# TRANSMISSION CHARACTERISTICS OF SPATIAL MECHANISMS CONTAINING HIGHER PAIRS

BY

CHIN-HUNG JWO

A DISSERTATION PRESENTED TO THE GRADUATE SCHOOL
OF THE UNIVERSITY OF FLORIDA IN PARTIAL FULFILLMENT
OF THE REQUIREMENTS FOR THE DEGREE OF
DOCTOR OF PHILOSOPHY

UNIVERSITY OF FLORIDA

1989

ACKNOWLEDGMENTS

The author wishes to express his deep and sincere appreciation to the chairperson of his supervisory committee, Dr. George N. Sandor, for his unfailing support and enthusiastic encouragement throughout the author's graduate pursuits. The author gratefully acknowledges the contribution to his education and practical knowledge of engineering given by the members of his supervisory committee, Dr. Joseph Duffy, Dr. Dr. Ron W. Dareing, Dr. Carl D. Crane, Dr. Chen-Chi Hsu, and his former advisor Dr. Gary K. Matthew. Special thanks are extended toward Dr. Dilip Kohli of the University of Wisconsin at Milwaukee for his valuable suggestions and his colleagues for sharing their knowledge.

Most of all, the author would like to thank his parents, Chin-Po and Tsai-Chung, for their endless support and encouragement and to his wife and son, Mei-Jung and Kaiwei(Kevin), for their companionship and patience during this undertaking.

Appreciation is also extended to the financial assistance by the National Science Foundation (Grant No. DMC-8508029).

TABLE OF CONTENTS


| | Page |
|---|---|
| ACKNOWLEDGMENTS | ii |
| ABSTRACT | v |
| CHAPTERS | |
| 1 INTRODUCTION | 1 |
| 1.1 Motivation | 1 |
| 1.2 Literature Review | 4 |
| 1.2.1 Kinematics of the Mechanisms Containing Higher pairs | 4 |
| 1.2.2 Coulomb Friction in Higher-pair Mechanisms. | 7 |
| 1.2.3 Coulomb Friction Coefficient | 10 |
| 1.2.4 Transmission Criteria for Linkages | 12 |
| 1.3 Objectives and Summary | 15 |
| 2 THE MECHANISMS AND THE HIGHER PAIRS | 17 |
| 2.1 The Mechanisms | 17 |
| 2.2 Force Analysis for Higher and Lower Pairs | 18 |
| 2.2.1 Slotted-sphere($S_L$) pair | 18 |
| 2.2.2 Sphere-slotted-cylinder(Sc) pair | 22 |
| 2.2.3 Sphere-groove(Sg) pair | 27 |
| 2.2.4 Sphere-plane(Sp) pair | 30 |
| 2.2.5 Cylinder-plane(Cp) pair | 32 |
| 2.2.6 Plane($P_L$) pair | 37 |
| 3 TRANSMISSION CRITERIA | 41 |
| 3.1 Deviation Angles | 41 |
| 3.1.1 Deviation angles for producing output force and moment | 42 |
| 3.1.2 Deviation angles for internal force and moment | 45 |
| 3.1.2.1 $S_L$(slotted sphere) pair | 47 |
| 3.1.2.2 Cp and Sp pairs | 49 |
| 3.1.2.3 $P_L$ pair | 55 |
| 3.1.2.4 Sg and Sc pairs | 55 |
| 3.1.2.5 R, P, and C pairs | 58 |
| 3.2 Force and Moment Transmissivities | 61 |
| 3.2.1 R-Sp-R mechanism | 62 |
| 3.2.2 R-Cp-C mechanism | 64 |
| 3.2.3 R-$P_L$-C-R mechanism | 67 |
| 3.3 Frictional Effects | 71 |
| 3.4 Mechanical Advantage and Instantaneous Efficiency | 75 |

3.5 Acceleration Ratio..... 78

4 STATIC FORCE AND TORQUE ANALYSIS..... 79
4.1 R-Sp-R Mechanisms..... 79
4.2 R-Cp-C Mechanisms..... 84
4.3 R-$P_L$-C-R Mechanism..... 89

5 DESIGN METHOD AND FORMULATION..... 94
5.1 Optimization Strategy in Mechanisms Design..... 94
5.2 Problem Formulation..... 98
5.2.1 Rotatability of mechanisms..... 98
5.2.1.1 Rotatability of R-Sp-R mechanism... 99
5.2.1.2 Rotatability of R-Cp-C and R-$P_L$-C-R mechanisms..... 102
5.2.2 Formulation of R-Sp-R mechanism..... 108
5.2.2.1 Objective function..... 112
5.2.2.2 Inequality constraints..... 113
5.2.2.3 Equality constraint..... 114
5.2.3 Formulation of R-Cp-C mechanism..... 114
5.2.3.1 Objective function..... 115
5.2.3.2 Inequality constraints..... 116
5.2.3.3 Equality constraint..... 116
5.2.4 Formulation of R-$P_L$-C-R Mechanism..... 116
5.2.4.1 Objective Function..... 117
5.2.4.2 Inequality constraints..... 118
5.2.4.3 Equality constraints..... 118
5.2.5 Feasible mechanism..... 119

6 NUMERICAL EXAMPLES..... 121
6.1 R-Sp-R Mechanism..... 121
6.2 R-Cp-C Mechanism..... 126
6.3 R-$P_L$-C-R Mechanism..... 142

7 CONCLUSIONS AND RECOMMENDATIONS FOR FUTURE RESEARCH.. 163
7.1 Conclusions..... 163
7.2 Recommendations..... 165

APPENDICES..... 167

A RELATIVE DISPLACEMENTS OF AN Sp PAIR..... 167
B RELATIVE DISPLACEMENTS OF A Cp PAIR..... 170
C RELATIVE DISPLACEMENTS OF A $P_L$ PAIR..... 174
D DISPLACEMENT EQUATIONS OF R-SP-R MECHANISM..... 177
E DISPLACEMENT EQUATIONS OF R-Cp-C MECHANISM..... 180
F DISPLACEMENT EQUATIONS OF R-$P_L$-C-R MECHANISM..... 184
G ROTATABILITY OF R-Sp-R MECHANISM..... 190

REFERENCE..... 193

BIOGRAPHICAL SKETCH..... 200

Abstract of Dissertation Presented to the Graduate School of the University of Florida in Partial Fulfillment of the Requirements for the Degree of Doctor of Philosophy

TRANSMISSION CHARACTERISTICS OF SPATIAL MECHANISMS CONTAINING HIGHER PAIRS

BY

CHIN-HUNG JWO

May, 1989

Chairman: Dr. George N. Sandor
Major Department: Mechanical Engineering

One of the essential problems in the design of mechanisms is the force and torque transmission. The transmission problem for both planar mechanisms and the spatial mechanisms containing lower pairs has been discussed extensively. However, this is not so for the spatial mechanisms containing higher pairs. The objective of this work is to study the transmission problem of the particular mechanisms.

The transmission characteristics of spatial mechanisms containing higher pair joints are investigated by way of the deviation angles and the transmissivities, which are expressed by way of geometric parameters. Sliding friction forces are included in the force and torque analysis due to their significant affect on the direct contact between the higher pair elements. Thus, mechanical advantage and instantaneous efficiency are also investigated for obtaining the efficiency of the mechanisms. In order to maintain

continuous motion, sliding friction forces must be overcome by the effective force produced by the input power. Thus, a geometric relationship between the friction force, which is opposes the direction of the relative velocity on the contact plane, and the effective force on the same contact plane must be satisfied in addition to the deviation angles.

Higher pair elements may have point or line contact. To reduce the complexity of the formulations caused by distributed friction forces, line contact is modeled by two concentrated normal force applied at the ends of the contact line. Similarly, for the plane pair, a lower pair, which is considered as a higher pair despite of the surface contact, is modeled by three concentrated normal forces acting on three of the corners of the contact plane.

Numerical examples are given for the design of mechanisms containing one-point, line, and surface contact higher pairs, respectively, which includes the consideration of optimum deviation angles and minimized peak acceleration to improved the high speed performance.

# CHAPTER 1
# INTRODUCTION

## 1.1 Motivation

The kinematic synthesis and analysis of closed loop spatial mechanisms have been studied extensively on mechanisms with lower pairs, but less so on mechanisms containing higher pairs. The use of higher pairs leads to more compact spatial mechanisms, which in general can be designed to produce better motion approximations and to have better dynamic performance than lower-pair mechanisms.

One of the essential problems in the design of mechanisms is the force and torque transmission which is also a criterion to avoid the "lock up" positions (Sutherland, 1981) or uncertainty configurations as defined by Hunt (1978). The transmission problem for both planar mechanisms and spatial mechanisms containing lower pairs has been discussed extensively in existing literature. However, this is not the case for spatial mechanisms containing higher pairs. Therefore, the objective of this work is to study the transmission problem of spatial mechanisms with higher pairs.

Instead of using transmission angles as defined in the design of planar mechanisms and some spherical and also in spatial mechanisms containing lower pairs only, deviation

angles are used as the design criteria. The deviation angles are defined as the angles between the input force and the resistant force at each joint in the sequence of force transmission which describe the transmitted force at the floating joints. The deviation angles for moment transmission are also defined similarly to those for the force transmission. For each floating joint there will be deviation angles for the transmission of internal force and moment, i.e., the force and moment transmitted between the pair elements. If the joint connects the coupler link and the output link, then there will also be deviation angles for the force and moment to produce the output force and output moment. The force and moment transmissivities are introduced to take all deviation angles in sequence into account. For three-link mechanisms, the transmissivities are classified as force-to-force and force-to-torque. These are the indexes of how well the coupler force produces the output translational and rotational motions, respectively. The torque-to-torque transmissivity is the index of how well the coupler produces the rotational motion of the output joint. For four-link mechanisms, the coupler force will produce a moment at the joint connecting the coupler link and the output link. Thus a force-torque-to-torque transmissivity is needed to show how this moment produces the output rotational motion. To take the frictional effects into account, the mechanical advantage and the instantaneous efficiency are also investigated. The mechanical advantage is defined

as the ratio between the output force exerted by the output link and the input force applied to input link. The instantaneous efficiency is defined as the ratio between the output power and the input power. When there is no energy loss due to the frictional effects, the instantaneous efficiency should be unity. The mechanical advantage and the instantaneous efficiency of the mechanism are affected by the power loss due to frictional effects between pair elements. In the consideration of high speed performance, the dynamic behavior of the mechanism should also be of concern. This can be evaluated by the angular and linear accelerations of the mechanism links. The output acceleration ratios can be defined as the ratio between the maximum and minimum output angular and linear accelerations, which depend on the type of the output joint. If the output link has only angular motion, the acceleration ratio may be defined as the ratio between the output angular acceleration and the square of the constant input angular velocity, as used in tandem mechanisms (Hain, 1971). Since the input angular velocity is assumed to be constant in this work, therefore, the acceleration ratio will be replaced by the magnitude of the output angular acceleration itself. It also may be desired to minimize the deviation between the maximum and minimum output angular or linear accelerations.

Once the transmission criteria are defined, the transmission characteristics of a certain mechanism can be evaluated by way of the deviation angles, the force and mo-

ment transmissivities, the mechanical advantage, and the instantaneous efficiency. The following step then is to optimize the mechanism to create better transmission and better dynamic performance. The other critical factors to be considered are

1. the rotatablity of the mechanism;
2. the physical size of the higher pair, which may create a restriction of the relative motion between two pair elements; and
3. the avoidance of possible redundant translational freedoms, i.e., the possible collinearity of sliding axes.

## 1.2 Literature Review

### 1.2.1 Kinematics of the Mechanisms Containing Higher Pairs

Kohli and Soni (1973a, b) use successive screw displacements to conduct kinematic analysis of single-loop and two-loop spatial mechanisms involving lower pairs. Kohli and Soni (1975) and Singh and Kohli (1979) developed pair geometry constraint equations for lower pairs such as Revolute (R), Prismatic (P), Helical (H), Sphere (S), and Cylinder (C) pairs, and for higher pairs such as Slotted Sphere ($S_L$), Sphere-in-slotted Cylinder (Sc), Sphere-Plane (Sp), Sphere-Groove (Sg) and Cam pairs. Figure (1-1) illustrates these higher pairs. The higher pairs can also be represented by various combinations of lower pairs as seen in the work of Chen and Roth (1969). Litvin and Gutman

Sphere-Slotted-Cylinder (Sc)

2 Rotations

1 Translations

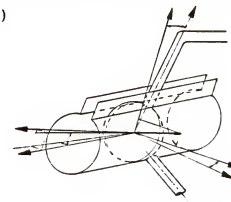

Plane ($P_L$)

1 Rotation

2 TranslationS

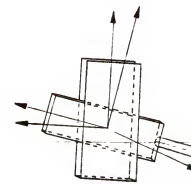

Slotted-Sphere ($S_L$)

2 Rotations

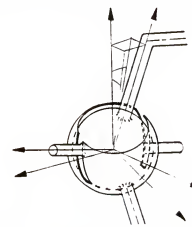

Figure 1-1 Pair Types.

Sphere-Plane (Sp)

3 Rotations

2 Translations

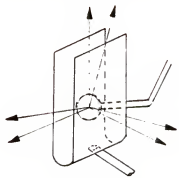

Sphere-Groove (Sg)

3 Rotations

1 Translation

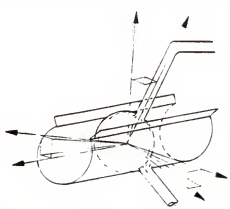

Cylinder-Plane (Cp)

2 Rotations

2 Translations

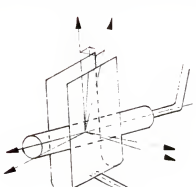

Figure 1-1 continued.

(1980) use matrix methods for a three-link mechanism with an intermediate higher pair of two crossed cylinders. Sandor, Kohli, Hernandez and Ghosal (1981) and then Ghosal, Kohli and Sandor (1982) applied higher pair geometry constraint equations to analyze three-link spatial mechanisms that contain Sp and Sg pairs and four-link mechanisms that contain Sg and Sc pairs, respectively. A more complete kinematic analysis is done by Ghosal in his thesis (1982) including three, four and five link mechanisms. Hernandez presented the kinematic synthesis and analysis of three-link spatial function generators containing higher pairs including pair element design (1983). Miesch (1984) gave optimal design of the R-Sp-R function generator. However, transmission characteristics have not been discussed fully as yet for higher pair mechanisms, although this is imperative in the design of such mechanisms.

### 1.2.2 Coulomb Friction in Higher-pair Mechanisms

The contact between higher pair elements is likely to be influenced by friction forces that are often distributed along a line or curve, rather than being a concentrated force acting at a single point. Although the friction can be neglected in the case of well lubricated bearings in lower pairs, for some circumstances the lubrication is poor or not allowed at all (for example, in space applications); then the friction is to be taken into account. There are not many publications in mechanism dynamics that consider

the effects of friction in lower-pair bearings. Keler (1973) derived the static forces, including friction of lower and some higher pairs using dual numbers based on an iterative technique, that is applicable to all single-loop mechanisms which are kinematically and statically determinate. Sadler (1973) uses the concept of the friction circle to investigate the effects of Coulomb friction in a pin joint with equilibrium equations in the dynamic analysis of four bar mechanisms. Bagci (1975a) presented the dynamic motion analysis of statically determinate planar mechanisms via the joint-force analysis including Coulomb and viscous damping. The methods used by Sadler (1973) and Bagci (1975a) parallel the graphical approach. Imam, Skreiner, and Sadler (1981) utilize similar method but they add the approximate closed-form solution to force analysis in the application of circuit-breaker mechanisms. Recently, Bagci and Khosravi (1986) extended their previous work (1975) to the application to spatial mechanisms with lower pairs, such as revolute, cylinder, prismatic, and sphere pairs. In the above work, all line contacts are treated as contacts at a single point with the assumption that only one concentrated reaction force exists at the center of gravity of the contact line. This is allowable because of the relative linear translation between pair elements, and does not involve the relative rotation on the tangential plane of the contact. This assumption is also applicable to higher pairs with one-point contact, but not for higher pairs with more-than-

one-point contact, where the relative velocity is different for each contact point along the line of contact.

Consideration of Coulomb friction is also seen in the design of cam systems. Pisano (1984) modeled a high-speed cam system using Coulomb friction alone at the rocker arm pivot. The static and dynamic coefficients of Coulomb friction are calculated directly from experimental data taken at low camshaft speeds. The incorporation of Coulomb friction into the model gives very good agreement with experiment. Chew (1985) used the concept of rolling-contact to reduce friction at highly loaded rocker-pivot without the use of rolling element bearings.

Another subject is the friction in the sliding surface of slider mechanisms. The study in this area is more dynamic, which may include surface combination (different sliding surfaces in contact), surface finish, viscosity of the lubricant, the composition of the lubricant, the geometry of the lubricating grooves and the nominal area of contact with apparent pressure on the slideway (Bell & Burdekin, 1966). Obviously, these subjects are outside the scope of what is considered in this work.

Two techniques for reducing the friction between kinematic pairs which connect a movable link to a frame are described by Litvin and Coy (1984). One way is arranging the design so that the relative velocities of the link with respect to two grounded kinematic pairs are equal in magnitude and opposite in direction. The other way is moving

the link in a direction perpendicular to the direction of the working motion. Although these techniques are not applicable in higher pairs, since higher pairs are usually at floating joints, it may be applied to grounded lower pairs if frictional effects are considered.

### 1.2.3 Coulomb Friction Coefficient

The static coefficient of Coulomb friction in the kinematic pairs of a mechanism is usually used when the mechanism is about to move. When the mechanism is already in motion, the kinetic coefficient of friction is applied, which in general is about 75 percent of the static coefficient (Bagci, 1975a).

In sliding motion, it may happen that the magnitude of the relative velocity goes to zero, for instance at the moment when the mechanism is starting up, reversing, or a position is broken. To deal with zero relative velocities, several models have been seen in the design of mechanisms containing a sliding joint. The most straightforward model is that the direction of the friction force, $\underline{F}$, depends on the sign of the relative velocity, $\underline{V}_S$, which is expressed

$$\underline{F} = \mu|\underline{N}|(-\text{sign}(\underline{V}_S)) \qquad (1\text{-}1)$$

where $|\underline{N}|$ is the absolute magnitude of the normal force applied at the contact point p. Figure (1-2a) illustrates Equation (1-1) where the effect of zero relative velocity is not included. Bell and Bardekins' experimental measurements

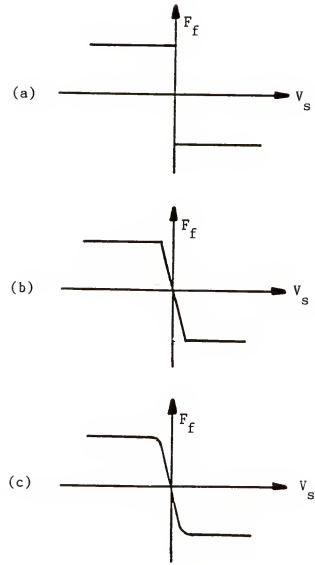


Figure 1-2 Approximations of static friction coefficient at zero relative velocity.

(1966) show that Equation (1-1) is especially good for moderate sliding velocities and cyclic conditions. Some other models are discussed by Rooney and Deravi (1982), which includes a straight line approximation when the relative velocity goes to zero, as shown in Figure (1-2b), and the one proposed by Rooney and Deravi, which has a nonlinear approximation nears zero velocity, as shown in Figure (1-2c). Keler (1973) suggests using the relative acceleration vector as the direction of the sliding friction force and using the adhesion coefficient instead of the frictional coefficient. In the present work, Equation (1-1) is applied. However, generally the sliding velocity on the contact plane of the higher pairs does not go to zero and changes to the opposite direction during the motion of the mechanism, i.e., generally the sliding motion is not along a straight line, and therefore application of Equation (1-1) is not quite straightforward.

### 1.2.4 Transmission Criteria for Linkages

For planar and spherical four-bar mechanisms, transmission criteria are defined by the well-known transmission angle, i.e., the angle between the coupler and the output link. The first application of optimal design including the transmission angle in planar mechanisms probably is the work done by Roth, Freudenstein, and Sandor (1962). In the ensuing two decades and more, voluminous publications considering the optimal transmission angle were published (Shoup &

Pelan, 1971; Freudenstein & Primrose, 1972; Bagci, 1975b; Gupta, 1977 & 1978; Freudenstein & Chew, 1979; and Tsai, 1983). Most of these works use the transmission angle to define the transmission characteristics, which is generally adequate for planar mechanisms. Graphical procedures for the optimization of the transmission angle in planar mechanisms are seen in Hall's work (1966) and also in the work by Sun and Waldron (1981).

The transmission angle is also used in the design of spherical mechanisms (Dukkipati & Soni, 1975; Huang, Pamidi, & Soni, 1970, Soni & Harrisberger, 1967; Hossne, 1979; Chiang, 1986a, b; Huang & Soni, 1969) and in spatial mechanisms (Soni & Harrisberger, 1969, 1971). Brasfield and Bagci (1975b) claimed that the use of transmission angle defined similarly to those used for planar mechanisms may not be appropriate for spherical and spatial mechanisms.

To express the transmission criteria for spatial mechanisms with lower pairs, various works have used different approaches. Hamid and Soni use the definition of transmission ratio, which is the ratio of the force exerted by the coupler link to the applied force received by the output link. They applied these in the design of RSSR (Hamid & Soni, 1971) and RSSP (Hamid & Soni, 1972) mechanisms. In the publication of Shoup, Steffen and Weatherford (1972), two deviation angles are defined as the force and torque effectiveness, which are 1) the angle between the direction of the force exerted by the coupler on

the output link and the direction of the velocity of their joint and 2) the angle between the axis of the torque exerted by the coupler on the output link and the direction of the axis of the angular velocity of the output link. Bagci (1971) uses 3x3 screw matrices to investigate the force-to-force, force-to-torque, torque-to-torque, and force torque-to-torque transmissivities which are solved through dual equilibrium equations. Transmission criteria are thus determined by how the force and moment exerted by the coupler affect the output force and moment. Bagci (1971) also indicated that the transmissivities can be used to avoid passive or redundant freedom. This is because the transmissivities vanish when there is passive or redundant freedom. The torque-to-torque transmission ratio concept is also used in the later work of Bagci (1973) for the spherical crank-rocker mechanism. Also, in the design of RCRRC mechanism, the transmissivities are applied by Lee and Bagci (1975) again. Sutherland (1973) established a transmission index by using the definition of wrenches and screws related to the mechanical error in a linkage. The transmission index can be used as an index of the quality of motion (Sutherland, 1981). Litvin (1980) uses dual vectors to develop the force transmission criteria for spatial linkages of any structure where he defines the transmission criteria by the ratios of the force and moment of every joint to the resisting moment at the joint. A definition of transmission angle similar to the definition of transmission ratio is

used by Hamid and Soni (1971, 1972), and it is also seen in the works of Gupta and Kazerounian (1983), Rao and Lakshminarayana (1984a, b, c), and Söylemez and Freudenstein (1982). In these works, the transmission ratios are used to denote the ratios between the force and moment exerted by the coupler to the output force and moment.

The use of transmission angle or ratio is well suited for single force transmitting mechanisms such as the RSSR mechanism. For mechanisms containing higher pairs, which may have both force and torque transmitted, the definition similar to those given by Bagci (1971) or Litvin (1980) would be more appropriate. Similar definition of transmissivities to that used by Bagci (1971) is applied with a different approach in this work. Funabashi and Freudenstein (1979a, b) gave some transmission criteria for high speed planar and spherical crank-and-rocker linkages. These criteria may be also applicable in the design of those particular mechanisms discussed in this work which are usually used for high speed applications. This is similar to the design of cam mechanisms, where the ratio of the output angular acceleration to the square of the input angular velocity is considered (Hain, 1971).

## 1.3 Objectives and Summary

Most works mentioned previously deal with lower pairs without Coulomb friction while the purpose of this work is to determine the transmission criteria of spatial mechanisms

including Coulomb-frictional effects in higher pair joint. The friction forces do not affect the deviation angles, but they do affect the reaction forces and moments. Thus, beside the deviation angles, mechanical advantage and instantaneous efficiency are also needed. Developing definitions of better transmission criteria will be of benefit in the seeking of optimal designs of spatial mechanisms with higher-pair joints.

In this chapter we have reviewed the works related to the topics of this dissertation and have also covered the design concept considered for transmission characteristics in the literature. Chapter 2 covers the force analysis for the higher pairs including friction forces. A discussion of design criteria including Coulomb frictional effects is covered in Chapter 3. Chapter 4 carries out the static force and torque analysis, which is needed to define the mechanical advantages and the instantaneous efficiency. Then, Chapter 5 gives the formulations of optimal design according to the transmission criteria defined in the previous chapters and other necessary constraints. Three numerical examples are given in Chapter 6, which are R-Sp-R, R-Cp-C, and R-$P_L$-C-R mechanisms, respectively. The R-Cp-C mechanism is statically indeterminate, and therefore it is modeled with specified output resistant force and torque. Conclusions and recommendations for future research are given in the final chapter.

# CHAPTER 2
# THE MECHANISMS AND THE HIGHER PAIRS

## 2.1 The Mechanisms

Higher pairs can be represented by combinations of prismatic and revolute pairs with special axis locations and orientations. This means that the direct constraints can be formulated for the higher pairs themselves. This simplifies the synthesis and analysis of the mechanisms with higher pairs. Due to the multiple degrees of freedom of relative motion of higher pairs, the number of links for a certain function can be reduced as compared to lower-pair mechanisms. This means that more compact mechanisms can be constructed by the use of higher pairs. The kinematic synthesis and analysis of mechanisms containing higher pairs has been shown by Ghosal (1982) for three, four and five-link mechanisms. Displacement equations based on Ghosal's work are listed in the appendices for two of the numerical examples in later chapters. The displacement equations for one of the examples, namely the R-$P_L$-C-R mechanism, are not in the existing literature. These equations are derived in a similar manner as those in Ghosal's work and are illustrated in Appendix F. In constructing the mechanisms, if the two-DOF lower pair is grounded instead of being a floating joint, the mechanisms so formed will be statically

indeterminate. For example, the R-Cp-C and R-$P_L$-R-C mechanisms are statically indeterminate if only the input torque is specified.

## 2.2 Force Analysis for Higher and Lower Pairs

Without Coulomb friction, the force analysis is rather straightforward for higher pairs, especially for those having a plane element, since the reaction force is always along the direction of the normal of the contact surface. However, when Coulomb friction is involved, the direction of the reaction force will be affected by the direction of the relative velocity between the contact pair elements. The analysis procedure will be shown later.

### 2.2.1 Slotted-sphere($S_L$) pair

A slotted-sphere pair is a lower pair with two degrees of freedom of relative rotation between pair elements and may be viewed as two perpendicular revolute pairs with intersecting axes. Figure (2-1) shows an $S_L$ pair where the inner sphere and the spherical shell are denoted as the i-th and j-th link, respectively. The origins of the two moving coordinates coincide. The relative rotations between the two coordinate systems are denoted as $\Theta_{xij}$ and $\Theta_{zij}$, respectively. One moment and three force components are acting between the two pair elements. If the i-th link is the input link and the j-th link is the output link, the transmitted moment, $\underline{M}_{ij}$, must be simultaneously perpendicular to

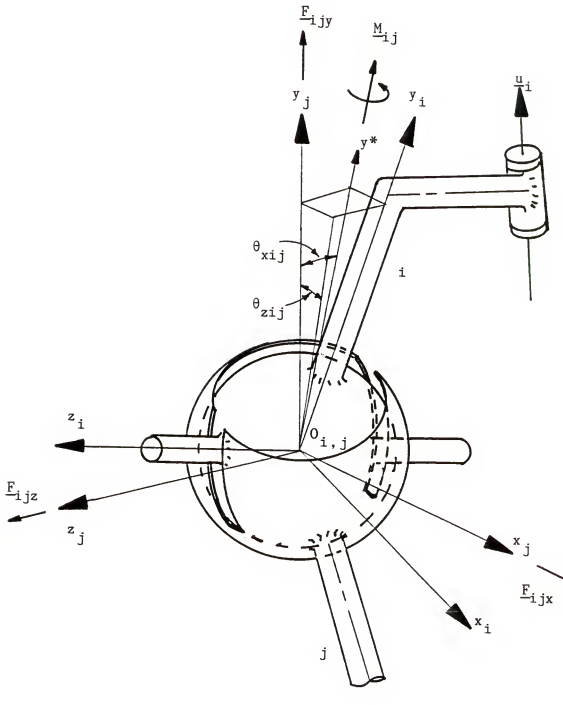


Figure 2-1 Slotted-sphere($S_L$) pair

$z_i$ and $x_j$ axes, i.e., in the direction of $y^*$. To count the frictional effects induced by this moment, a force couple consisted of $\underline{F}_{c1}$ and $\underline{F}_{c2}$ are illustrated at the two assumed contact points $P_1$ and $P_2$ to replace the moment, as shown in the force diagram for the $S_L$ pair in Figure (2-2). The two forces forming the couple will cause two Coulomb sliding friction forces, $\underline{F}_{f1}$ and $\underline{F}_{f2}$. The directions of the two friction forces are opposite to the relative sliding velocities $\underline{V}_{s1}$ and $\underline{V}_{s2}$, respectively. The directions of the two relative sliding velocities must be opposite to each other, since the relative motion is caused by the relative rotations only, and will produce tangent velocities at the two contact points. Thus, the directions of the friction forces $\underline{F}_{f1}$ and $\underline{F}_{f2}$ are also opposite to each other. The resultant friction moment, $\underline{M}_f$, must be in the direction of the $x_j$ axis, i.e., normal to $y_j z_j$ plane. The transmitted force, $\underline{F}_{ij}$, can have three components and its line of action intersects the inner surface of the spherical shell at the modelled contact point P. Also, there is a sliding friction force, $\underline{F}_f$, caused by $\underline{F}_{ij}$ at point P. The direction of $\underline{F}_f$ is opposite to the relative sliding velocity which is caused by the two relative rotations at point P.

To summarize the forces and moments at the pair, we may write the resultant force at the center of the sphere, as

$$\underline{F}_{rij} = \underline{F}_{ij} + \underline{F}_f \qquad (2\text{-}1)$$

where

$$\underline{F}_f = -\mu|\underline{F}_{ij}|\underline{v}_s; \qquad \underline{v}_s = \underline{V}_s/|\underline{V}_s|; \quad \underline{V}_s = \underline{\Omega}_{ij} \times r\underline{f}_{ij}.$$

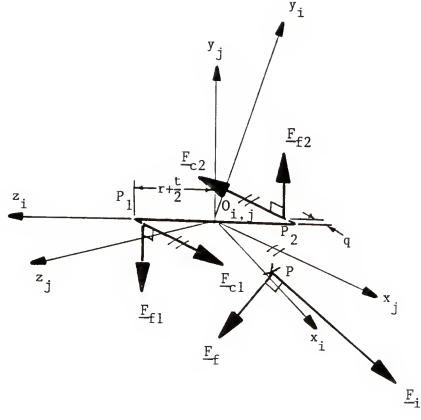


Figure 2-2 Force diagram of $S_L$ pair.

The quantity $\mu$ is the friction coefficient, a positive scalar; r is the radius of the sphere; $\underline{f}_{ij}$ is the unit vector of the transmitted force $\underline{F}_{ij}$, $\underline{f}_{ij} = \underline{F}_{ij} / |\underline{F}_{ij}|$; $\underline{\Omega}_{ij}$ is the relative angular velocity of element i with respect to element j. The resultant moment may be expressed

$$\underline{M}_{rij} = \underline{M}_{ij} + r\underline{f}_{ij} \times \underline{F}_f + 2[(r + t/2)\underline{z}_i + q\underline{x}_i] \times \underline{F}_{f1} \qquad (2\text{-}2)$$

where

$$\underline{F}_{f1} = -\mu|\underline{F}_{c1}|\underline{v}_{s1};$$

$$|\underline{F}_{c1}| = |\underline{F}_{c2}| = |\underline{M}_{ij}|/(r + t/2);$$

$$\underline{v}_{s1} = \underline{V}_{s1}/|\underline{V}_{s1}|;$$

$$\underline{V}_{s1} = \underline{\Omega}_{ij} \times [(r + t/2)\underline{z}_i + q\underline{x}_i].$$

The quantity t, a positive scalar, is the thickness of the spheric shell, which may be neglected; q is the radius of the inserted round bar on the two sides of the inner sphere; The direction of $\underline{M}_{ij}$ is initially assumed having the positive direction along $y^*$. If q and t are both neglected, Equation (2-2) becomes

$$\underline{M}_{rij} = \underline{M}_{ij} + r\underline{f}_{ij} \times \underline{F}_f + 2r\underline{z}_i \times \underline{F}_{f1} \qquad (2\text{-}3)$$

Here, $\underline{M}_{rij}$ is the resultant moment both the external and frictional moments.

### 2.2.2 Sphere-slotted-cylinder(Sc) pair

Figure (2-3) shows an Sc pair where the sphere and the cylinder elements are connected to the i-th link and the j-th link, respectively. Initially, the origins of the two

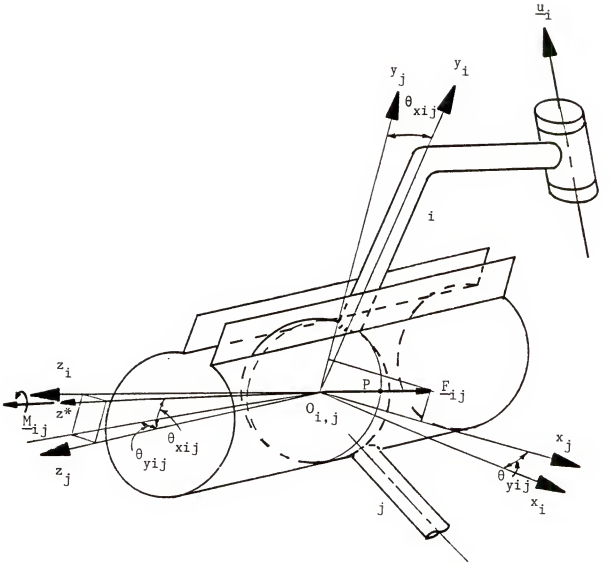


Figure 2-3 Sphere-slotted-cylinder(Sc) pair

moving coordinate systems coincide. An Sc pair permits two relative rotations, $\theta_{xij}$ and $\theta_{yij}$; and a relative translation, $l_{zij}$(initially assumed to be zero), along the direction of the $z_j$ axis. The Sc pair may be treated as a combination of two revolute pairs and one prismatic pair, where the two revolute axes intersect on the axis of the prismatic pair. One moment and two force components are transmitted between the two pair elements, whose directions are shown in Figure (2-3). The transmitted moment, $\underline{M}_{ij}$, is in the direction of $z^*$, which is normal to the $x_jy_i$ plane. If the pair is considered to be in surface-contact, the moment may be replaced by a force couple, consisting of $\underline{F}_{c1}$ and $\underline{F}_{c2}$, acting at the two assumed contact points, $P_1$ and $P_2$. Figure (2-4) illustrates the force diagram of the Sc pair. The vector of the force couple is parallel to the $x_j$ axis and is passing through the $y_i$ axis. Point $P_1$ is the intersection with the normal surface of the sphere rod and the edge of the cylinder slot. Point $P_2$ is where $\underline{F}_{c2}$ going from the center of the inner sphere and passing through the inner surface of the cylinder element. Thus, two friction forces, $\underline{F}_{f1}$ and $\underline{F}_{f2}$, are induced, whose directions are opposite to the directions of the relative sliding velocities, $\underline{V}_{s1}$ and $\underline{V}_{s2}$, respectively. Since these two relative sliding velocities are parallel with the $y_jz_j$ plane, the direction of the vector of the friction moment, $\underline{M}_f$, must be in a plane normal to the $y_jz_j$ plane, i.e., collinear to $x_j$ axis. The transmitted force, $\underline{F}_{ij}$, has two components in the direction

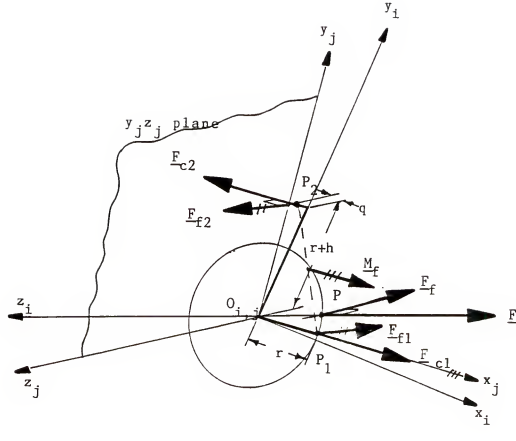


Figure 2-4 Force diagram of Sc pair.

of $x_j$ and $y_j$ axes, respectively. Thus, the transmitted force lies on the $x_jy_j$ plane. The contact point P is the intersection with the arc of contact of the normal to the axis of the cylinder, coplanar with the axis and the line of action of the force acting on and going through the center of the sphere. The forces and moments may be summarized at the center of the sphere. The resultant force is

$$\underline{F}_{rij} = \underline{F}_{ij} + \underline{F}_f + \underline{F}_{f1} + \underline{F}_{f2} \qquad (2\text{-}4)$$

where

$$\underline{F}_f = -\mu|\underline{F}_{ij}|\underline{v}_s;$$

$$\underline{F}_{f1} = -\mu|\underline{F}_{c1}|\underline{v}_{s1};$$

$$\underline{F}_{f2} = -\mu|\underline{F}_{c2}|\underline{v}_{s2};$$

and

$$\underline{v}_s = \underline{V}_s/|\underline{V}_s|;$$

$$\underline{V}_s = \underline{\Omega}_{ij} \times r\underline{f}_{ij} + \underline{V}_{zij};$$

$$|\underline{F}_{c1}| = |\underline{F}_{c2}| = |\underline{M}_{ij}|/[0.5(r + h)/\cos\Theta_{xij}];$$

$$\underline{v}_{s1} = \underline{V}_{s1}/|\underline{V}_{s1}|;$$

$$\underline{V}_{s1} = \underline{\Omega}_{ij} \times r\underline{x}_j + \underline{V}_{zij};$$

$$\underline{v}_{s2} = \underline{V}_{s2}/|\underline{V}_{s2}|;$$

$$\underline{V}_{s2} = \underline{\Omega}_{ij} \times \{[(r + h)/\cos\Theta_{xij}]\underline{y}_i - q\underline{x}_j\} + \underline{V}_{oij};$$

The quantity r is the radius of the sphere; q is the radius of the sphere rod; h is the height of the slot of the cylinder element; $\underline{V}_{zij}$ is the relative linear velocity along the cylinder axis; and $\underline{M}_{ij}$ is initially assumed in the direction of $z^*$ axis. The resultant moment may be written

$$\underline{M}_{rij} = \underline{M}_{ij} + r\underline{f}_{ij} \times \underline{F}_f + r\underline{x}_j \times \underline{F}_{f1} + \{[(r + h)/\cos\Theta_{xij}]\underline{Y}_i - q\underline{x}_j\} \times \underline{F}_{f1} \qquad (2\text{-}5)$$

When the force $\underline{F}^*$ of the sphere element exerts onto the grooved cylinder element is directed toward the open slot in the cylinder, then P splits into two points. Although the exact contact points $P_1^*$ and $P_2^*$ are at the edges of the slot as shown in Figure (2-5), we can use the theoretical contact point $P^*$, which lies on the line of action of $\underline{F}^*$ through the center of the sphere, since this does not change the resultant force.

### 2.2.3 Sphere-groove(Sg) pair

The Sg pair allows three relative rotations and one translation between the pair elements. An Sg pair may be viewed as a combination of three revolute pairs and one prismatic pair, where the three revolute pair axes are concurrent on the axis of the prismatic pair. Figure (2-6) illustrates an Sg pair where the inner sphere and the groove are denoted as the i-th and the j-th link, respectively. There are two force components transmitted through the two pair elements and no moments transmitted. The location of the acting point P of the resultant force at an Sg pair can be described similarly to that at an Sc pair (see Figure (2-6)). The resultant force may be summarized at the sphere center, as

$$\underline{F}_{rij} = \underline{F}_{ij} + \underline{F}_f \qquad (2\text{-}6)$$

where

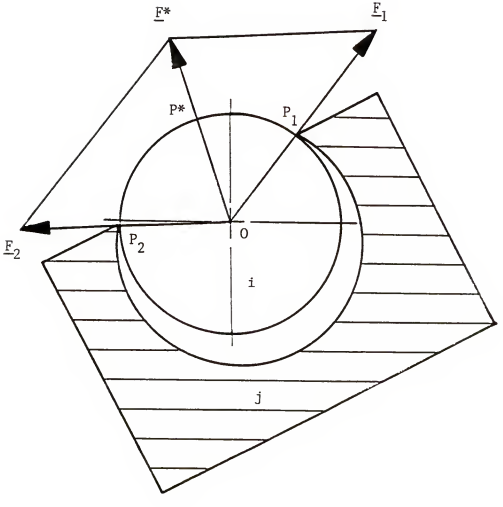


Figure 2-5 Theoretical contact point of Sc or Sg pair.

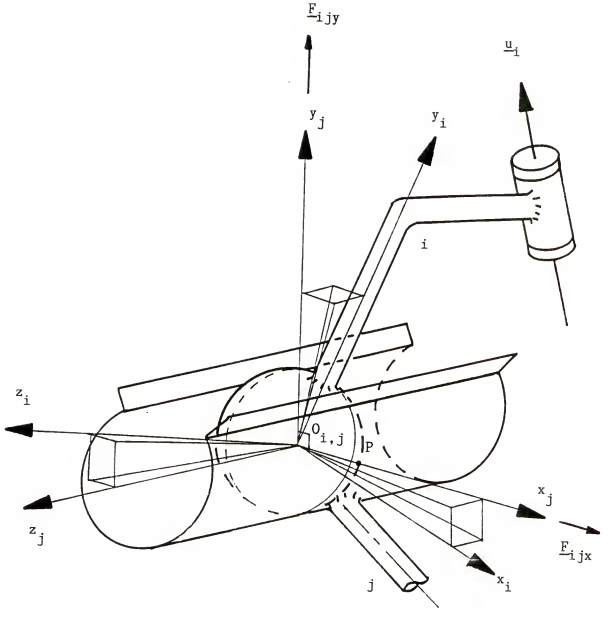


Figure 2-6 Sphere-groove(Sg) pair

$$\underline{F}_f = \frac{-\mu|\underline{F}_{ij}|(\underline{\Omega}_{ij} \times r\underline{f}_{ij} + \underline{V}_{zij})}{|\underline{\Omega}_{ij} \times r\underline{f}_{ij} + \underline{V}_{zij}|}$$

The quantity r is the radius of the sphere, $\underline{\Omega}_{ij}$ is the relative angular velocity vector; $\underline{f}_{ij}$ is the unit vector of $\underline{F}_{ij}$; $\underline{V}_{zij}$ is the relative linear velocity along the froove. The resultant moment at the sphere center is

$$\underline{M}_{rij} = r\underline{f}_{ij} \times \underline{F}_f \qquad (2\text{-}7)$$

In the force and torque analysis for the mechanisms containing an Sg pair, the resultant force can be summarized at the contact point instead of the sphere center and the resultant moment is eliminated. It is to be noted, however, that when the sphere rod reaches the edge of the groove, a moment about the $z^*$ axis will be transmitted.

### 2.2.4 Sphere-plane(Sp) pair

Figure (2-7) shows the Sp pair where the inner sphere and the plane elements are denoted as the i-th and the j-th link, respectively. The pair permits three relative rotations and two relative translations. The three rotation axes are concurrent at the center of the sphere. There is only one force acting on the contact surface. The contact point P for a Sp pair must lie at the intersection of the plane and the force vector $\underline{F}_{ij}$ passing through the center of the sphere and normal to the plane. The point P can be on either side of the plane element depending on the direction of the transmitted force. When friction is present, the resultant force can be summarized at the contact point

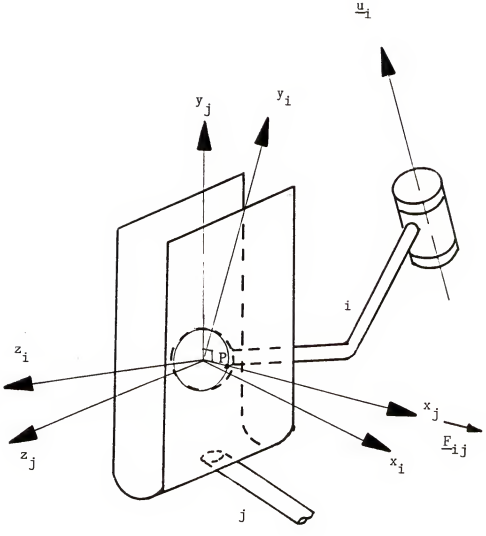


Figure 2-7 Sphere-plane(Sp) pair.

instead of the sphere center. Thus, there will be no moment but only forces acting at the contact point, and

$$\underline{F}_{rij} = \underline{F}_{ij} + \underline{F}_{f} \qquad (2\text{-}8)$$

where

$$\underline{F}_{f} = -\mu|\underline{F}_{ij}|\underline{v}_{s}$$

The unit vector of the relative sliding velocity at the contact point, $\underline{v}_s$, can be obtained directly from the displacement equations.

### 2.2.5 Cylinder-plane(Cp) pair

There are two relative rotations and two translations between the pair elements of a Cp pair denoted by $\theta_{xij}$ and $\theta_{zij}$, as shown in Figure (2-8). In such an interpretation, the axes of one revolute pair and one prismatic pair coincide, namely $z_i$, and the other two pair axes are perpendicular to each other and to the two coincident axes. The relative translations are along the $y_j$ and $z_j$ axes, respectively. There is only one moment component and one force component transmitted between the pair elements, which are acting on the contact line. The contact line for the Cp pair is the intersection between the plane element and the normal plane that passes through the axis of the cylinder, as shown in Figure (2-8). Without friction, the direction of the transmitted moment vector, $\underline{M}_{ij}$, must be perpendicular to the contact line and lies in the contacting plane element. The direction of the transmitted force, $\underline{F}_{ij}$, must be normal to the contacting plane element. The moment vector

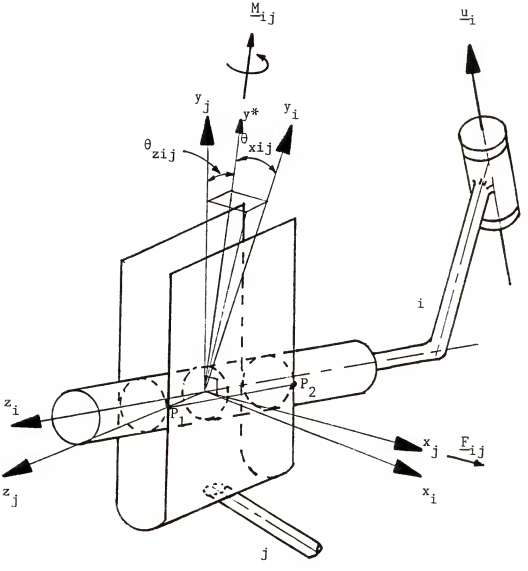


Figure 2-8 Cylinder-plane(Cp) pair

$\underline{M}_{ij}$ may be modeled as a force couple consisting of $\underline{F}_{c1}$ and $\underline{F}_{c2}$ acting at the ends of the contact line (Figure (2-9)). When friction is present, two sliding friction forces are to be added, which lie on the contacting plane element surfaces. Thus the direction of the friction moment, $\underline{M}_f$, must be substantially normal to the plane element. Unlike the previous pairs, which all have a sphere element and the transmitted force components can be regarded as a single force passing through the sphere center, the Cp pair has a cylinder element and the transmitted force components are distributed along the contact line normal to the plane element. These forces will produce distributed friction forces opposing the direction of the relative sliding velocities, which vary both in direction and in magnitude along the contact line. Therefore, it is difficult to determine the transmitted forces and moments analytically when considering distributed transmitted forces.

To simplify the force and torque analysis, the transmitted force and moment may be modeled by two concentrated forces acting at the two ends of the contact line, where the two forces may have different magnitudes and their directions are parallel to each other. This is assuming that the cylinder and the plane elements are rigid and there may exist some small clearance between cylinder and the plane elements. As shown in Figure (2-9), the normal forces are $\underline{F}_{ij1}$ and $\underline{F}_{ij2}$. Their directions are initially assumed to be opposite to each other, parallel to the $x_j$ axis. Two friction

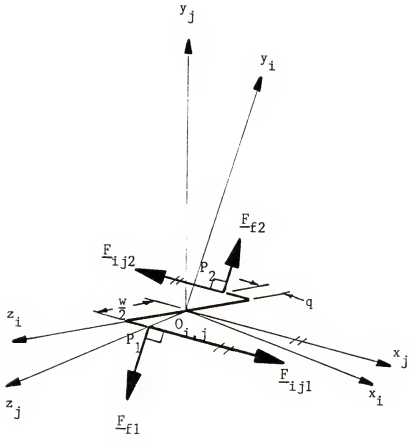


Figure 2-9 Force diagram of Cp pair.

forces are induced at the two contact points, $P_1$ and $P_2$. To determine the assumed location of the resultant force, the two normal forces are first assumed acting at the axis of the cylinder element. The forces may be summarized at the gravity center (the midpoint of the contact line). The resultant force can be written

$$\underline{F}_{rij} = \underline{F}_{ij1} + \underline{F}_{ij2} + \underline{F}_{f1} + \underline{F}_{f2} \tag{2-10}$$

where

$$\underline{F}_{f1} = -\mu|\underline{F}_{ij1}|\underline{V}_{s1}/|\underline{V}_{s1}|;$$

$$\underline{F}_{f2} = -\mu|\underline{F}_{ij2}|\underline{V}_{s2}/|\underline{V}_{s2}|;$$

$$\underline{V}_{s1} = \underline{\Omega}_{ij} \times \underline{OP}_1 + \underline{V}_{ij};$$

$$\underline{V}_{s2} = \underline{\Omega}_{ij} \times \underline{OP}_2 + \underline{V}_{ij};$$

$$\underline{OP}_1 = (w/2)\underline{z}_i + q\underline{x}_j;$$

$$\underline{OP}_2 = -(w/2)\underline{z}_i - q\underline{x}_j.$$

The vector $\underline{\Omega}_{ij}$ and $\underline{V}_{ij}$ are the relative angular and linear velocities, respectively; $\underline{OP}_1$ and $\underline{OP}_2$ are the vectors from the midpoint of cylinder axis in contact to the two contact points $P_1$ and $P_2$, respectively; and q is the radius of the cylinder. The transmitted moment can be written

$$\underline{M}_{rij} = \underline{OP}_1 \times (\underline{F}_{ij1} + \underline{F}_{f1}) + \underline{OP}_2 \times (\underline{F}_{ij2} + \underline{F}_{f2}) \tag{2-11}$$

If the radius of the cylinder, q, is neglected in force and torque analysis, the two vectors $\underline{OP}_1$ and $\underline{OP}_2$ can be simplified, as

$$\underline{OP}_1 = (w/2)\underline{z}_i \tag{2-12}$$

and

$$\underline{OP}_2 = -(w/2)\underline{z}_i, \tag{2-13}$$

respectively. This means that the two normal forces and the

two friction forces are assumed acting at the axis of the cylinder.

2.2.6 Plane($P_L$) pair

A $P_L$ pair has planar surface contact. It is illustrated in Figure (2-10). The pair allows one relative rotation, $\Theta_{xij}$, and two relative translations, $l_{yij}$ and $l_{zij}$, between the pair elements. The plane pair may be viewed as a combination of one revolute pair and two prismatic pairs, where the two prismatic pair axes intersect at and the revolute pair axis is perpendicular to the two prismatic axes. There are two moment components and one force component acting between the pair elements. The directions of the transmitted moments, $\underline{M}_{yij}$ and $\underline{M}_{zij}$, are in the direction of $y_j$ and $z_j$, respectively; and the direction of the transmitted force, $\underline{F}_{ij}$ is normal to the contact surface, i.e., in the direction of $x_i$ and $x_j$. Similarly to the Cp pair, the transmitted force is distributed on the contact surface and can not readily be represented by a concentrated force and moment.

Although the contact in the $P_L$ pair is a surface contact, we may assume three concentrated normal force, $\underline{F}_{ij1}$, $\underline{F}_{ij2}$, and $\underline{F}_{ij3}$, applied at three of the four corners of the contact plane, as shown in Figure (2-11). This is also based on the assumption of the existence of clearance between pair elements. It is reasonable to neglect the thickness of the inner plane element, and the three transmitted

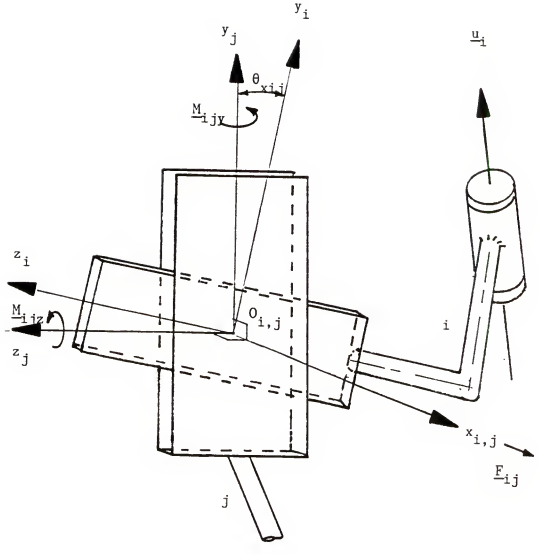


Figure 2-10 Plane ($P_L$) pair.

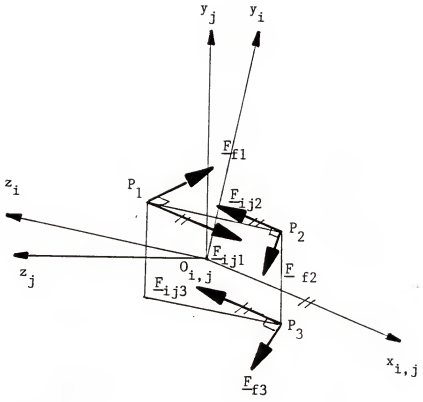


Figure 2-11 Force diagram of $P_L$ pair.

forces can be assumed acting at the same contact surface. The directions of the three transmitted forces are in the direction of the $x_j$ axis. The three normal forces will produce three sliding friction forces lying in the contact plane. The resultant force and moment may be summarized at the gravity center as

$$\underline{F}_{rij} = \sum_{k=1}^{3} (\underline{F}_{ijk} + \underline{F}_{fk}) \tag{2-14}$$

and

$$\underline{M}_{rij} = \sum_{k=1}^{3} \underline{OP}_k \times (\underline{F}_{ijk} + \underline{F}_{fk}) \tag{2-15}$$

# CHAPTER 3
# TRANSMISSION CRITERIA

The transmission criteria for spatial mechanisms can be fully evaluated by the deviation angles of each joint for force and moment transmission, the mechanical advantage and the instantaneous efficiency of the mechanism, and the accelerations for better dynamics performance. The following sections define these criteria according to the geometry of each pair mentioned in Chapter 2 and for some typical mechanisms.

## 3.1 Deviation Angles

To explore the transmission characteristics of mechanisms, not only must the force and moment transmission from the coupler to the output link to be evaluated, but also the force and moment transmission in each floating joint. Good force and moment transmission in each floating joint provides the basis of good transmission characteristics for the mechanism. Furthermore, it ensures the avoidance of separation of force-closed pair elements. It is therefore necessary to separately define deviation angles for the internal force and moment transmission of each floating joint and for the force and moment transmission at the joint connecting the coupler link and the output link for the output motion. In order to define the deviation

angles, the transmitted force and moments for the $C_p$[1] and $P_L$[2] pairs are regarded as acting at the center of gravity of the pair contact. When considering the deviation angles for force and moment transmission, the directions of the transmitted force and moment vectors are of concern.

3.1.1 Deviation angles for producing output force and moment

Figure (3-1) illustrates a coupler link and an output link, which are assumed to be connected by a joint, Q, that will transmit both force and moment. This floating joint may be either a lower or higher pair. The grounded output joint is assumed to be a cylindrical joint so there are both angular and linear output displacements. Then, the deviation angle for the force transmitted to produce the translational motion of the output link can be defined, as

$$\delta_{FT} = \cos^{-1} \frac{\underline{F}_{co} \cdot \underline{V}_{ot}}{|\underline{F}_{co}||\underline{V}_{ot}|} \qquad (3\text{-}1)$$

where $\underline{F}_{co}$ is the force exerted from the coupler link onto the output link through the floating joint Q, $\underline{V}_{ot}$ is the absolute velocity at the joint Q caused by the translational motion of the output joint. The deviation angle for the force transmitted to produce the rotational motion of the output link is defined

$$\delta_{FR} = \cos^{-1} \frac{\underline{F}_{co} \cdot \underline{V}_{or}}{|\underline{F}_{co}||\underline{V}_{or}|} \qquad (3\text{-}2)$$

---

1. Cylinder-on-plane

2. Plane-on-plane

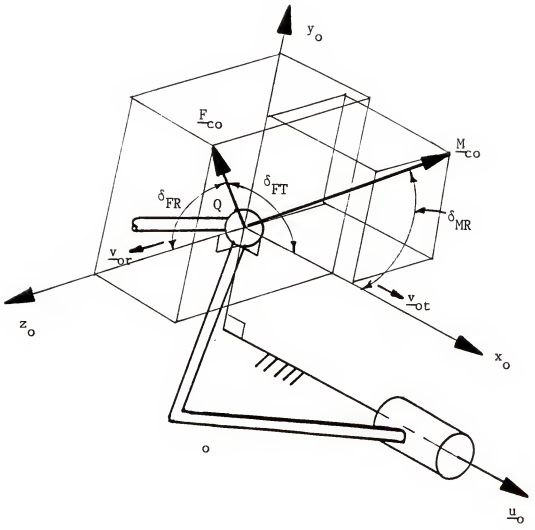


Figure 3-1 Deviation angles for producing output force and moment.

where $\underline{V}_{or}$ is the absolute velocity at the joint Q caused by the rotational motion of the output joint. The deviation angle for the moment transmitted to produce the rotational motion of the output joint is

$$\delta_{MR} = \cos^{-1} \frac{\underline{M}_{co} \cdot \underline{u}_{O}}{|\underline{M}_{co}|} \qquad (3\text{-}3)$$

where $\underline{M}_{co}$ is the moment exerted by the coupler to the output link at the joint Q; and $\underline{u}_{O}$ is the unit vector of the direction of the output joint axis, i.e., the direction of the output resistant moment vector. For the four-link mechanisms, the moment exerted by the coupler link to the output link at the Q joint may consist of two components, one is caused by the driving torque and the other one is caused by the transmitted force at the previous floating joint. Thus, for the four-link mechanisms, there will be two deviation angles to distinguish the effort of each moment. Similarly, for five-link mechanisms the exerted moment at the Q joint may consist of three components, one of them is caused by the driving torque directly and the other two components are caused by the two transmitted forces at the previous two floating joints, respectively. If the cosine of these deviation angles approaches to zero, there may be redundant freedoms generated in the output link, i.e., the transmitted force or moment does not contribute to the output force or moment. For example: $\cos\delta_{FT} = 0$ indicates there is no translation displacements at the output joint; both $\cos\delta_{FR} = 0$ and $\cos\delta_{MR} = 0$ indicate that the

rotational displacements is lost in the output joint. In practice, the absolute value of the cosine of the minimum deviation angle may be used to define the design criteria, as

$$|\cos\delta_{min}| \geq \beta \qquad (3\text{-}4)$$

where $\beta$ is a positive value less than one and away from zero.

Equations (3-1) to (3-3) apply to any pair that is adjoining the coupler link and the output link. These three deviation angles are for the use of defining how the exerted force and moment from the coupler link to the output link affect the resistant force and moment at the output joint.

### 3.1.2 Deviation angles for internal force and moment transmission

In cam mechanisms, the force transmission characteristic between the cam and the follower is defined by the pressure angle, which is the angle between the direction of motion of the follower and the normal to the cam surface at the contact between the cam and the follower (Chen, 1982). In higher pairs other than the cam pair, a similar definition can be applied.

For either the higher or the lower pair that is located in the joint connecting the coupler link and the output link, the angles between the directions of the transmitted force and moment vectors at the contact point or center of gravity of the contact line, curve, or area and

the direction-of-motion vectors serve as the deviation angles. The friction angle is also involved in determining the transmission criteria. The deviation angles measure how the coupler force and moment produce the linear and angular motion at the output joint. This effect upon the transmission characteristics between the coupler and the output link has been shown in the previous section. Besides these deviation angles, there are also deviation angles involving internal force and moment transmission needs to be considered between other mechanism joints especially when the mechanism contains a higher pair. This is due to the nature of the external-groove, cylinder and plane elements of higher pairs in transmitting force and/or moment. When the forces are transmitted through an $Sg^3$ or $Sc^4$ pair, the transmitted forces must lie on the plane that contains the contact point and perpendicular to the axis of the external grove or the cylinder element as illustrated in Chapter 2. Thus, the direction of the transmitted force is restricted, as is also the transmitted moment. If the deviation angle for the force or moment transmission approaches to 90 degrees, the higher pairs may be separated or generate relative passive freedom in the higher pair. Similarly, for the mechanisms containing a $Sp^5$, Cp, or $P_L$ pair which have an

---

3. Sphere-in-groove
4. Sphere-in-cylinder
5. Sphere-on-plane

external plane element, the transmitted force must be along the direction of the normal of the contact plane and the direction of the vector of the transmitted moment must be on the contact plane. Even in lower pairs such as the revolute (R), prismatic (P), or the cylindrical (C) joint, the direction of the transmitted force and moment may also be restricted. Therefore, it is necessary to discuss the definition of deviation angles for internal force and moment transmission according to the geometrical constraints of each pair.

3.1.2.1 $S_L$(slotted sphere) pair

The direction of the force transmitted between the pair elements of an $S_L$ pair is not restricted since it does not have any relative translational freedoms. When an $S_L$ pair is connecting the coupler link and the output link, Equation (3-1) to (3-2) for force transmission can be applied. However, the direction of the transmitted moment is restricted, which has been shown in Chapter 2. Thus, a deviation angle for the internal moment transmission needs to be defined. An R-$S_L$ dyad is shown in Figure (3-2), where the R joint is assumed to be the input joint with an input driving torque $\underline{M}_d$. The inner sphere is connected to the input link. The input moment is applied from the inner sphere to the outside sphere; the direction of the transmitted normal moment vector $\underline{M}_{23}$ must be along the direction of the $y^*$ axis, which lies in the $y_3z_3$ plane, i.e., the plane in

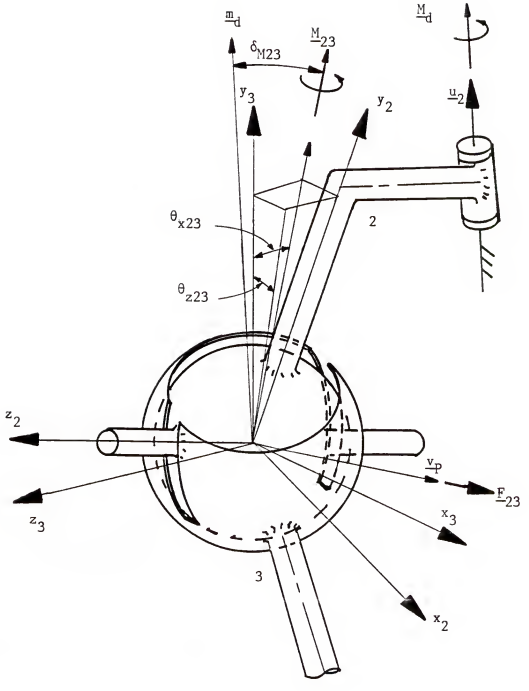


Figure 3-2 Deviation angles of an $S_L$ pair.

which the centerline of the cut slot of the external sphere lies. The deviation angle for the moment transmission may therefore be expressed:

$$\delta_{M23} = \cos^{-1}\underline{u}_2 \cdot \underline{y}^* \qquad (3\text{-}5)$$

where $\underline{u}_2$ is the unit vector of the input joint axis and $\underline{y}^*$ is the unit vector resulted by rotating $y_3$ about the $x_3$ axis by the angle of $\theta_{x23}$.

3.1.2.2 Cp and Sp pairs

For a three-link mechanism containing an Sp or Cp pair, the only floating joint is the higher pair, where the transmitted forces must be along the direction of the normal of the contacting tangential plane and the transmitted moment must lie on the contacting plane. Thus, the deviation angels for internal force and moment transmissions are explicitly defined by the transmitted normal force and moment and the directions of the output velocity which causes the translation or rotation of the output joint. However, this is assuming that the plane element is connected to the input link. If the plane element is attached to the output link, then the deviation angles are defined otherwise. Figures (3-3) and (3-4) illustrate the two different constructions of R-Cp dyads. In Figure (3-3), the cylinder element is connected to the input link denoted as link 2. Two moving coordinates are attached at the intersection of the two contact forces. The deviation angle for force transmission, $\delta_{F23}$, is the angle between the unit vector of the direction

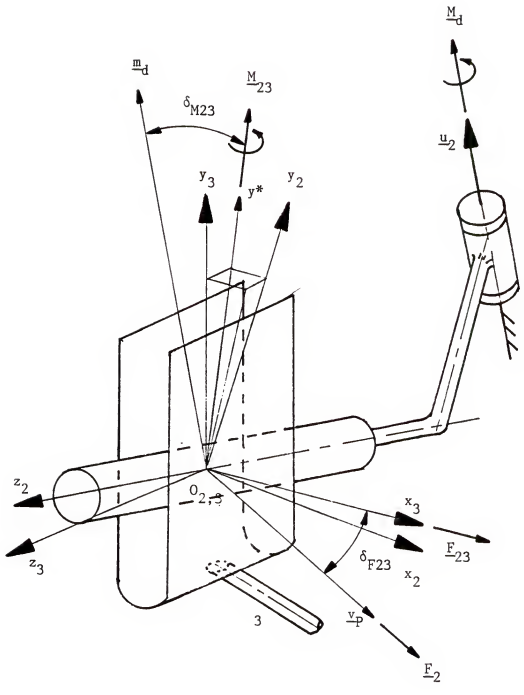


Figure 3-3 Deviation angles of a Cp pair (the cylinder element is connected to the input link).

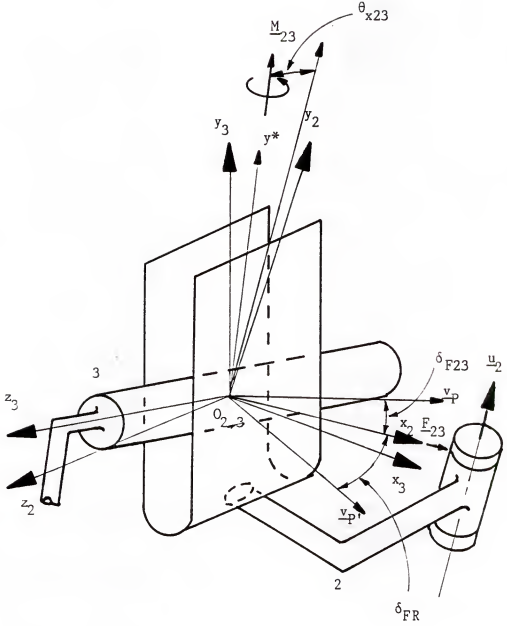


Figure 3-4 Deviation angles of a Cp pair (the plane element is connected to the input link).

of the input effort force, $\underline{F}_2$, caused by the input torque at the center of gravity of the line contact and the direction of the transmitted force normal to the plane element, $\underline{F}_{23}$. Thus, we have

$$\delta_{F23} = \cos^{-1}\underline{v}_p \cdot \underline{x}_3 \tag{3-6}$$

where $\underline{v}_p$ is the unit vector of the absolute velocity $\underline{V}_p$ and $\underline{x}_3$ is the unit normal of the contact plane in the direction from the cylinder element to the plane element. If link 3 is the output link, such as in an R-Cp-C mechanism, the deviation angle between the transmitted normal force and the absolute translational motion caused by link 3 is predetermined by the geometry of link 3, i.e., the value determined by Equations (3-1) is fixed. The other variable deviation angle for force transmission is the angle between the normal force vector and the absolute rotational output motion. It can be defined as

$$\delta_{FR} = \cos^{-1}\underline{x}_3 \cdot \underline{v}_{p'} \tag{3-7}$$

where $\underline{v}_{p'}$ is the unit vector of the absolute velocity $\underline{V}_{p'}$ starting out from the output joint. The deviation angle for internal moment transmission is defined

$$\delta_{M23} = \cos^{-1}\underline{u}_2 \cdot \underline{y}^* \tag{3-8}$$

where $\underline{u}_2$ is the unit vector of the input joint axis and $\underline{y}^*$ is the unit vector of the direction of the moment vector transmitted from the cylinder element to the plane element. If link 3 is the output link, the deviation angle between the transmitted moment vector and the absolute rotational motion(angular velocity vector) is also a variable

parameter, which may be defined by using Equation (3-3).

On the other hand, when the plane is connected to the input link, as shown in Figure (3-4), the deviation angles $\delta_{F23}$ and $\delta_{FR}$ are defined similarly to Equations (3-6) and (3-7). But, the deviation angle for producing translational output motion is variable now. It can be defined as

$$\delta_{FT} = \cos^{-1} \underline{x}_2 \cdot \underline{u}_3 \qquad (3\text{-}9)$$

where $x_2$ is the unit vector of the normal of the contact plane and $\underline{u}_3$ is the unit vector of the output joint axis. The deviation angles for moment transmission are the same as the in previous case.

It can be observed from Figure (3-3) when $\delta_{F23}$ approaches to 90 degrees, the relative sliding between the cylinder and the plane will approach a maximum. This is the so called indeterminate slipping, which will cause the uncertainty configuration as defined by Hunt (1979). Also, when $\delta_{M23}$ goes to 90 degrees, there will be a rotational redundant freedom between the two pair elements. Similar definition applies to the four, or five-link mechanisms that have a higher pair with a plane element.

For the Sp pair, as shown in Figure (3-5), the definition for the internal force transmission is similar to that for the Cp pair, except that the Sp pair does not transmit moment.

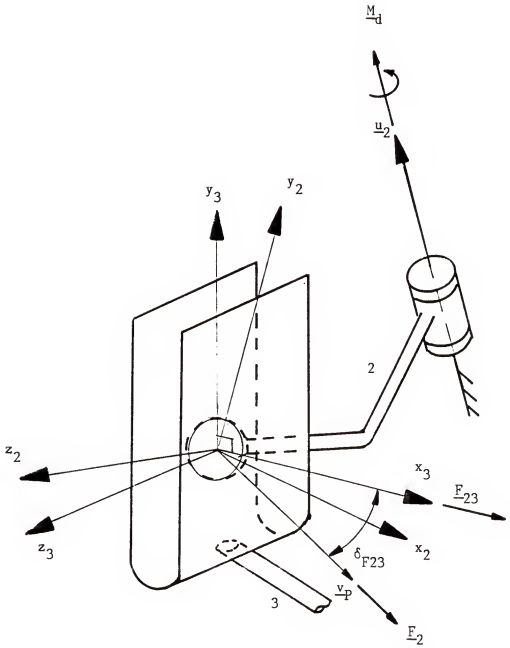


Figure 3-5 Deviation angle of an Sp pair.

3.1.2.3 $P_L$ pair

For the $P_L$ pair, the deviation angle for the internal force transmission is a variable parameter since the positions where the forces applied are variable. Figure (3-6) shows an R-$P_L$ dyad, where the R joint is an input joint with an input moment $\underline{M}_d$. The deviation angle $\delta_{F23}$ is the angle between the input effort force $\underline{F}_2$ and the transmitted force $\underline{F}_{23}$. The transmitted moment vector must lie on the contact surface. As shown in Chapter 2, the moment has two components on the $y_j$ and $z_j$ axes, respectively. The direction of the transmitted moment vector $\underline{M}_{23}$ is the projection of the driving moment vector $\underline{M}_d$ on the contact surface. Thus, the deviation angle $\delta_{M23}$ for the moment transmission is defined as the angle between the vectors of the driving torque and the transmitted moment. $\delta_{M23}$ is a fixed value here.

3.1.2.4 Sg and Sc pairs

The deviation angles of force transmission for the Sg and Sc pairs are defined similarly as those for the Sp and Cp pairs, except that the direction of the transmitted force is now located on the plane perpendicular to the joint axis and passes through the center of the sphere and the contact point. Figure (3-7) illustrates an R-Sc dyad where the sphere is connected to the link 2 with an R input joint and the cylinder element is connected to link 3. Two coordinates are located at the sphere center as described in

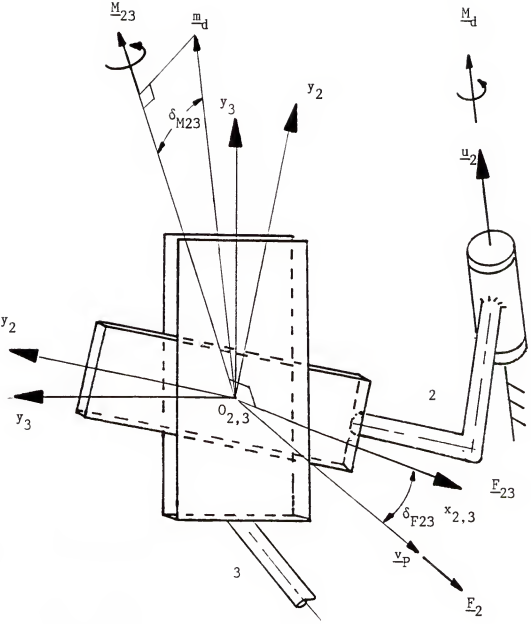


Figure 3-6 Deviation angles of a $P_L$ pair.

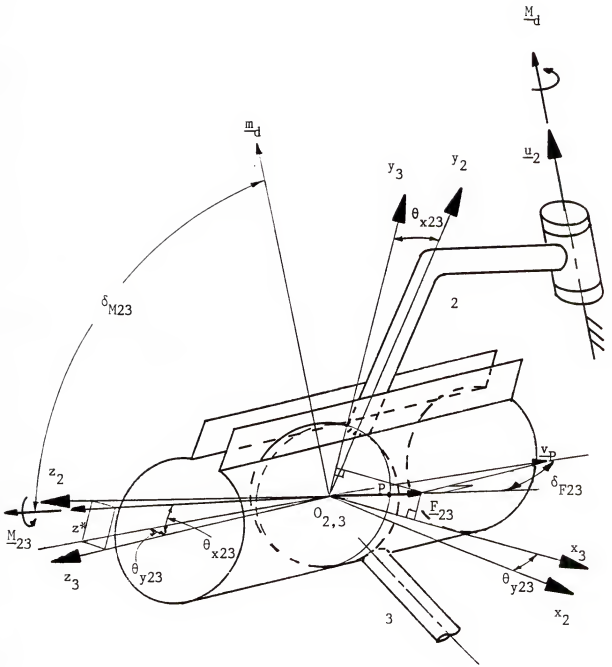


Figure 3-7 Deviation angles of a Sc pair.

Chapter 2. The deviation angle for the force transmission is defined, as

$$\delta_{F23} = \cos^{-1}\underline{v}_p \cdot \underline{x}^* \tag{3-10}$$

where $\underline{v}_p$ is the direction of the input effort force, i.e., the unit vector of the absolute velocity of the contact point; and $\underline{x}^*$ is the unit vector of the transmitted force, which is the projection of $\underline{v}_p$ on the plane passing through the sphere center and normal to the axis of the cylinder. The deviation angle for the moment transmission is

$$\delta_{M23} = \cos^{-1}\underline{u}_2 \cdot \underline{z}^* \tag{3-11}$$

where $\underline{u}_2$ is the direction of the unit vector of the driving torque, and $\underline{z}^*$ is the direction of the transmitted moment vector, which lies on the $y_3$ and $z_3$ plane. Similar definition applies to the mechanisms containing an Sg pair except there is no moment transmission.

3.1.2.5 R, P, and C pairs

The revolute and prismatic pairs do not have moment and force transmitted along the direction of the joint axis, respectively. There is neither moment nor force transmitted along the joint axis of a cylindric pair. These restraints of the force and moment for the lower pairs also affect the transmission characteristics of the mechanisms since the force or moment component in the direction of the joint axis vanishes. Thus, the deviation angles for the internal force and moment transmission of lower pairs should also be of concern. To define the deviation angels for these three

lower pairs, an R-C dyad is shown in Figure (3-8), where a force and a moment are exerted at the C joint, which are induced by the driving torque at the R joint. The joint axes of the R and C joint are denoted as $\underline{u}_i$ and $\underline{u}_j$, respectively. The transmitted force and moment may be expressed

$$\underline{F}_{ij} = (\underline{u}_j \times \underline{F}_i) \times \underline{u}_j \tag{3-12}$$

and

$$\underline{M}_{ij} = (\underline{u}_j \times \underline{M}_d) \times \underline{u}_j \tag{3-13}$$

respectively. $\underline{F}_i$ is the effort force caused by the input torque at the R joint applied to the j-th link through the C joint, which is in the direction of the absolute velocity of the i-th link at the C joint, $\underline{v}_i$; and $\underline{M}_d$ is the driving torque vector, which is in the direction of the joint axis, $\underline{u}_i$. Then, the cosine value of the deviation angles for internal force and moment transmission of the C joint can be expressed

$$\cos\delta_{Fij} = \frac{\underline{F}_i \cdot \underline{F}_{ij}}{|\underline{F}_i||\underline{F}_{ij}|} \tag{3-14}$$

and

$$\cos\delta_{Mij} = \frac{\underline{M}_i \cdot \underline{M}_{ij}}{|\underline{M}_i||\underline{M}_{ij}|} \tag{3-15}$$

The two values of Equations (3-14) and (3-15) are equal to the $\sin\sigma_{Fij}$ and $\sin\sigma_{Mij}$, respectively, where

$$\sigma_{Fij} = \cos^{-1} \frac{\underline{F}_i \cdot \underline{u}_j}{|\underline{F}_i|} \tag{3-16}$$

and

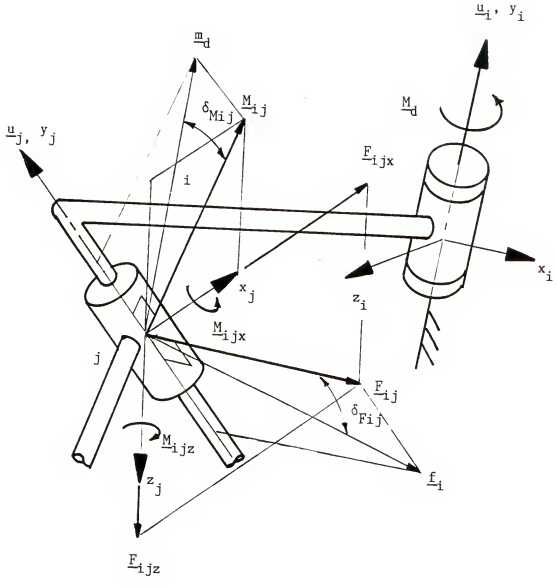


Figure 3-8 Deviation angles of a lower pair.

$$\sigma_{Mij} = \cos^{-1} \frac{\underline{M}_i \cdot \underline{u}_j}{|\underline{M}_i|} \qquad (3\text{-}17)$$

Equations (3-16) and (3-17) also apply to the P or R joint in place of the C joint.

## 3.2 Force and Moment Transmissivities

In the previous sections, the deviation angles for producing output force and moment and for the internal force and moment transmission of both higher pairs and lower pairs were introduced. Using these deviation angles in practice, the force and moment transmissivities are now to be defined. This will expand the usefulness of the deviation angles. The force and moment transmissivities are defined as the effectiveness of how the input effort force and input moment affect the output resistance force and moment. There are four force and moment transmissivities: force-to-force, force-to-torque, torque-to-torque, and force torque-to-torque. The force-to-force transmissivity is defined as how the driving force of an input prismatic joint or input effort force caused by an input revolute joint at the joint connecting the input link and the coupler link affects the translational motion of the output link, or in other words, how it produces the output force. The force-to-torque transmissivity is defined as how the driving force or the input effort force affects the rotational motion of the output link or how it produces the output torque. The torque-to-torque transmissivity is how the driving torque intro-

duced at an input revolute joint or the input effort torque caused by the driving force at an input prismatic joint or at the joint connecting the input link and the coupler link affects the rotational motion of the output link or produces the output torque. For four-or-more-link mechanisms, the exerted force at a floating link will produce a moment at a successive floating joint. The force-torque-to-torque transmissivity is defined as how this moment produces the output torque. These transmissivities are determined by the geometry of the mechanism. The following sections will discuss the usage of these transmissivities according to the construction of the mechanisms.

3.2.1 R-Sp-R mechanism

Figure (3-9) shows an R-Sp-R mechanism where the inner sphere is connected to the input link. The contact point is denoted as P; $\underline{P}$ and $\underline{P}'$ are the position vectors from the input joint axis and the output joint axis to the contact point, respectively; a moving coordinate system is attached to the contact point, which consists of the orthonormal unit vectors $\underline{a}$, $\underline{b}$, and $\underline{c}$, where $\underline{a}$ is the normal of the plane element. The force-to-torque transmissivity for mechanisms having such geometry can be defined, as

$$\tau_{FM} = |\cos\delta_{F23}\cos\delta_{FR}| \qquad (3\text{-}18)$$

where $\delta_{F23}$ is defined similarly to Equation (3-6), i.e., the deviation angle between the input effort force, $\underline{F}_2$, and the transmitted normal force, $\underline{F}_{23}$; and $\delta_{FR}$ is defined similarly

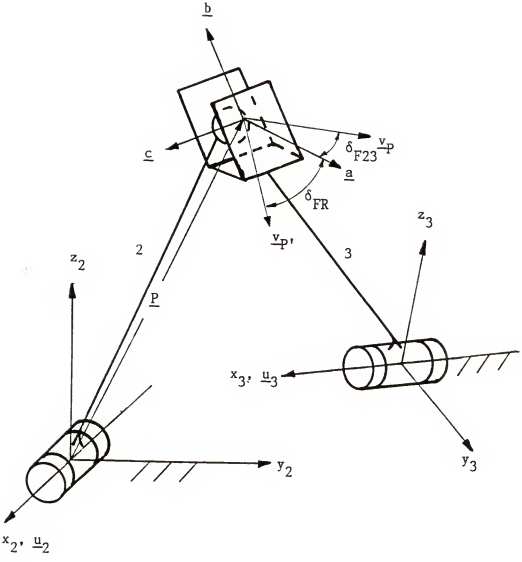


Figure 3-9 Transmissivities of an R-Sp-R mechanism.

to Equation (3-2), i.e, the angle between the direction of the transmitted normal force, $\underline{F}_{23}$, and the direction of the output joint resistant force(or the absolute velocity of the contact point as a point of the output link). The deviation angles of Equation (3-18) can be expressed in terms of the geometrical parameters, as

$$\cos\delta_{F23} = \underline{v}_p \cdot \underline{a} \tag{3-19}$$

and

$$\cos\delta_{FR} = \underline{a} \cdot \underline{v}_{p'} \tag{3-20}$$

where $\underline{v}_p$ and $\underline{v}_{p'}$ are the unit vectors of the absolute velocities of the contace point as a point of the input or output link, respectively; $\underline{a}$ is the unit vector of the normal of the plane element.

### 3.2.2 R-Cp-C mechanism

For the mechanisms having geometry as the R-Cp-C mechanisms shown in Figure (3-10), there are two force transmissivities, since the output joint has both translational and rotational motions. There is also one moment transmissivity. The center of gravity of the contact line is denoted as P and the normal of the plane element is denoted as $\underline{a}$; $\underline{b}^*$ is the unit vector on the contact plane perpendicular to $\underline{a}$; the axis of the cylinder element is $\underline{c}^*$. The force-to-torque transmissivity to produce rotational motion of the output link at the output joint is defined similarly to Equation (3-18). The additional force-to-force transmissivity is defined as

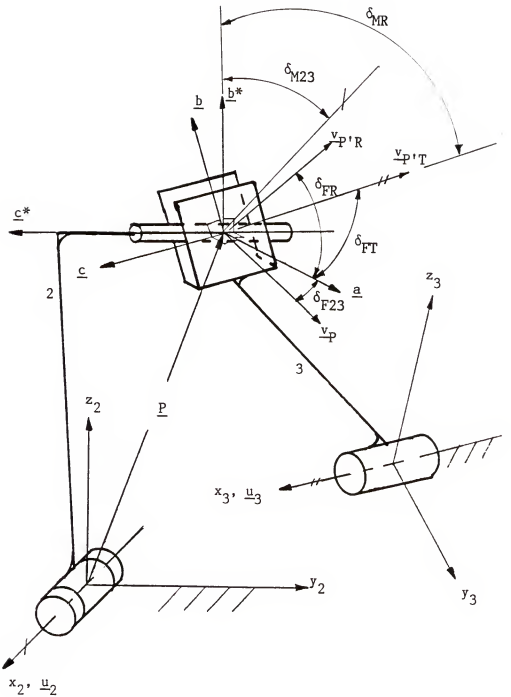


Figure 3-10 Transmissivities of an R-Cp-C mechanism.

$$f_{FF} = |\cos\delta_{F23}\cos\delta_{FT}| \tag{3-21}$$

where $\delta_{F23}$ is defined similarly to Equation (3-19); and $\delta_{FT}$ is defined similarly to Equation (3-1) and can be determined by:

$$\cos\delta_{FT} = \underline{a} \cdot \underline{u}_3 \tag{3-22}$$

where $\underline{u}_3$ is the unit vector of the output joint axis. Also, there is a torque-to-torque transmissivity for the input moment to produce the rotational motion of the output link at the output joint, which can be expressed

$$f_{MM} = |\cos\delta_{M23}\cos\delta_{MR}| \tag{3-23}$$

where $\delta_{M23}$ is defined by Equation (3-8), which is the angle between the driving torque vector and the transmitted normal moment vector; $\delta_{MR}$ is defined similarly to Equation (3-3), which is the angle between the transmitted normal moment vector and the output resistant moment vector. The cosine of deviation angles of Equation (3-23) can be expressed by the geometrical parameters disregarding the sign, as

$$\cos\delta_{M23} = \underline{u}_2 \cdot \underline{b}^* \tag{3-24}$$

and

$$\cos\delta_{MR} = \underline{b}^* \cdot \underline{u}_3 \tag{3-25}$$

where $\underline{u}_2$ and $\underline{u}_3$ are the unit vectors of the input and output joint axes, respectively. Unlike the deviation angles for the force transmission, the values of $\cos\delta_{M23}$ and $\cos\delta_{MR}$ are variable parameters, since the direction of $\underline{b}^*$ is determined both the axis of the cylinder element and the normal of the plane element, i.e., $\underline{b}^* = \underline{a} \times \underline{c}^*$.

3.2.3 R-$P_L$-C-R mechanism

For four or more-link mechanisms, the deviation angles at all floating joints are of concern. Consider an R-$P_L$-C-R mechanism as shown in Figure (3-11). An input effort force, $\underline{F}_i$, and moment, $\underline{M}_d$, are caused by the input driving torque at the $P_L$ joint. We may assume the transmitted normal force $\underline{F}_{23}$ is in the same direction as the normal of the plane elemnt of the $P_L$ pair, $\underline{a}$, since the sign of the cosine values are not concerned. The force-to-torque transmissivity is defined

$$\tau_{FR} = |\cos\delta_{F23}\cos\delta_{F34}\cos\delta_{FR}| \tag{3-26}$$

where $\delta_{F23}$ is the angle between the input effort force and the normal of the plane elements; $\delta_{F34}$ is the angle between the coupler force and the transmitted force, $\underline{F}_{34}$, at the floating C joint. The transmitted force $\underline{F}_{34}$ can be expressed, as

$$\underline{F}_{34} = (\underline{u}_3 \times \underline{F}_{23}) \times \underline{u}_3 \tag{3-27}$$

$\delta_{F34}$ is the angle between the normal of the plane element and the unit vector of the direction of $\underline{F}_{34}$, whose consine value is the same as the sine value of the angle contained by $\underline{F}_{23}$ and $\underline{u}_3$. Thus, we may write

$$\cos\delta_{F34} = \sin(\cos^{-1}\underline{a} \cdot \underline{u}_3) \tag{3-28}$$

It can be observed that $\delta_{F34}$ is a fixed angle since the plane element is attached to joint 3. The third deviation angle $\delta_{FR}$ is defined similarly to Equation (3-2), i.e., the angle between $\underline{F}_{34}$ and the direction of the resistant force for the rotation of the output link, which can be expressed

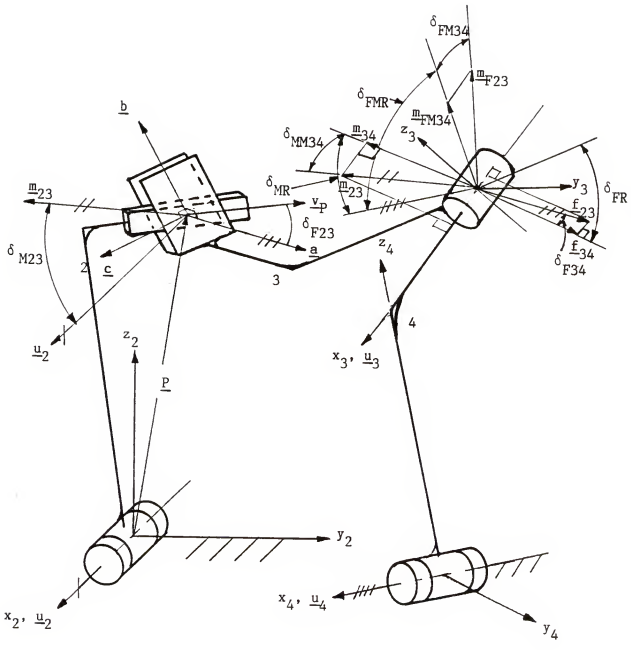


Figure 3-11 Transmissivities of an R-$P_L$-C-R mechanism.

$$\cos\delta_{FR} = \underline{f}_{34} \cdot \underline{v}_{3'}$$

$$= \frac{(\underline{u}_3 \times \underline{a}) \times \underline{u}_3 \cdot \underline{v}_{3'}}{|(\underline{u}_3 \times \underline{a}) \times \underline{u}_3|} \tag{3-29}$$

where $\underline{v}_{3'}$ is the unit vector of the direction of the absolute velocity of the center of the floating C joint as a point of the output link. The torque-to-torque transmissivity is

$$f_{MM} = |\cos\delta_{M23}\cos\delta_{MM34}\cos\delta_{MR}| \tag{3-30}$$

The fixed angle $\delta_{M23}$ is the deviation angle of the internal moment transmission of the $P_L$ joint. It is defined by

$$\cos\delta_{M23} = \underline{u}_2 \cdot \underline{m}_{23} \tag{3-31}$$

where

$$\underline{m}_{23} = \frac{(\underline{a} \times \underline{u}_2) \times \underline{a}}{|(\underline{a} \times \underline{u}_2) \times \underline{a}|}$$

is the unit vector of the direction of the transmitted moment vector $\underline{M}_{23}$. Equation (3-31) can be also be written, as

$$\cos\delta_{M23} = \sin(\cos^{-1}\underline{u}_2 \cdot \underline{a}) \tag{3-32}$$

The angle $\delta_{MM34}$ is the deviation angle for the sequential moment transmission at the floating R joint, i.e., the angle between the vectors of $\underline{M}_{23}$ and $\underline{M}_{34}$. The unit vector of the direction of the transmitted moment through joint 3 can be expressed as

$$\underline{m}_{34} = \frac{(\underline{u}_3 \times \underline{m}_{23}) \times \underline{u}_3}{|(\underline{u}_3 \times \underline{m}_{23}) \times \underline{u}_3|} \tag{3-33}$$

Then, $\cos\delta_{M34}$ can be written

$$\cos\delta_{M34} = \underline{m}_{23} \cdot \underline{m}_{34}$$

$$= \sin(\cos^{-1}\underline{m}_{23} \cdot \underline{u}_3) \tag{3-34}$$

The third angle $\delta_{MR}$ is defined as the angle between the transmitted moment vector at the floating C joint and the output resistant torque vector, i.e.,

$$\cos\delta_{MR} = \frac{(\underline{u}_3 \times \underline{m}_{23}) \times \underline{u}_3 \cdot \underline{u}_4}{|(\underline{u}_3 \times \underline{m}_{23}) \times \underline{u}_3|} \tag{3-35}$$

The transmitted normal force at the $P_L$ joint will produce a moment about the floating C joint. Then, the force torque-to-torque transmissivity for this moment to produce the output torque is

$$f_{FMM} = |\cos\delta_{F23}\cos\delta_{FM34}\cos\delta_{FMR}| \tag{3-36}$$

The angle of $\delta_{F23}$ is defined similarly to Equation (3-19). The direction of the force-produced moment can be written

$$\underline{m}_{F23} = \underline{P}_3 \times \underline{a} \;/\; |\underline{P}_3 \times \underline{a}| \tag{3-37}$$

where $\underline{P}_3$ is the distance vector from joint 3 to the center of gravity of the contact surface of the $P_L$ pair. The unit vector of the direction of the transmitted moment at the C joint is

$$\begin{aligned} \underline{m}_{FM34} &= (\underline{u}_3 \times \underline{m}_{F23}) \times \underline{u}_3 \;/\; |(\underline{u}_3 \times \underline{m}_{F23}) \times \underline{u}_3| \\ &= \frac{[\underline{u}_3 \times (\underline{P}_3 \times \underline{a})] \times \underline{u}_3}{|\underline{P}_3 \times \underline{a}||[\underline{u}_3 \times (\underline{P}_3 \times \underline{a})] \times \underline{u}_3|} \end{aligned} \tag{3-38}$$

Thus, $\cos\delta_{FM34}$ can be written, as

$$\begin{aligned} \cos\delta_{FM34} &= \underline{m}_{F23} \cdot \underline{m}_{FM34} \\ &= \sin(\cos^{-1}(\underline{u}_3 \cdot \underline{P}_3 \times \underline{a}) \end{aligned} \tag{3-39}$$

The angle $\delta_{FMR}$ is the angle between the transmitted moment and the output resistance torque. It can be defined as

$$\cos\delta_{FMR} = \underline{m}_{FM34} \cdot \underline{u}_4$$

$$= \frac{[\underline{u}_3 \times (\underline{P}_3 \times \underline{a})] \times \underline{u}_3 \cdot \underline{u}_4}{|\underline{P}_3 \times \underline{a}||[\underline{u}_3 \times (\underline{P}_3 \times \underline{a})] \times \underline{u}_3|} \qquad (3\text{-}40)$$

## 3.3 Frictional Effects

In Figure (3-12), a sphere and a plane are in contact at point P, where the sphere is connected to the input link which has revolute joint and the plane is connected to the output link which has the other revolute joint. The absolute velocity at the contact point P as a point of the input link is $\underline{V}_p$ and as a point of the output link, it is $\underline{V}_{p'}$. Then, the relative velocity is denoted by $\underline{V}_{pp'}$ where $\underline{V}_{pp'} = \underline{V}_p - \underline{V}_{p'}$. The sliding relative velocity, i.e., the projected component of the relative velocity on the contact plane is given as

$$\underline{V}_s = \underline{V}_{pp'} - (\underline{V}_{pp'} \cdot \underline{a})\underline{a} \qquad (3\text{-}41)$$

where $\underline{a}$ is the unit vector of the normal of the contact plane. Now, if there is an input torque applied at the input link at the input revolute, an input effort force $\underline{F}_2$, which is in the direction of $\underline{V}_p$, acts on the contact point from the sphere to the plane. The input effort force will cause a normal force $\underline{F}_n$ applied from the sphere to the plane through the contact point. The deviation angle in this case then is defined as the angle between $\underline{F}_2$ and $\underline{F}_n$. If the roles of the sphere and the plane are reversed, the deviation angle needs to be defined differently, as discussed in the previous sections. Also, there is another force component of the input effort force projected on the contact

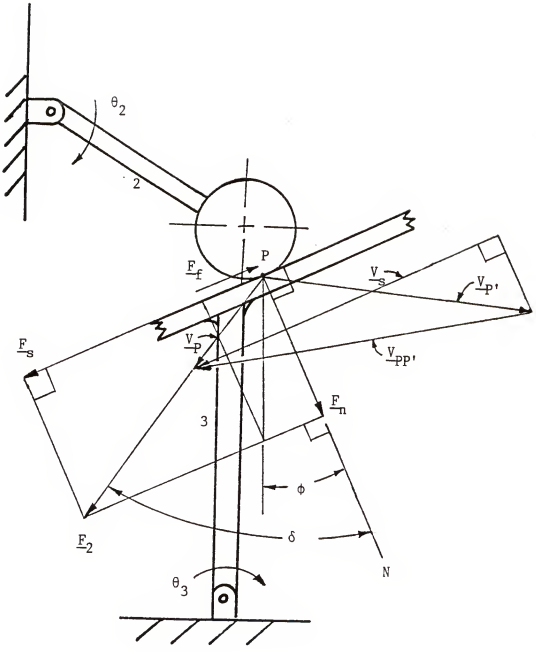


Figure 3-12 Frictional effects in plane motion.

plane, which is denoted as $\underline{F}_s$. This is the force causing the relative movement between the sphere and the plane on the contact plane. Now, if there is friction between the sphere and the plane, a friction force, $\underline{F}_f$, will be induced. The direction of the friction force is opposite to the direction of the relative sliding velocity, $\underline{V}_s$, as shown in Figure (3-12). The resultant reaction force, $\underline{F}_r$, consists of the resistant normal force and the friction force. It can be observed that the friction force must be overcome by the sliding force in order to keep the mechanism in motion. This can be easily followed by first considering the plane motion between the sphere and the plane, as shown in Figure (3-12), where the direction of the sliding force $\underline{F}_s$ and the direction of the friction force $\underline{F}_f$ are collinear but opposite in sense. If the deviation angle $\delta$ is smaller than the friction angle $\varphi$, then the mechanism will not move at all. Thus, the condition that the sliding force must overcome the friction force should be satisfied if a continuous motion is desired. It is also observed from Figure (3-12) that a very small deviation angle may not be desired although the smaller is the deviation angle, the better is the transmissibility of the mechanisms.

To establish the general condition, considering Figure (3-13), the sphere and the plane are now assumed moving in the space. The x coordinate is assumed to be in the direction of the friction force and the y coordinate is in the direction of the normal force, as shown in the figure. The

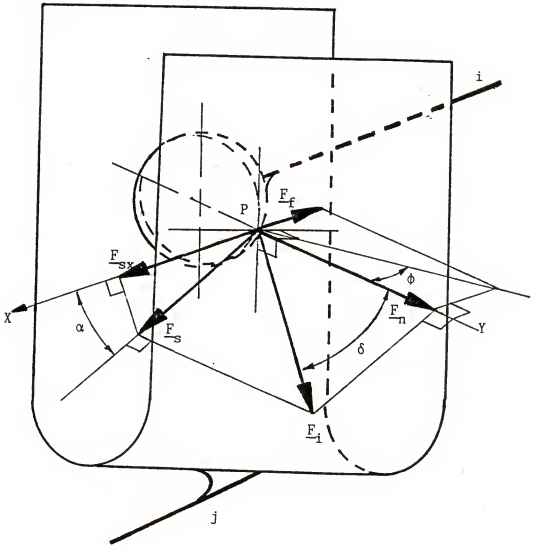


Figure 3-13 Friction effects in spatial motion.

absolute magnitude of the component of the sliding force in the direction of the relative motion may be expressed in terms of the input effort force, as

$$|\underline{F}_{sx}| = |\underline{F}_i||\sin\delta\cos\alpha| \tag{3-42}$$

where $\alpha$ is the angle between the sliding force $\underline{F}_{sx}$ and the direction of the relative sliding velocity $\underline{V}_s$. The magnitude of the friction force may also be written

$$|\underline{F}_f| = \mu|\underline{F}_i||\cos\delta| \tag{3-43}$$

where $\mu$ is the static friction coefficient. Since we must have the condition of $|\underline{F}_{sx}| \geq |\underline{F}_f|$ to satisfy for the requirement for continuous motion of the mechanism, the following expression is given

$$|\cos\alpha| > \mu|\cot\delta| \tag{3-44}$$

In the other words, the above equation may also be employed to restrict the allowable friction coefficient between the two elements in contact, i.e.,

$$\mu < |\cos\alpha\tan\delta| \tag{3-45}$$

## 3.4 Mechanical Advantage and Instantaneous Efficiency

The friction forces will cause loss of energy, which can be observed directly from the virtual work equation. For example, considering the mechanisms containing a one-point contact higher pair, the virtual work equation for these mechanisms can be expressed

$$\underline{M}_d \cdot \underline{\Omega}_d + \underline{F}_d \cdot \underline{V}_d + \underline{F}_f \cdot \underline{V}_s + \underline{M}_r \cdot \underline{\Omega}_r + \underline{F}_r \cdot \underline{V}_r = 0 \tag{3-46}$$

where the subscript d and r denotes the driving link and the

resistant link, respectively; $\underline{M}$ and $\underline{F}$ denotes the torque and force, respectively; $\underline{F}_f$ is the sliding friction force; $\underline{V}_s$ is the relative sliding velocity at the contact point. The first two terms of Equation (3-46) are the input power (I.P.), the last two terms is the output power (O.P.), and the power loss (P.L.) is then given by the third term. Since the direction of the friction force is opposite to the direction of the relative sliding velocity, the power loss can be simplified as

$$\text{P.L.} = -|\underline{F}_f||\underline{V}_s| \tag{3-47}$$

Observing from equation (3-47), the power loss is proportional to the magnitude of the normal force and the magnitude of the relative sliding velocity. The power ratio may be defined as the ratio of the output power to the input power, as

$$\text{P.R.} = \left|\frac{\text{O.P.}}{\text{I.P.}}\right| = 1 - \left|\frac{\text{P.L.}}{\text{I.P.}}\right| \tag{3-48}$$

The power ratio is actually the instantaneous efficiency (Alizade and Sandor, 1985). The instantaneous efficiency may be defined as

$$\text{I.E.} = \frac{|\underline{M}_d{}^*|}{|\underline{M}_d|} = \text{P.R.} \tag{3-49}$$

where $|\underline{M}_d{}^*|$ is the absolute value of the input moment required without friction in the higher pair to overcome the output resistance, and $|\underline{M}_d|$ is the absolute value of the input moment required in the higher pair when there is friction.

The mechanical advantage (M.A.) is one of the criteria for the ability of a mechanism to transmit torque or force and is defined as the ratio of the magnitudes of force out over force in (Erdman & Sandor, 1984, pp. 110 - 113):

$$M.A. = \frac{F_{out}}{F_{in}} \tag{3-50}$$

The mechanical advantage may also be investigated on the information of input and output displacements (Midha, etl., 1984). To investigate the mechanical advantage, we may assume an input and an output force applied at a unit normal distance from the input and output link pivots, respectively. If the output joint is a cylindric joint, the force output has two components, one for the translational and one for the rotational motion, respectively. Then, we may define two mechanical advantages for each of the force output components, i.e.,

$$M.A._t = \frac{F_{out}{}^t}{F_{in}} \tag{3-51}$$

and

$$M.A._r = \frac{F_{out}{}^r}{F_{in}} \tag{3-52}$$

where $F_{out}{}^t$ and $F_{out}{}^r$ are the two force components for the translational and rotational motion, respectively. These two mechanical advantages must satisfy the relationship of

$$M.A. = (M.A._t{}^2 + M.A._r{}^2)^{1/2} \tag{3-53}$$

## 3.5 Acceleration Ratio

The output acceleration ratio can be defined as the ratio of the maximum and minimum accelerations of the output link. If the output link is in oscillation, then the maximum and minimum accelerations happen when the output link is at the limit positions. Thus, we have

$$\alpha = |\varphi_{max} / \varphi_{min}| \tag{3-54}$$

where $\varphi_{max}$ and $\varphi_{min}$ are the maximum and minimum output angular or linear acceleration. By minimizing the quantity $|1 - \alpha|$, the acceleration can be forced to be symmetrically distributed in the positive and negative directions. To minimize the maximum magnitude of the acceleration, another criterion is needed. If the input joint is a revolute joint and the input link has complete rotation and constant angular velocity, such other criterion can be defined as the ratio between the maximum magnitude of the output acceleration and the square of the input angular velocity. Thus,

$$\alpha^* = |\varphi|_{max} / \theta^2 \tag{3-55}$$

When the constant input angular velocity is unity, the ratio is simply the maximum output acceleration itself. The other way to minimize the maximum magnitude of the maximum acceleration is to minimize the deviation between the maximum and minimum accelerations. Thus, we may define the acceleration deviation, as

$$\sigma = |(\varphi_{max} - \varphi_{min})/\varphi_{max}| \tag{3-56}$$

Equations (3-54) and (3-56) may be also applied to output linear acceleration.

# CHAPTER 4
# STATIC FORCE AND TORQUE ANALYSIS

The static force and torque analysis is carried out by vector methods for three numerical examples. The first one is an R-Sp-R mechanism, which has one contact force in the model of the Sp pair and is statically determinate. The second one is an R-Cp-C mechanism, which has two contact forces in the model of the Cp pair. The R-Cp-C mechanism is a statically indeterminate mechanism, therefore, the output force and moment are specified instead of the input moment. The last one is an R-$P_L$-C-R mechanism, which has three contact forces in the model of the $P_L$ pair and is also statically determinate. The static force and torque analysis for other mechanisms can be followed in a similar manner.

## 4.1 R-Sp-R Mechanisms(Figure (4-1))

In the case of statically determinate three-link mechanisms such as the R-Sp-R mechanism with one point contact between the higher pair elements, which is shown in Figure (4-1), the moment equilibrium equation for the input link can be written as

$$(\underline{M}_d + \underline{P}_2 \times \underline{R}_{32}) \cdot \underline{u}_2 = 0 \qquad (4\text{-}1)$$

where $\underline{M}_d$ is the driving torque; $\underline{R}_{32}$ is the reaction force at the contact point; $\underline{P}_2$ is the vector from the input R joint

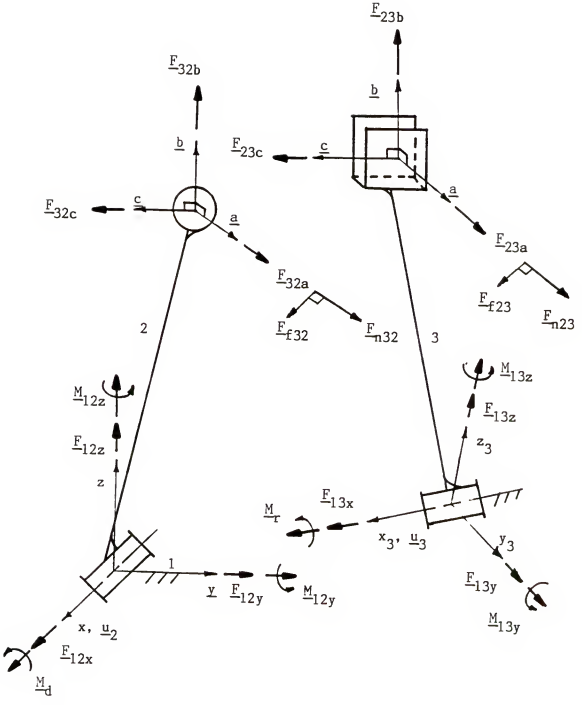


Figure 4-1 Free-body diagram of R-Sp-R mechanism.

to the contact point; and $\underline{u}_2$ is the unit vector of the input R joint axis. The reaction force consists of the transmitted normal force, $\underline{F}_{n32}$, and the sliding friction force, $\underline{F}_{f32}$. This can be expressed, as

$$\underline{R}_{32} = \underline{F}_{n32} + \underline{F}_{f32}$$
$$= |\underline{F}_{n32}|(\text{sign}^1(\underline{f}_{n32})\underline{f}_{n32} + \mu\underline{f}_{f32}) \qquad (4\text{-}2)$$

where

$$\underline{f}_{n32} = -\underline{a}$$
$$\underline{f}_{f32} = -\underline{v}_s$$
$$\underline{v}_s = \underline{V}_s/|\underline{V}_s|$$
$$\underline{V}_s = \underline{V}_{p'p} - (\underline{V}_{p'p} \cdot \underline{a})\underline{a}$$
$$\underline{V}_{p'p} = \underline{V}_{p'} - \underline{V}_p$$
$$\underline{V}_{p'} = \underline{\Omega}_3 \times \underline{P}_3$$
$$\underline{V}_p = \underline{\Omega}_2 \times \underline{P}_2$$

The magnitude of the normal force is given by substituting Equation (4-2) into Equation (4-1), i.e.,

$$F_n = \frac{-M_d}{\underline{P}_2 \times (\text{sign}(\underline{f}_{n32})\underline{f}_{n32} + \mu\underline{f}_{f32}) \cdot \underline{u}_2} \qquad (4\text{-}3)$$

or

$$R = \frac{-M_d}{\underline{P}_2 \times \underline{r}_{32} \cdot \underline{u}_2} \qquad (4\text{-}4)$$

where $\underline{r}_{32} = \text{sign}(\underline{f}_{n32})\cos\varphi\underline{f}_{n32} + \sin\varphi\underline{f}_{f32}$ and R is the mag-

---

1. The direction of the normal force applied from the cylinder to the plane is initially defined the same as the normal vector of the contact plane, $\underline{f}_{n23} = \underline{a}$, i.e, $\underline{f}_{n32} = -\underline{a}$. Then, it is verified by the sign of the absolute magnitude of the normal force, $|\underline{F}_n|$. If the resulting $|\underline{F}_n|$ is positive then it agrees with the assumption. A negative $|\underline{F}_n|$ means that $\underline{f}_{n32} = \underline{a}$.

nitude of the reaction force, $\underline{R}_{32}$. The above equation is then employed to check the sign of $\underline{f}_{n32}$. The moment equilibrium equation for the output link can be written

$$(\underline{M}_r + \underline{P}_3 \times \underline{R}_{23}) \cdot \underline{u}_3 = 0 \tag{4-5}$$

where $\underline{M}_r$ is the output resistant torque, $\underline{P}_3$ is the distance vector from the output joint to the contact point. Thus, the resistant torque is given by substituting Equation (4-4) into the above equation, as

$$M_r = \frac{-M_d(\underline{P}_3 \times \underline{r}_{32} \cdot \underline{u}_3)}{\underline{P}_2 \times \underline{r}_{32} \cdot \underline{u}_2} \tag{4-6}$$

To derive the instantaneous efficiency to show the frictional effects explicitly, we may write the virtual work equation for the mechanism, as

$$\underline{M}_d \cdot \underline{\Omega}_2 + \underline{F}_f \cdot \underline{V}_s + \underline{M}_r \cdot \underline{\Omega}_3 = 0 \tag{4-7}$$

$\underline{F}_f$ is the friction force where $\underline{F}_f = -\mu|\underline{F}_n|\underline{v}_s$. The power loss is

$$\begin{aligned} \text{P.L.} &= \underline{F}_f \cdot \underline{V}_s \\ &= -\sin\varphi|\underline{R}||\underline{V}_s| \end{aligned} \tag{4-8}$$

Now, the instantaneous efficiency can be written in terms of the power loss and the input power, as

$$\text{I.E.} = 1 - \left| \frac{\text{P.L.}}{\text{I.P.}} \right| \tag{4-9}$$

where

$$\text{I.P.} = \underline{M}_d \cdot \underline{\Omega}_2$$

Substituting Equation (4-8) into the above equation gives the instantaneous efficiency in terms of the geometrical parameters, as

$$\text{I.E.} = \frac{\sin\varphi|\underline{V}_s|}{\underline{P}_2 \times \underline{r}_{32} \cdot \underline{\Omega}_2} \tag{4-10}$$

To investigate the mechanical advantage, we may assume a force input and a force output applied at the input and output link, respectively. The directions of the force input and force output are assumed to be the same as the directions of the absolute velocities of the contact point P as a point of the input link and the output link, respectively. Then, the force input and force output may be written in terms of the magnitudes of the input torque and resistant torque, respectively, as

$$|\underline{F}_i| = \frac{|\underline{M}_d|}{|\underline{P}_i|} \tag{4-11}$$

and

$$|\underline{F}_o| = \frac{|\underline{M}_r|}{|\underline{P}_o|} \tag{4-12}$$

where $|\underline{F}_i|$ and $|\underline{F}_o|$ are the absolute magnitude of the force input and the force output, respectively; $|\underline{P}_i|$ and $|\underline{P}_o|$ are the absolute magnitude of shortest distance from the input and output joint axes to the force input and output, respectively. Thus, the mechanical advantage for this particular mechanism can be written in terms of the input and output moment, as

$$\text{M.A.} = \frac{|\underline{F}_o|}{|\underline{F}_i|} = \frac{|\underline{M}_r||\underline{P}_i|}{|\underline{M}_d||\underline{P}_o|} \tag{4-13}$$

or can be written in terms of the instantaneous efficiency, as

$$\text{M.A.} = \frac{|\underline{\Omega}_2||\underline{P}_i|}{|\underline{\Omega}_3||\underline{P}_o|} \text{ I.E.} \tag{4-14}$$

If more mechanical advantage is desired, one may simply increase $|\underline{P}_i|$, i.e., the distance from the input joint axis to the input force; or decrease $|\underline{P}_o|$, i.e, the distance from the output joint axis to the output force.

## 4.2 R-Cp-C Mechanisms(Figure (4-2))

For the R-Cp-C mechanisms, which is a statically indeterminate mechanism, we may model it as a function generator, i.e., the output link is oscillating in a limited range, and specify the output resistant force and torque. In order to do so, the output cylinder joint is coupled with a translation(compression or tension) spring and a torsion spring, as shown in Figure (4-2). Assuming the cylinder joint is free of friction, then the resistant force and moment are simply proportional to the linear and angular displacements, respectively, as

$$\underline{F}_r = k_t(-\underline{S}_3) \tag{4-15}$$

and

$$\underline{M}_r = k_r(-\underline{\Theta}_3) \tag{4-16}$$

where $k_t$ and $k_r$ are the translation and torsion spring constants, respectively; $\underline{S}_3$ and $\underline{\Theta}_3$ are the linear and angular displacements of the output joint, respectively.

Now, if the output motion is known, the resistant force and moment would be given, we may write the force equilibrium for the output link as follows:

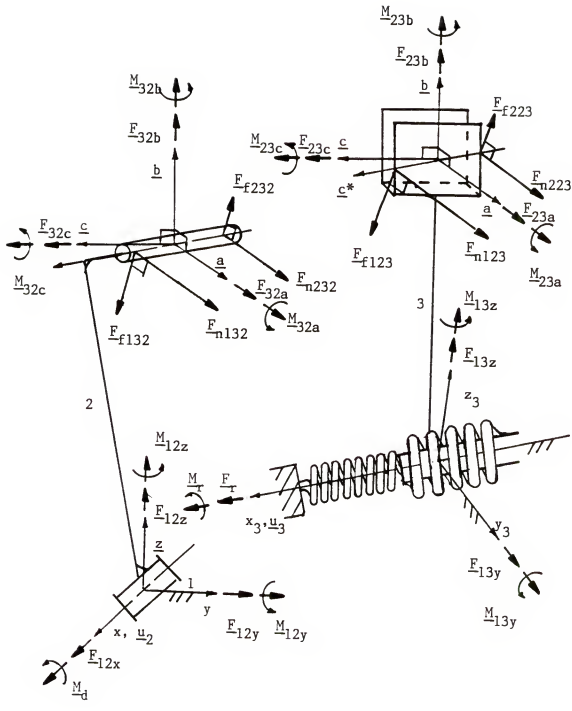


Figure 4-2 Free-body diagram of R-Cp-R mechanism.

$$a_1|\underline{R}_1| + a_2|\underline{R}_2| = - F_r \tag{4-17}$$

where

$$a_i = (\text{sign}(\underline{f}_{ni23})\cos\varphi\underline{f}_{ni23} + \sin\varphi\underline{f}_{fi23}) \cdot \underline{u}_3; \quad i = 1, 2$$

$\underline{f}_{ni23}$ are the unit vectors initially assumed in the direction of $\underline{a}$, $\underline{f}_{fi23}$ are the unit vectors in the the opposite directions of the relative sliding velocities at the two contact points, respectively. The moment equilibrium is expressed

$$b_1|\underline{R}_1| + b_2|\underline{R}_2| = - M_r \tag{4-18}$$

where

$$b_i = \underline{P}_{3i} \times (\text{sign}(\underline{n}_{i23})\cos\varphi\underline{f}_{ni23} + \sin\varphi\underline{f}_{fi23}) \cdot \underline{u}_3;$$

$i = 1, 2$

and $\underline{P}_{3i}$ is the vector from the axis of the output joint to the contact point $P_i$. Solving Equations (4-17) and (4-18) simultaneously, gives

$$|\underline{R}_1| = \frac{- b_2F_r + a_2M_r}{D} \tag{4-19}$$

and

$$|\underline{R}_2| = \frac{- a_1M_r + b_1F_r}{D} \tag{4-20}$$

where $D = a_1b_2 - a_2b_1$. Equations (4-19) and (4-20) are utilized to check the signs of $\underline{f}_{n123}$ and $\underline{f}_{n223}$.

Then, the driving torque can be obtained by the use of the torque equilibrium for the input link, which gives

$$M_d + (\underline{P}_{21} \times \underline{R}_{132} + \underline{P}_{22} \times \underline{R}_{232}) \cdot \underline{u}_2 = 0 \tag{4-21}$$

Equation (4-21) can be rewritten into the form containing the magnitudes of $\underline{F}_r$ and $\underline{M}_r$, as

$$M_d = [(c_1b_2 - c_2b_1)F_r + (-c_1a_2 + c_2a_1)M_r]/D \qquad (4\text{-}22)$$

where

$$c_i = \underline{P}_{2i} \times (\text{sign}(\underline{f}_{ni23})\cos\varphi\underline{f}_{ni23} + \sin\varphi\underline{f}_{fi23}) \cdot \underline{u}_2;$$

$$i = 1, 2$$

Equation (4-22) shows that the driving torque is determined by two parts, one is by the resistant force and the other is by the resistant moment. To illustrate the effects of the Coulomb friction, we may write the virtual work equation for the mechanism, as

$$\underline{M}_d \cdot \underline{\Omega}_2 - \sin\varphi(|\underline{R}_1||\underline{V}_{S1}| + |\underline{R}_2||\underline{V}_{S2}|) + \underline{M}_r \cdot \underline{\Omega}_3 + \underline{F}_r \cdot \underline{V}_3 = 0 \qquad (4\text{-}23)$$

where $|\underline{V}_{S1}|$ and $|\underline{V}_{S2}|$ are the absolute magnitude of the relative sliding velocities at the two contact points of the Cp pair, respectively, and $\underline{\Omega}_2$ and $\underline{\Omega}_3$ are the angular velocities of the input and the output links. Thus, the power loss is explicitly expressed, as

$$\text{P.L.} = \sin\varphi(|\underline{R}_1||\underline{V}_{S1}| + |\underline{R}_2||\underline{V}_{S2}|) \qquad (4\text{-}24)$$

Substituting Equations (4-19) and (4-20) into the above equation gives the P.L. in terms of the magnitude of the resistant force and moment, as

$$\text{P.L.} = \sin\varphi[(-b_2|\underline{V}_{S1}| + b_2|\underline{V}_{S2}|)F_r + (a_2|\underline{V}_{S1}| - a_1|\underline{V}_{S2}|)M_r]/D \qquad (4\text{-}25)$$

The output power is consisted of two components and the instantaneous efficiency may be expressed as the summation of two instantaneous efficiencies for output force and output moment, respectively, as

$$\text{I.E.} = \text{I.E.}_F + \text{I.E.}_M \qquad (4\text{-}26)$$

where

$$I.E._F = \left| \frac{O.P._F}{I.P.} \right| = \frac{F_r V_3}{M_d \Omega_2}$$

and

$$I.E._M = \left| \frac{O.P._M}{I.P.} \right| = \frac{M_r \Omega_3}{M_d \Omega_2}$$

Here, instead of using the absolute magnitudes, the signed scalar are used, since the output force and moment may contribute either positive or negative work. To express the total instantaneous efficiency in terms of the total power loss, one may write

$$I.E. = \left| \frac{O.P.}{I.P.} \right| = \frac{M_r \Omega_3 + F_r V_3}{M_d \Omega_2} = 1 - \left| \frac{P.L.}{I.P.} \right| \qquad (4\text{-}27)$$

where

$$\frac{P.L.}{I.P.} = \frac{(A_1 F_r + A_2 M_r)\sin\varphi}{B_1 F_r + B_2 M_r}$$

$$A_1 = -b_2 |\underline{V}_{s1}| + b_2 |\underline{V}_{s2}|$$

$$A_2 = a_2 |\underline{V}_{s1}| - a_1 |\underline{V}_{s2}|$$

$$B_1 = b_2 |\underline{V}_{p1} \cdot \underline{r}_{132}| - b_1 |\underline{V}_{p2} \cdot \underline{r}_{232}|$$

$$B_2 = -a_2 |\underline{V}_{p1} \cdot \underline{r}_{132}| + a_1 |\underline{V}_{p2} \cdot \underline{r}_{232}|$$

The mechanical advantage may also be expressed in two terms but not by the way of superposition as the power ratio. This is because the force output consists of two components: one is favoring in the translational motion and the other one is favoring the rotational motion. The magnitude of the resultant force is the square root of the sum of the squares of the magnitudes of force components. Thus,

the total mechanical advantage may be written in terms of the mechanical advantages for force output produced by output force and output moment, respectively, as

$$M.A. = (M.A._t^2 + M.A._r^2)^{1/2} \tag{4-28}$$

where

$$M.A._t = \frac{|\underline{F}_{ot}|}{|\underline{F}_i|} = \frac{|\underline{F}_r||\underline{P}_i|}{|\underline{M}_d|}$$

$$M.A._r = \frac{|\underline{F}_{or}|}{|\underline{F}_i|} = \frac{|\underline{M}_r||\underline{P}_i|}{|\underline{M}_d||\underline{P}_o|}$$

The absolute magnitudes $|\underline{F}_{ot}|$ and $|\underline{F}_{or}|$ are the force output components for translational motion and rotational motion, respectively; $|\underline{P}_i|$ and $|\underline{P}_o|$ are the distances from the joint axes to the locations of the force input and force output. Unlike the previous case, the power ratio and mechanical advantages for the R-Cp-C mechanism can not be expressed explicitly in terms of velocities.

## 4.3 R-$P_L$-C-R Mechanism(Figure 4-3)

Considering an R-$P_L$-C-R mechanism, as shown in Figure (4-3), the moment equilibrium for the input link can be expressed

$$M_d + (\underline{P}_{21} \times \underline{R}_{132} + \underline{P}_{22} \times \underline{R}_{232} + \underline{P}_{23} \times \underline{R}_{332}) \cdot \underline{u}_2 = 0 \tag{4-29}$$

where $\underline{P}_{2i}$, i = 1, 2, 3, are the vectors from $\underline{u}_2$ to the three contact points (two in the outter plane element and the one in the inner plane element), respectively. Recognize that if there is no force or moment transmitted in the direction

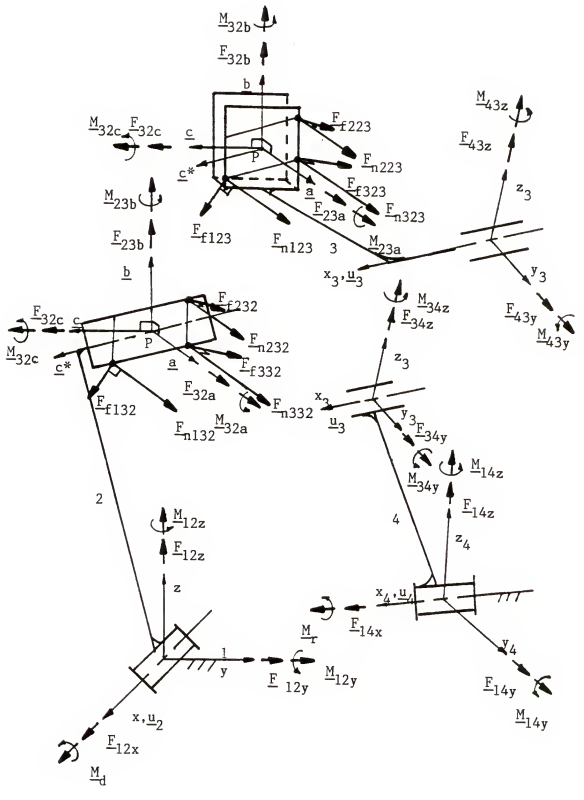


Figure 4-1 Free-body diagram of R-$P_L$-C-R mechanism.

of $\underline{u}_3$ (i.e., there is no friction), then from the force and moment equilibrium equations for the coupler link(link 3) we have

$$(\underline{R}_{123} + \underline{R}_{223} + \underline{R}_{323}) \cdot \underline{u}_3 = 0 \qquad (4\text{-}30)$$

$$(\underline{P}_{31} \times \underline{R}_{123} + \underline{P}_{32} \times \underline{R}_{223} + \underline{P}_{33} \times \underline{R}_{323}) \cdot \underline{u}_3 = 0 \qquad (4\text{-}31)$$

Then, the magnitude of the reaction forces can be obtained by solving Equations (4-29) to (4-31) simultaneously. Using the above three equations we obtain three equations linear in the three absolute magnitudes of the normal forces, as

$$a_1|\underline{R}_1| + b_1|\underline{R}_2| + c_1|\underline{R}_3| = -M_d \qquad (4\text{-}32)$$

$$a_i|\underline{R}_1| + b_i|\underline{R}_2| + c_i|\underline{R}_3| = 0 \qquad i = 2, 3 \qquad (4\text{-}33)$$

where

$$a_1 = \underline{P}_{21} \times \underline{r}_{132} \cdot \underline{u}_2$$

$$b_1 = \underline{P}_{22} \times \underline{r}_{232} \cdot \underline{u}_2$$

$$c_1 = \underline{P}_{23} \times \underline{r}_{332} \cdot \underline{u}_2$$

$$a_2 = \underline{r}_{123} \cdot \underline{u}_3$$

$$b_2 = \underline{r}_{223} \cdot \underline{u}_3$$

$$c_2 = \underline{r}_{223} \cdot \underline{u}_3$$

$$a_3 = \underline{P}_{31} \times \underline{r}_{123} \cdot \underline{u}_3$$

$$b_3 = \underline{P}_{32} \times \underline{r}_{223} \cdot \underline{u}_3$$

$$c_3 = \underline{P}_{33} \times \underline{r}_{323} \cdot \underline{u}_3$$

$$\underline{r}_{i32} = \text{sign}(\underline{f}_{ni32})\cos\varphi\underline{f}_{ni32} + \sin\varphi\underline{f}_{fi32} = -\underline{r}_{i23};$$

$$i = 1, 2, 3$$

Applying Cramer's rule, the reaction forces can be expressed

$$|\underline{R}_1| = M_d D_1/D \qquad (4\text{-}34)$$

$$|\underline{R}_2| = M_d D_2/D \qquad (4\text{-}35)$$

and

$$|\underline{R}_3| = M_d D_3/D \tag{4-36}$$

respectively; where

$$D = \begin{vmatrix} a_1 & b_1 & c_1 \\ a_2 & b_2 & c_2 \\ a_3 & b_3 & c_3 \end{vmatrix}$$

$$D_1 = b_2c_3 - b_3c_2$$

$$D_2 = a_3c_2 - a_2c_3$$

$$D_3 = a_2b_3 - a_3b_2$$

Equations (4-34) to (4-36) are employed to check to the sign of the normal forces. The resistant moment can be obtained by solving the moment equilibrium equation for the dyad consisting of the coupler link and the output link, as

$$(\underline{P}_{41} \times \underline{R}_{123} + \underline{P}_{42} \times \underline{R}_{223} + \underline{P}_{43} \times \underline{R}_{323}) \cdot \underline{u}_4 + \underline{M}_r \cdot \underline{u}_4 = 0 \tag{4-37}$$

Thus, by substituting Equations (4-34) to (4-36) into the above equation, the resistant moment can be expressed in terms of the input moment, as

$$M_r = \{[(\underline{P}_{41} \times \underline{r}_{123})D_1 + (\underline{P}_{42} \times \underline{r}_{223})D_2 + (\underline{P}_{43} \times \underline{r}_{323})D_3]M_d \cdot \underline{u}_4\}/D \tag{4-38}$$

To derive the instantaneous efficiency, the virtual work equation for the mechanism may be written

$$\underline{M}_d \cdot \underline{\Omega}_2 - \sin\Phi(|\underline{R}_1||\underline{V}_{s1}| + |\underline{R}_2||\underline{V}_{s2}| + |\underline{R}_3||\underline{V}_{s3}|) + \underline{M}_r \cdot \underline{\Omega}_4 = 0 \tag{4-39}$$

Thus, the instantaneous efficiency for this particular mechanism may be expressed in terms of the power loss, as

$$\text{I.E.} = \left|\frac{\text{O.P.}}{\text{I.P.}}\right| = \frac{|\underline{M}_r||\underline{\Omega}_4|}{|\underline{M}_d||\underline{\Omega}_2|} = 1 - \left|\frac{\text{P.L.}}{\text{I.P.}}\right| \tag{4-40}$$

where the ratio of power loss to the input power is

$$\frac{\text{P.L.}}{\text{I.P.}} = \frac{(|D_1||\underline{V}_{s1}| + |D_2||\underline{V}_{s2}| + |D_3||\underline{V}_{s3}|)\sin\phi}{|D\Omega_2|} \tag{4-41}$$

The mechanical advantage may also be written in terms of the instantaneous efficiency, as

$$\text{M.A.} = \frac{|\underline{F}_o|}{|\underline{F}_i|} = \frac{|\underline{\Omega}_2||\underline{P}_i|}{|\underline{\Omega}_4||\underline{P}_o|}\ \text{I.E.} \tag{4-42}$$

where $\underline{F}_o$ and $\underline{F}_i$ the input force and output force, respectively.

# CHAPTER 5
# DESIGN METHOD AND FORMULATION

## 5.1 Optimization Strategy in Mechanisms Design

The application of optimization in mechanism design may be classified into two groups, one is in precision point synthesis and the other one is the mathematical programming problem (Fox & Gupta, 1973). This work naturally falls into the second group. The optimization methods may also be classified into three groups: objective function without constraints, objective function with constraints using unconstrained optimization methods, and the direct solution of constrained problems. The second group may be called indirect methods for constrained problems or sequential unconstrained minimization techniques (SUMT) (Fiacco & McCormick, 1968). The indirect methods handle the constraints implicitly so that the detailed structure of the constraint equations does not need to be considered. The third group may be called direct solution methods of constrained problems. The direct methods take the constraint equations directly into account. Most application of optimal engineering design involve nonlinear equation systems with both linear and nonlinear constraint equations. Thus, generally the second or the third method is needed. The comparison of these methods for constrained problems has

been studied by several publications, such as the one by Eason and Fenton (1974) and more recently by Sandgren and Ragsdell (1980). A summary for these and other comparison is seen in Reklaitis, Ravindran, and Ragsdell, 1983. Hock and Schittkowski (1983) also compared 27 nonlinear programming codes. For those problems where the gradients are available for the constraint equations, the sequential quadratic programming method and the generalized reduced gradient method may give the best approach(Hock and Schittkowski, 1983). Otherwise, the indirect methods will be a better choice. Although, the gradients can be obtained by numerical methods, it does not necessary give a better result, as indicated by Eason and Fenton (1974).

The general optimal design problem may have the form (Rao, 1978)

Minimize $U(\underline{X})$ $\underline{X}= [x_1, x_2, \ldots, x_N]^T$

Subject to

$G_j(\underline{X}) \geq 0$ $j = [1, J]$

$H_k(\underline{X}) = 0$ $k = [J+1, K]$

where $U(\underline{X})$ is the objective function, $\underline{X}$ is the design vector, $G_j(\underline{X})$ are the inequality constraints, and $H_k(\underline{X})$ are the equality constraints. To use the penalty function with an unconstrained optimization method, the original objective function and the constraints are converted into the form

$$U_M(\underline{X}, \underline{R}) = U(\underline{X}) + M(\underline{R}, G(\underline{X}), H(\underline{X})) \qquad (5\text{-}1)$$

where $\underline{R}$ is a set of penalty parameters and M is a function of $\underline{R}$ and the constraint equations. Now, the constrained op-

timization problem is treated as an unconstrained optimization problem with the objective function $U_M$.

Powell's method using conjugate directions (1964) for the unconstrained optimization with the method of penalty multipliers (Powell, 1969; Fletcher, 1974) for the penalty function, provides an efficient optimization scheme for constrained optimization without the need of derivatives. The codes form OPTIVAR (Siddall, 1982) are adopted here due to its efficiency(Reklaitis, Ravindran, and Ragsdell, 1983) and easy implementation with different penalty functions. The objective function illustrated by Siddall has the form

$$U_M = U(\underline{X}) + \frac{1}{2}\sum_j r_j \langle G_j - g_j \rangle^2 + \frac{1}{2}\sum_k r_k (H_k - h_k)^2 \qquad (5\text{-}2)$$

where $r_j$ and $r_k$ are the multipliers and may vary for successive optimization runs, which are recommended to be increased by an arbitrary factor of 10. The <*> notation has the meaning

$$\langle * \rangle = \begin{cases} * & \text{if } * \le 0 \\ 0 & \text{if } * > 0 \end{cases} \qquad (5\text{-}3)$$

The other two parameters $g_j$ and $h_k$ are updated by the following equations between successive iteration i and i+1, as

$$g_j^{(i+1)} = g_j^{(i)} - \min\left(G_j^{(i)}, g_j^{(i)}\right) \qquad (5\text{-}4)$$

$$h_k^{(i+1)} = h_k^{(i)} - H_k^{(i)} \qquad (5\text{-}5)$$

The first run uses $g_j$ and $h_k$ equal to zero. Figure (5-1) illustrates a flow chart adapted from the algorithm listed by Siddall for Powell's strategy.

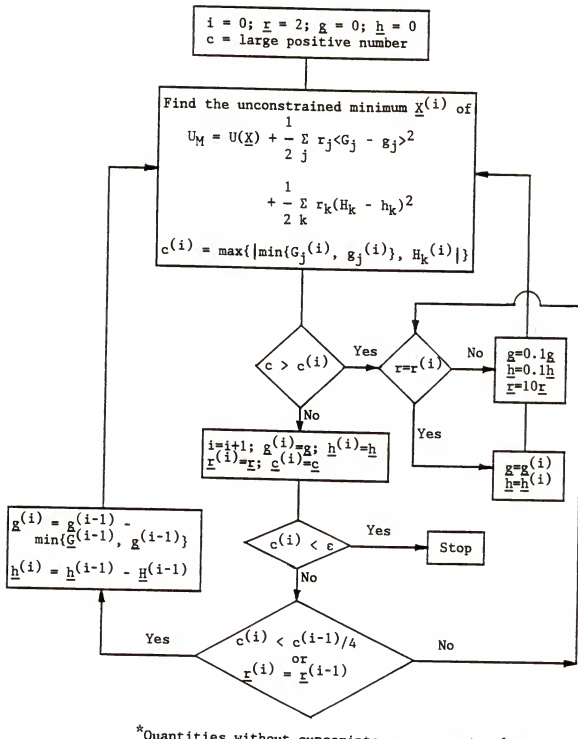


*Quantities without supscripts are current values.

Figure 5-1 Flow chart of Powell's algorithm for method of multipliers (adapted from Siddall, 1982).

## 5.2 Problem Formulation

Involving the transmission criterion in optimal design of mechanisms has been seen in numerous publications. Some of them work on finding the optimal transmission angle or deviation angles for a certain mechanism, some others take the transmission angle as one of the design criteria. Here, the goal is to find the best transmission characteristics which includes not only minimizing the maximum deviation angles but also minimizing the peak acceleration ratio. Having the transmission criteria defined in the previous chapters, we need to formulate the design problem for each particular mechanism. Before doing so, some basic constraints need to be clarified first.

### 5.2.1 Rotatability of mechanisms

To investigate the transmission characteristics, a fully rotatable input link is desired, therefore the rotatability of the mechanism must be considered. The term "rotatability" applies to not only the input link but also the output link. Thus, multiple conditions of rotatability should be established to cover different Grashof-type linkages namely crank-rocker or crank-crank.

Generally, the rotatability for the mechanisms having quadratic input-output displacement equation may be determined by the natures of the roots of equation's discriminant, as seen in Nolle's work (1969) for RSSR mechanism. Alizade and Sandor (1985) also apply the ine-

quality constraints derived from the coefficients of the determinant to the design of RSSR and RSSP mechanisms with complete crank rotation. Reinholtz (1983) uses a similar approach to determine the input crank rotatability for the RSSR mechanism. Recently, Angeles and Bernier (1986) use the discriminant of the input-output equations by geometric approach to the analyses of the mobility of planar and spatial four-bar mechanisms. The determining of rotatability for the R-Sp-R mechanism (see Figure 5-2) will need to utilize a similar approach.

5.2.1.1 Rotatability of R-Sp-R mechanism

The discriminant a quadratic displacement equation can be rearranged into a quartic equation in terms of either the output or input rotation angle. After the discriminant of the quartic equation is obtained, Sturm's theory may be applied to judge the roots of the equation (Cajori, 1943). If the discriminant of the quartic equation has four real roots, then the original displacement equation must have complex roots only, i.e., the input link must have no limit positions, which also means the input link has a complete rotation. On the other hand, if the discriminant of the quartic equation has no real roots at all, the original displacement equation must have real roots, i.e., there are limit position, for the input link. In another words, the input link does not have full rotatability. Similar situations are applied to the output-input equation to determine

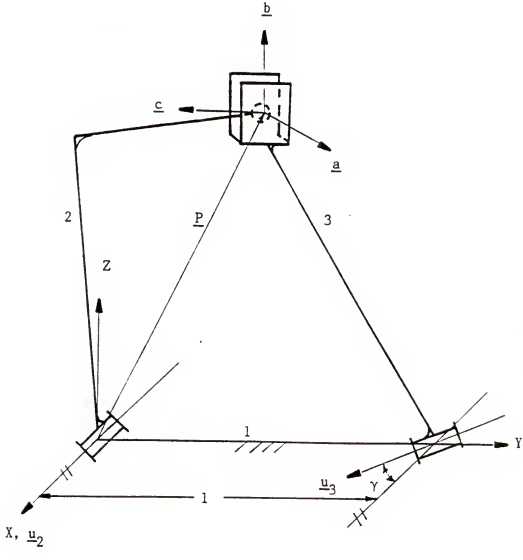


Figure 5-2 An R-Sp-R mechanism

the rotatability of the output link.

To state the criteria for the quartic equation having either all real roots or all imaginary roots, some brief expressions from Cajori's work (1943, Sec. 50) are adopted as follows:

A general quartic equation may have the form

$$b_0x^4 + 4b_1x^3 + 6b_2x^2 + 4b_3x + b_4 = 0 \qquad (5\text{-}6)$$

which can be transformed into a new equation, deprived of its second term as follows:

$$y^4 + 6Hy^2 + 4Gy + b_0{}^2I - 3H^2 = 0 \qquad (5\text{-}7)$$

where

$$y = b_0x + b_1$$

$$H = b_0b_2 - b_1{}^2$$

$$G = b_0b_3 - 3b_0b_1b_2 + 2b_1{}^3$$

$$I = b_0b_4 - 4b_1b_3 + 3b_2{}^2$$

The nature of the roots of the general quartic equation can then be stated as follows:

a. all roots real, if

$(I^3 - 27J^2) > 0,$

$(3b_0J - 2HI) > 0,$

and

$H < 0;$

b. all roots imaginary, if

$(I^3 - 27J^2) > 0,$

and if

$H > 0$

or else

$$(3b_0J - 2HI) < 0;$$

where

$$J = (b_0{}^2HI - G^2 - 4H^3)/b_0{}^3.$$

To apply the above two conditions in mechanism design, we may affirm the following conditions:

1. if the determinant of the quadratic output-input equation of a mechanism satisfies the first condition, then the output link is a rocker, i.e., it is oscillating in a limited range;
2. if the determinant of the quadratic output-input equation of a mechanism satisfies the second condition, then the output link is a crank, i.e., it can rotate 360 degrees;
3. if the determinant of the quadratic input-output equation of a mechanism satisfies the second condition, then the input link is a crank, i.e., it has full rotatability.

Generally, these conditions can be applied to the four-link spatial mechanisms with lower pairs only and the three-link spatial mechanisms with one higher pair.

5.2.1.2 Rotatability of R-Cp-C and R-$P_L$-C-R mechanisms

It is noted that the R-Cp-C and R-$P_L$-C-R mechanisms, as far as rotations are concerned, are equivalent to a spherical RRRR four-link mechanism as shown in Figure 5-3. The parameters used to specify it are as follows:

$\underline{s}$ the unit vector along the ith pair axis

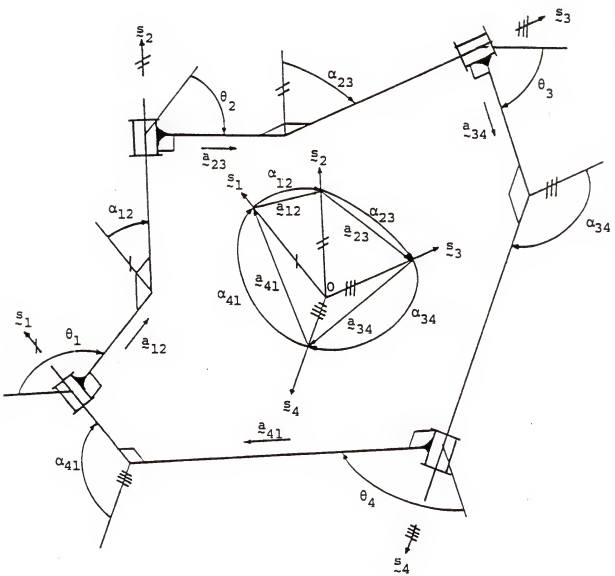


Figure 5-3 A spherical RRRR four-link mechanism.

$\underline{a}_{ij}$ the unit vector along the common perpendicular between $\underline{s}_i$ and $\underline{s}_j$

$\alpha_{ij}$ the positive angle from $\underline{s}_i$ to $\underline{s}_j$ measured clockwise looking in the direction on $\underline{a}_{ij}$, i.e., in the right-hand direction about $\underline{a}_{ij}$

$\theta_i$ the positive angle from $\underline{a}_{ij}$ to $\underline{a}_{jk}$ measured clockwise looking in the direction of $\underline{s}_j$

In the equivalent mechanism, the $\alpha_{ij}$'s become arcs of great circles physically representing the link lengths. Since angular relationships are maintained, the spherical mechanism has the same Grashof type as the spatial mechanism.

The input-output equation for the 4R spherical mechanism is a cosine law for a spherical quadrilateral (Duffy, 1980). If all the link lengths lie within certain ranges, the Grashof rule for the planar four-link four-revolute mechanism can be directly applied to the spherical four-link four-revolute mechanism using the arc angles between joints as link lengths. Gilmartin and Duffy (1972) derived the criteria for determining types of the spherical four-link four-revolute mechanism with general proportions. The criteria for the crank-rocker type mechanism are stated as three inequalities:

$$\alpha_{23} + \alpha_{34} > \alpha_{12} + \alpha_{41} \tag{5-8}$$

$$\alpha_{23} + \alpha_{41} > \alpha_{12} + \alpha_{34} \tag{5-9}$$

$$\alpha_{34} + \alpha_{41} > \alpha_{12} + \alpha_{23} \tag{5-10}$$

The criteria for the crank-crank type mechanism are stated as another three inequalities:

$$\alpha_{12} + \alpha_{23} > \alpha_{34} + \alpha_{41} \tag{5-11}$$

$$\alpha_{23} + \alpha_{34} > \alpha_{23} + \alpha_{41} \tag{5-12}$$

$$\alpha_{23} + \alpha_{34} > \alpha_{12} + \alpha_{34} \tag{5-13}$$

To utilize these inequalities, we must first observe that the R-Cp-C and R-$P_L$-C-R mechanisms are equivalent to the spherical four-link four-revolute mechanism. This can be observed by modeling all the pairs with lower pairs only. Figure 5-4 shows an R-Cp-C mechanism. The Cp pair can be modeled by the C-P-R dyad. Figure 5-5 shows an R-CPR-C mechanism which is equivalent to the R-Cp-C mechanism. In Figure 5-5, the axes of the turning pairs are $\underline{s}_1$, $\underline{s}_2$, $\underline{s}_4$, and $\underline{s}_5$. These axes are corresponding to $\underline{u}_2$, $\underline{c}^*$, $\underline{a}$, and $\underline{u}_3$, respectively, as shown in Figure 5-4. The input-output equation for the angular motions is related to the input and output angles and the angles between the axes of the revolute pairs only. This can also be observed from the displacement equation (E-3) in Appendix E. To obtain a crank-rocker type mechanism, equations (5-8) to (5-10) are applied. With proper substitutions of the corresponding angles between the axes, the inequality constraints can be expressed as:

$$\alpha_{24} + \alpha_{45} - (\alpha_{12} + \alpha_{51}) > 0 \tag{5-14}$$

$$\alpha_{24} + \alpha_{51} - (\alpha_{12} + \alpha_{45}) > 0 \tag{5-15}$$

$$\alpha_{45} + \alpha_{51} - (\alpha_{12} + \alpha_{24}) > 0 \tag{5-16}$$

Notice that in Figure 5-5 the angle between $\underline{s}_2$ and $\underline{s}_4$, $\alpha_{24}$, is the same angle between $\underline{c}$ and $\underline{a}$ in Figure 5-4, which is $\pi/2$. The other angles can be expressed as:

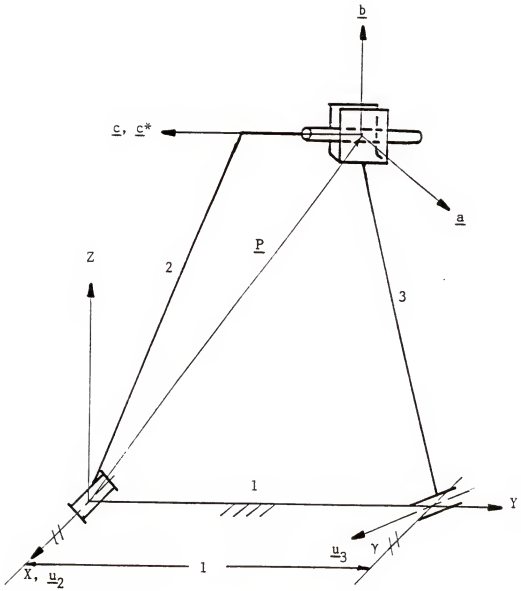


Figure 5-4 An R-Cp-C mechanism.

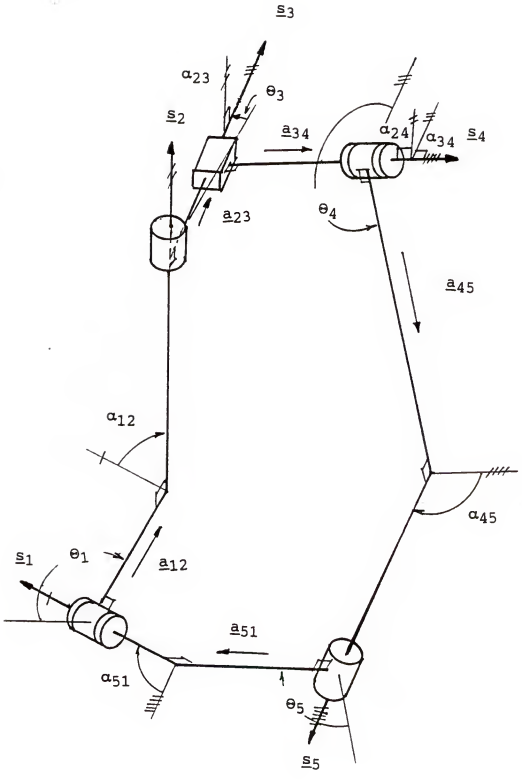


Figure 5-5 An R-CPR-C mechanism.

$$\alpha_{12} = \cos^{-1} \underline{u}_2 \cdot \underline{c} \tag{5-17}$$

$$\alpha_{45} = \cos^{-1} \underline{a} \cdot \underline{u}_3 \tag{5-18}$$

$$\alpha_{51} = \cos^{-1} \underline{u}_3 \cdot \underline{u}_2 \tag{5-19}$$

Similarly, an R-$P_L$-C-R mechanism (shown in Figure 5-6) can be modeled as an R-PRP-C-R mechanism (shown in Figure 5-7). The axes of the turning pairs in Figure 5-7 are $\underline{s}_1$, $\underline{s}_3$, $\underline{s}_5$, and $\underline{s}_6$, which are corresponding to $\underline{u}_2$, $\underline{a}$, $\underline{u}_3$, and $\underline{u}_4$, respectively. To obtain a crank-crank type mechanism, equations (5-11) to (5-13) are applied. With proper substitutions of the corresponding $\alpha$ angles, the inequality constraints can be written as:

$$\alpha_{13} + \alpha_{35} - (\alpha_{56} + \alpha_{61}) > 0 \tag{5-20}$$

$$\alpha_{13} + \alpha_{56} - (\alpha_{35} + \alpha_{61}) > 0 \tag{5-21}$$

$$\alpha_{35} + \alpha_{56} - (\alpha_{12} + \alpha_{41}) > 0 \tag{5-22}$$

where the $\alpha$ angles can be obtained from observing Figure 5-6, as

$$\alpha_{13} = \cos^{-1} \underline{u}_2 \cdot \underline{a} \tag{5-23}$$

$$\alpha_{35} = \cos^{-1} \underline{a} \cdot \underline{u}_3 \tag{5-24}$$

$$\alpha_{56} = \cos^{-1} \underline{u}_3 \cdot \underline{u}_4 \tag{5-25}$$

$$\alpha_{61} = \cos^{-1} \underline{u}_4 \cdot \underline{u}_2 \tag{5-26}$$

### 5.2.2 Formulation of R-Sp-R mechanism

An R-Sp-R mechanism is shown in Figure (5-2). The input joint axis lies in the x coordinate axis, the output joint axis is a unit distance away from the x coordinate axis with a skew angle about the y coordinate. Thus the common normal of the input and output joint axes is

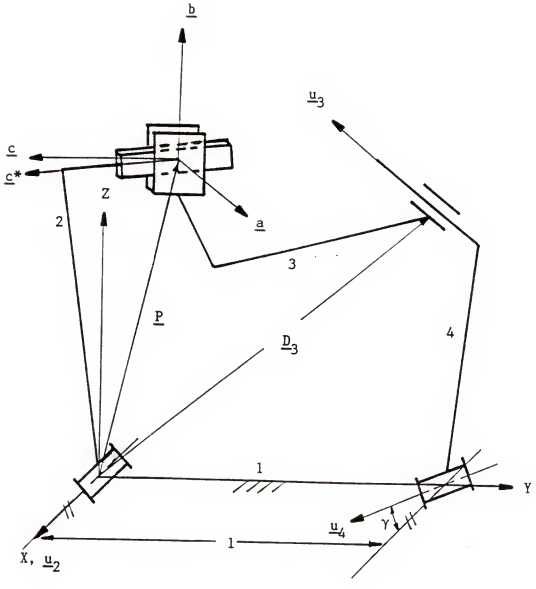


Figure 5-6 An R-$P_L$-C-R mechanism.

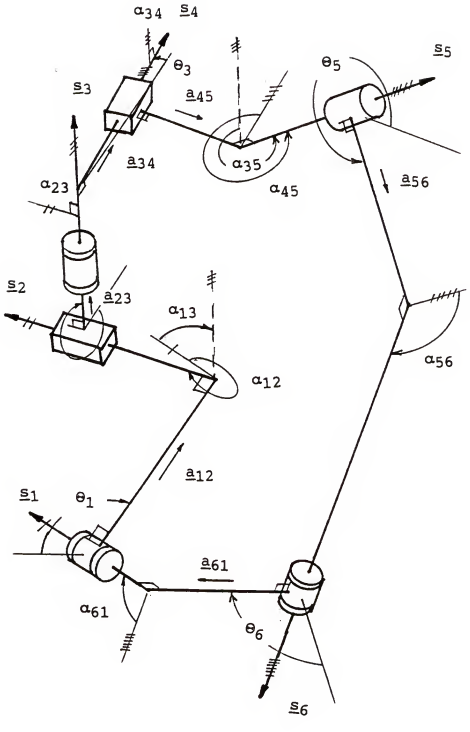


Figure 5-7 An R-PRP-C-R mechanism.

$[0,1,0]^T$. The skew angle of the output joint axis may be assigned as a fixed value. The position vector $\underline{P}$ locates the initial contact point and the shortest vector from the input joint axis to the contact point is denoted as $\underline{P}_2$. A coordinate system attached to the contact point has axis $\underline{a}$ in the direction of the normal vector of the plane element of the Sp pair, axes $\underline{b}$ and $\underline{c}$ are on the contact surface. The goal is to design a crank-crank mechanism with favorable transmission criteria for a specified link length ratio between the input crank and the ground link. The state variables are

$$\underline{u}_2,\ \underline{u}_3,\ \underline{D}_2,\ \underline{D}_3,\ \underline{P}_2,\ \underline{a},\ \underline{b},\ \underline{c}$$

where

$$\underline{a} \cdot \underline{b} = 0;$$

$$\underline{c} = \underline{a} \times \underline{b};$$

and

$$\underline{D}_2 = [0,\ 0,\ 0]^T,$$

$$\underline{D}_3 = [0,\ 1,\ 0]^T$$

are the vectors from the origin of the fixed coordinate system to the input joint and output joint, respectively. The design variables are the position vector $\underline{P}$ and the Euler angles of the unit vector $\underline{a}$. The use of Euler angles for the in-plane coordinate axes has the advantage of limiting the ranges of the magnitudes of the design variables. Thus the design vector may be expressed

$$\underline{X} = [\Theta_x,\ \Theta_y,\ \Theta_z,\ p_x,\ p_y,\ p_z]^T \qquad (5\text{-}27)$$

Then, we have

$\underline{P} = [p_x, p_y, p_z]$

$\underline{a}_i = [M_\Theta]\underline{a}$

$\underline{b}_i = [M_\Theta]\underline{b}$

$\underline{c}_i = \underline{a}_i \times \underline{b}_i$

where $[M_\Theta]$ is the rotation matrix based on $\Theta_x$, $\Theta_y$, $\Theta_z$; $\Theta_x$, $\Theta_y$, $\Theta_z$ are the angles(at the i-th iteration) of the moving coordinate system measured from the positive branch of the fixed coordinate axes, respectively; and $\underline{a}_i$, $\underline{b}_i$, and $\underline{c}_i$ designate the moving coordinate axes at the i-th iteration. Then, the rotation matrix for the moving coordinate system at the i-th iteration can be expressed

$$[M_\Theta] = \begin{bmatrix} c\Theta_y c\Theta_x & -c\Theta_y s\Theta_x & s\Theta_y \\ c\Theta_x s\Theta_y s\Theta_z + c\Theta_z s\Theta_x & -s\Theta_x s\Theta_y s\Theta_z + c\Theta_z c\Theta_x & -s\Theta_z c\Theta_y \\ -c\Theta_x s\Theta_y c\Theta_z + s\Theta_z s\Theta_x & s\Theta_x s\Theta_y c\Theta_z + s\Theta_z c\Theta_x & c\Theta_z c\Theta_y \end{bmatrix} \quad (5\text{-}28)$$

where $c\Theta_j = \cos\Theta_j$ and $s\Theta_j = \sin\Theta_j$; $\Theta_j = \Theta_x$, $\Theta_y$, $\Theta_z$.

5.2.2.1 Objective function

The objective function may be based on the deviation angles and the maximum and minimum acceleration of the output joint, as

$$U(\underline{X}) = - k_1|\cos\delta_{F23}|_{min} - k_2|\cos\delta_{FR}|_{min} + k_3\alpha_{\Theta 3} \quad (5\text{-}29)$$

where

$\underline{X} = [\Theta_x, \Theta_y, \Theta_z, p_x, p_y, p_z]^T$;

$\alpha_{\Theta 3} = |\theta_3|_{max} / \theta_2{}^2$.

$\theta_2$ and $\theta_3$ are the input angular velocity and the output an-

gular acceleration, respectively. The coefficients $k_1$, $k_2$, and $k_3$ are the weighting factors. The two deviation angles are defined in Equations (3-19) and (3-20).

5.2.2.2 Inequality constraints

The R-Sp-R mechanism is desired to be a crank-crank type mechanism, so that the second and third conditions of the rotatability are to be applied. Then, for the input-output and output-input equations we have six inequality constraint equations, i.e.,

$$G_1(\underline{X}) = (I_i^3 - 27J_i^2) > 0; \quad (5\text{-}30)$$

$$G_2(\underline{X}) = H_i > 0 \text{ or else} \quad (5\text{-}31)$$

$$G_3(\underline{X}) = (3b_{i0}J_i - 2H_iI_i) < 0; \quad (5\text{-}32)$$

$$G_4(\underline{X}) = (I_o^3 - 27J_o^2) > 0; \quad (5\text{-}34)$$

$$G_5(\underline{X}) = H_o > 0 \text{ or else} \quad (5\text{-}35)$$

$$G_6(\underline{X}) = (3b_{o0}J_o - 2H_oI_o) < 0; \quad (5\text{-}36)$$

where the subscripts i and o denote that the coefficients are derived from the coefficients of the input-output and output-input equations, respectively. The coefficients of the quartic equations are derived in Appendix G.

As pointed out in Chapter 3, the friction force may stop the relative sliding between the pair elements of the higher pair. To ensure this would not happen, Equation (3-45) must be satisfied, i.e.,

$$G_7(\underline{X}) = \mu - |\cos\alpha\tan\delta| \geq 0 \quad (5\text{-}37)$$

5.2.2.3 Equality constraint

To ensure that the mechanism will not have an infinitely small or large link length, it is necessary to set a fixed link length for either the input link or the output link. The link length is difficult to define for the link that attached to a higher pair. However, for this particular mechanism, the input link length can be defined as the shortest distance form the input join axis to the initial contact point (or the center of the sphere, if preferred), which is designated as $\underline{P}$ in Figure (5-2). Since the ground link length is already set to be unity, we may assign $P_2$ as the input link to the ground link length ratio. Then, an equality constraint equation can be formed, as

$$H_8(\underline{X}) = |(\underline{u}_2 \times \underline{P}) \cdot \underline{u}_2| - P_2 = 0 \qquad (5\text{-}38)$$

5.2.3 Formulation of R-Cp-C mechanism

An R-Cp-C mechanism is shown in Figure (5-4), which can be described similarly to the R-Sp-R mechanism except that there is one more design variable to define the axis of the cylinder element in the Cp pair. The state variables are the same as the R-Sp-R mechanism. The design vector is

$$\underline{X} = [\theta_x, \theta_y, \theta_z, \beta, p_x, p_y, p_z]^T \qquad (5\text{-}39)$$

where

$$\underline{P} = [p_x, p_y, p_z]$$

$$\underline{a}_i = [M_\theta]\underline{a}$$

$$\underline{b}_i = [M_\theta]\underline{b}$$

$$\underline{c}_i = \underline{a}_i \times \underline{b}_i$$

and

$$\underline{c}^*_i = \cos(\beta)\underline{b}_i + \sin(\beta)\underline{c}_i$$

is the unit vector of the axis of the cylinder element. The angle $\beta$ is measured from the in-plane axis $\underline{b}$ to the inner cylinder axis $\underline{c}^*$. The rotation matrix $[M_\theta]$ is defined the same as Equation (5-28).

5.2.3.1 Objective function

There are four deviation angles for the R-Cp-C mechanisms as illustrated in Chapter 3. If the R-Cp-C mechanism is desired to be a crank-rocker type mechanism, then the two deviation angles $\delta_{F23}$ and $\delta_{M23}$ will be a right angle during the entire motion of the mechanism. Thus, it is meaningless to maximize their minimum values. Therefore, the objective function will consist of two other deviation angles and the maximum and minimum accelerations, as

$$U(\underline{X}) = - k_1|\cos\delta_{FR}|_{min} - k_2|\cos\delta_{FT}| - k_3|\cos\delta_{MR}|_{min} + k_4\alpha_{\theta 3} + k_5\sigma_{\theta 3} + k_6\alpha_{S3} + k_7\sigma_{S3} \qquad (5\text{-}40)$$

where

$$\alpha_{\theta 3} = ||\theta_{3max} / \theta_{3min}| - 1|;$$

$$\sigma_{\theta 3} = |(\theta_{3max} - \theta_{3min})/\theta_{3max}|;$$

$$\alpha_{S3} = ||S_{3max} / S_{3min}| - 1|;$$

$$\sigma_{S3} = |(S_{3max} - S_{3min})/S_{3max}|;$$

and $\theta_3$ and $S_3$ are the angular and linear acceleration of the output link, respectively. The coefficients $k_i$, i = [1, 6], are the weighting factors. The deviation angles $\delta_{FR}$, $\delta_{FT}$, and $\delta_{MR}$ are defined in Chapter 3.

5.2.3.2 Inequality constraints

Equations (14) to (16) are applied to determine a crank-rocker type mechanism. The constraint for continuous motion is the same as the R-Sp-R mechanism. Thus, $G_7(\underline{X})$ can be similar to Equation (5-37).

5.2.3.3 Equality constraint

Similarly to the R-Sp-R mechanism, it is necessary to set a fixed link length ratio for the input link and the ground link. The input link length is defined as the length of the common normal between $\underline{u}_2$ and $\underline{c}$. Thus, the equality constraint can be written as

$$H_8(\underline{X}) = (\underline{P} - \underline{D}_2) \cdot \underline{c} \times \underline{u}_2 \; / \; |\underline{c} \times \underline{u}_2| - P_2 = 0 \quad (5\text{-}41)$$

where $P_2$ is a given link length ratio for the input link.

5.2.4 Formulation of R-$P_L$-C-R Mechanism

An R-$P_L$-C-R mechanism is shown in Figure (5-6), where the input joint axis $\underline{u}_2$ is in the direction of the x axis and the output join axis $\underline{u}_4$ has the common normal $(0, 1, 0)^T$ with $\underline{u}_2$ and has a skew angle $\tau$. A coordinate system $\underline{a}$, $\underline{b}$, and $\underline{c}$ is attached at the initial contact point of the outer plane element of the $P_L$ pair. The axis $\underline{a}$ is normal to the plane element. The axis $\underline{c}^*$ is the in the inner plane element. The axis of the floating C joint is denoted as $\underline{u}_3$ and the joint has a distance vector $\underline{D}_3$ away form the input joint which is located at the origin of the fixed coordinate system.

5.2.4.1 Objective Function

There are three deviation angles for force transmission, three deviation angles for moment transmission, and two deviation angles for the force-produced moment transmission. Thus, the objective function may be formed

$$U(\underline{X}) = - k_1|\cos\delta_{F23}|_{min} - k_2|\cos\delta_{F34}| - k_3|\cos\delta_{FR}|_{min} - k_4|\cos\delta_{M23}| - k_5|\cos\delta_{MM34}|_{min} - k_6|\cos\delta_{MR}|_{min} - k_7|\cos\delta_{FM34}|_{min} - k_8|\cos\delta_{FMR}|_{min} + k_9\alpha_{\Theta 3} + k_{10}\sigma_{\Theta 3} + k_{11}\alpha_{S3} + k_{12}\sigma_{S3} + k_{13}\alpha_{\Theta 4} + k_{14}\sigma_{\Theta 4} \quad (5\text{-}42)$$

where

$$\underline{X} = [\Theta_{Px}, \Theta_{Py}, \Theta_{Pz}, \Theta_{u3x}, \Theta_{u3y}, \Theta_{u3z}, \beta, p_x, p_y, p_z, d_{3x}, d_{3y}, d_{3z}]^T$$

$$\alpha_{\Theta 3} = ||\Theta_{3max} / \Theta_{3min}| - 1|$$

$$\sigma_{\Theta 3} = |(\Theta_{3max} - \Theta_{3min})/\Theta_{3max}|$$

$$\alpha_{S3} = ||S_{3max} / S_{3min}| - 1|$$

$$\sigma_{S3} = |(S_{3max} - S_{3min})/S_{3max}|$$

$$\alpha_{\Theta 4} = ||\Theta_{4max} / \Theta_{4min}| - 1|$$

$$\sigma_{\Theta 4} = |(\Theta_{4max} - \Theta_{4min})/\Theta_{4max}|$$

$$\underline{a}_i = [M_{\Theta P}]\underline{a}$$

$$\underline{b}_i = [M_{\Theta P}]\underline{b}$$

$$\underline{c}_i = \underline{a}_i \times \underline{b}_i$$

$$\underline{c}^*_i = \cos(\beta)\underline{b}_i + \sin(\beta)\underline{c}_i$$

$$\underline{u}_{3i} = [M_{\Theta u3}]\underline{u}_3$$

The coefficients $k_i$, i = [1, 14], are the weighting factors. $[M_{\Theta P}]$ is the rotation matrix for the in-plane coordinate system and $\Theta_{Pj}$, j = x, y, z, are the rotation angles for the

in-plane coordinate system at the i-th iteration measured from the positive branch of the fixed coordinate axes, respectively. Similarly, $[M_{\Theta u3}]$ is the rotation matrix for $\underline{u}_3$ and $\Theta_{u3j}$, j = x, y, z, are the rotation angles for $\underline{u}_3$ at the i-th iteration, respectively. $\beta$ is the angle measured from $\underline{b}$ to $\underline{c}^*$. $\Theta_3$ and $S_3$ are the relative angular and linear accelerations of the floating C joint. $\Theta_4$ is the angular acceleration of the output link. $p_j$, j = x, y, z, are components of the vector $\underline{P}$ from the origin to the origin of the initial moving coordinate system $\underline{a}$, $\underline{b}$, $\underline{c}$. $d_{3j}$, j = x, y, z, are the components of the vector $\underline{D}_3$ from the origin to the floating C joint.

5.2.4.2 Inequality constraints

Equations (20) to (22) are applied to obtain a crank-crank type mechanism. Also, Equation (5-37) applies for the continuous motion.

5.2.4.3 Equality constraints

Since the R-$P_L$-C-R is a four-link mechanism, it is therefore necessary to set two link length ratio instead of one as for the previous mechanisms. The input link length ratio can be defined to be the same as for the previous mechanisms. The second link length ratio can be set between the output link and the ground link, where the link length is the length of the common normal between the two joint axes. Thus, we have $H_8(\underline{X})$ to be defined by Equation (5-37)

and $H_9(\underline{X})$ to be defined, as

$$H_9(\underline{X}) = (\underline{D}_3 - \underline{D}_4) \cdot \underline{u}_3 \times \underline{u}_4 \; / \; |\underline{u}_3 \times \underline{u}_4| - P_4 = 0 \quad (5\text{-}43)$$

where $P_4$ is a given link length ratio for the output link.

5.2.5 Feasible mechanism

"Feasible mechanism" here means that the mechanism has the ability to move as excepted, namely, as a crank-crank, crank-rocker, or other Grashof-Type mechanisms. The design problems formulated are parametric, i.e., the original objective function and the inequality constraint equation for the continuous motion need to be calculated throughout the entire range of motion. It is always difficult to start the optimization search from an infeasible starting point and expect that the constraints will be satisfied when the original objective function converges. This is usually overcome by using the exterior penalty function. Therefore, it is desired to start the optimization search from a feasible starting point. In order to find the feasible starting point, an extra optimization search needs to be formulated. This can be done by using the equality constraint equation as the original objective function. The six nonparametric inequality constraint equations for classifying the type of mechanism are applied as the inequality constraints. Thus, the "pseudo-objective" function can be written

$$U^*_M = \sum_{k=8}^{9} H_k(\underline{X}) + M^*(\underline{R}, \underline{G}_j(\underline{X})); \qquad j = [1, 6] \quad (5\text{-}44)$$

The global minimum of Equation (5-44) is zero when all the inequality constraints are satisfied. Then, the design vector resulting from this optimization process will provide a feasible mechanism, i.e., a feasible starting point for the objective functions derived in the previous sections. It can be observed that Equation (5-44) contains non-parametric constraints and the original objective function is much simpler. Thus, it will be much easier to converge from an infeasible region to a feasible region than by using the parametric constraint function directly. However, the constraint for the continuous motion is not included in Equation (5-44), which is a parametric constraint.

# CHAPTER 6
# NUMERICAL EXAMPLES

## 6.1 R-Sp-R Mechanisms

Figure (5-1) illustrates the parameters of the R-Sp-R mechanism. The formulation of objective function and the constraints are illustrated in Chapter 5. The R-Sp-R mechanism is desired to be a crank-crank type mechanism. The input joint is assumed rotating with unit angular velocity ($\theta_2$ = 1 rad/sec) and unit input torque ($M_d$ = 1 lbf·in). The static friction coefficient is set at $\mu$ = 0.27. The given variables are:

$\underline{u}_2 = (1.000000,\ 0.000000,\ 0.000000)^T$

$\underline{D}_2 = (0.000000,\ 0.000000,\ 0.000000)^T$

$\underline{u}_3 = (0.866025,\ 0.000000,\ 0.500000)^T$

$\underline{D}_3 = (0.000000,\ 1.000000,\ 0.000000)^T$

The above vectors are illustrated in Section 5.2.2. The input link length is designated to be equal to 1.5. The following set of the weighting factors gives a better over all result considering the displacements and the deviation angles, which is

$$k_1 = k_2 = k_3 = 1$$

The local optimum point based on Equation (5-29) with the above weighting factors for one of the branches of the mechanism is found at (see Equation (5-27)):

$$\underline{X} = [\ 2.893710,\ \ 1.826581,\ \ 0.946411,$$
$$-0.025338,\ \ 1.426154,\ -0.464859]^T$$

The corresponding design parameters (see Figure (5-2)) are obtained carried out as

$$\underline{a} = (\ 0.247194,\ -0.856662,\ -0.452798)^T$$
$$\underline{b} = (-0.758864,\ \ 0.119415,\ -0.640207)^T$$
$$\underline{c} = (\ 0.602512,\ \ 0.501867,\ -0.620571)^T$$
$$\underline{P} = (-0.025338,\ \ 1.426154,\ -0.464859)^T$$

The actual input link length(the absolute value of $\underline{P}$) is 1.500003. The fixed cosine of deviation angle (see Equation (5-9)) for the output force to produce the output rotation is $\cos\delta_{FR} = 0.958777$. The minimum cosine of the variable deviation angle is $\cos\delta_{F23} = 0.632942$. The maximum allowable static friction coefficient to mechanism movability is 0.478643. The minimum plane element length and width are 1.511937 along the direction of the moving axis $\underline{b}$ and 1.962780 along the direction of the moving axis $\underline{c}$.

Figure (6-1) shows the output motions(in radian) of the mechanism. $\Theta_3$, $\dot{\Theta}_3$, and $\ddot{\Theta}_3$ are the angular displacement, angular velocity, and angular acceleration, respectively. Figure (6-2) shows the relative displacement of the Sp pair. The path is plotted by $\varepsilon_c$(the relative movement along the direction of moving axis $\underline{c}$) relative to $\varepsilon_b$(the relative movement along the direction of the moving axis $\underline{b}$). Figure (6-3) illustrates the thansmissivity and the corresponding deviation angles. The curve of force-to-torque transmissivity is the absolute value of the scalar product of

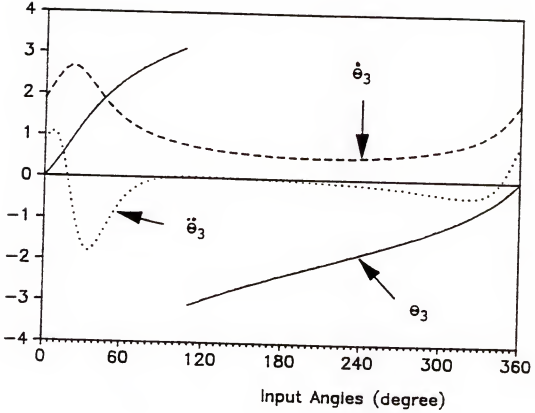


$\theta_3$: angular displacement (rad)

$\dot{\theta}_3$: angular velocity (rad/sec)

$\ddot{\theta}_3$: angular acceleration (rad/sec$^2$)

Figure 6-1 Output motion of R-Sp-R mechanism.

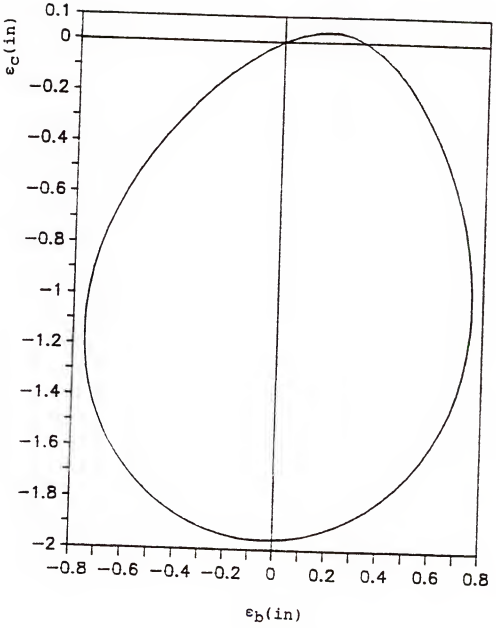


Figure 6-2 Relative path of the elements of the Sp pair.

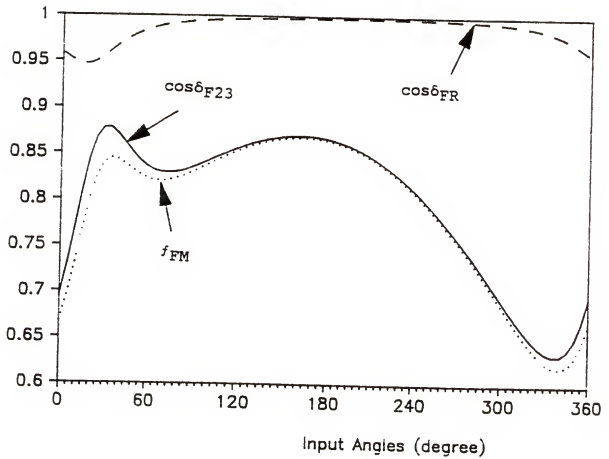


Figure 6-3 Force-to-Torque Transmissivity and the corresponding deviation angles.

$\cos\delta_{F23}$ and $\cos\delta_{FR}$ (see Equation (3-18)). Figure (6-4) shows the magnitudes of the normal force and sliding force with and without friction. Figure (6-5) shows the output torque with ($|M_r|$) and without ($|M_r^*|$) friction. Figure (6-6) shows the power loss which is the scalar product of the magnitude of sliding relative velocity and the magnitude of the friction force. The instantaneous efficiency (the ratio between the output power and the input power) is shown in Figure (6-7). Since the input power is unity, the instantaneous efficiency is numerically equal to the output power.

## 6.2 R-Cp-C Mechanisms

An R-Cp-C mechanism is illustrated in Figure (5-4), which is designed as a crank-rocker mechanism. The angular velocity of the input joint is unity. The output joint is attached to a translational and a rotational springs. The spring indexes for the translational and rotational springs are $k_t$ = 0.1 lbf/in and $k_r$ = 1 lbf/rad, respectively. The output force and torque are proportional to the translational and rotational displacements of the output link, as seen in Equations (4-15) and (4-16). Thus, the output link may contribute either positive or negative work. The input torque is an unknown quantity, which may also be doing positive or negative work to the input link. The static friction coefficient is set at $\mu$ = 0.27. The given variables are designated as follows:

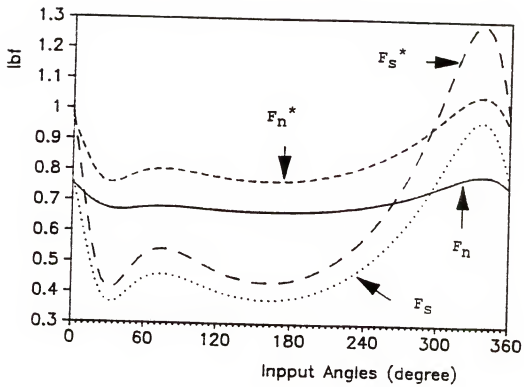


$F_n$: normal force with friction

$F_n^*$: normal force without friction

$F_s$: sliding force with friction

$F_s^*$: sliding force without friction

Figure 6-4 Normal forces and sliding forces at the Sp pair.

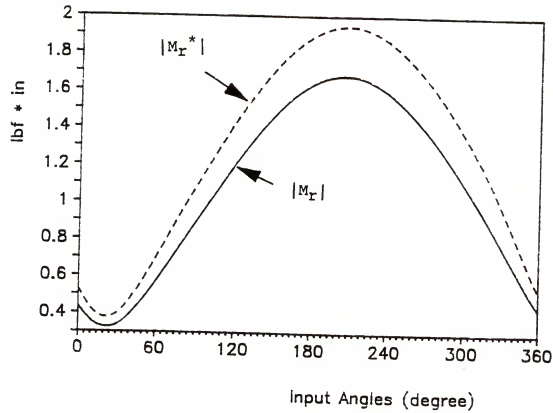


$M_r$: output torque with friction

$M_r^*$: output torque without friciton

Figure 6-5 Output torques.

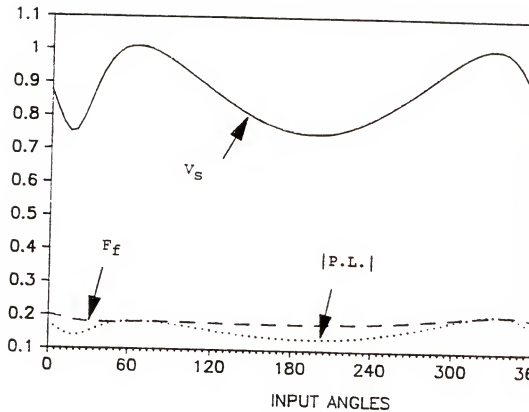


P.L.: power loss (lbf·in/sec)

$V_s$: relative sliding velocity (in/sec)

$F_f$: friction force (lbf)

Figure 6-6 Power loss.

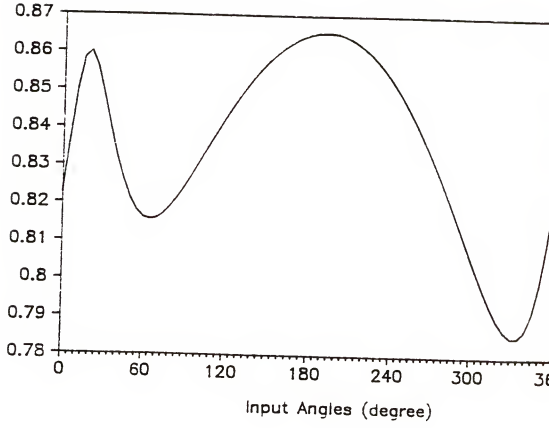


Figure 6-7 Instantaneous efficiency.

$\underline{u}_2 = (1.000000,\ 0.000000,\ 0.000000)^T$

$\underline{D}_2 = (0.000000,\ 0.000000,\ 0.000000)^T$

$\underline{u}_3 = (0.866025,\ 0.000000,\ 0.500000)^T$

$\underline{D}_3 = (0.000000,\ 1.000000,\ 0.000000)^T$

The input link length (the length of the common normal between $\underline{u}_2$ and $\underline{c}$) is set at 0.5. The following weighting factors set gives a better overall result considering the displacements and the deviation angles, which is

$$k_1 = k_2 = k_3 = k_4 = k_6 = 1, \quad k_5 = k_7 = 5$$

The local optimum point (see Equation 5-39) based on Equation (5-40) with the above weighting factors for one of the branches of the mechanism is found at

$\underline{X}$ = [-0.23213805E+00, 0.20730233E+01, 0.32297996E+01,
0.14631425E+01, 0.24620417E+00, 0.64163337E+00,
0.57991137E+00]$^T$

The corresponding parameters then are obtained as

$\underline{a} = (-0.036556,\ -0.700632,\ -0.712585)^T$

$\underline{b} = (\ 0.136410,\ \ 0.702889,\ -0.698097)^T$

$\underline{c} = (\ 0.998903,\ -0.046490,\ -0.005534)^T$

$\underline{P} = (\ 0.246204,\ \ 0.641633,\ \ 0.579911)^T$

The input link link length is equal to 0.500002. The minimum plane element length is 2.408281 along the direction of the moving axis $\underline{b}$. The minimum cylinder element length is 3.576647 along the direction of the moving axis $\underline{c}^*$. The fixed cosines of deviation angles for the output force to produce output translation and rotation are $\cos\delta_{FT}$ = 0.387951 and $\cos\delta_{FR}$ = 0.662558, respectively.

When the frictional effects are taken into account, the width of the plane element becomes essential. If the width of the plane element is small, i.e., the length of the contact line is short, the normal forces produced by the input torque at the two contact points at the edges of the plane element will be very large in order to produce enough transmitting moment. In this case, the corresponding friction forces become too large such that the mechanism may not be able to move at all. This can be observed from the virtual work equation such as Equation (4-23). The power loss is proportional to the absolute magnitudes of the normal force. The theoretical power loss may be larger than the input power if the absolute magnitudes of the normal force are too large. Then there is no way to produce positive output power in order to overcome the output resistant force and torque. Also, when solving the static equilibrium equations (4-19) and (4-20), there is no way to get positive values of the magnitudes of the reaction force no matter how the signs of the normal forces change due to a moment change. So, the width of the plane element is increased until Equations (4-19) and (4-20) can yield positive values for the magnitudes of the reaction forces with proper signs of the normal force vectors. The minimum plane width is found at W = 10 when the diameter of the cylinder element is neglected. Note that if the diameter of the cylinder element is counted, the width of the plane element needs to be increased. This is because there will be one more friction moment component as

illustrated in Equation (2-11). Thus, the power loss will be increased. Then, a longer contact line is needed to reduce the absolute magnitudes of the normal forces.

Figure (6-8) and (6-9) illustrate the translational and rotational output motions of the R-Cp-C mechanism. $\Theta_3$, $\dot{\Theta}_3$, and $\ddot{\Theta}_3$ are the angular displacement, angular velocity, and angular acceleration, respectively. $S_3$, $\dot{S}_3$, and $\ddot{S}_3$ are the linear displacement, linear velocity, linear acceleration, respectively. Figure (6-10) shows the relative displacement of the Cp pair. The path is plotted with the quantities $\varepsilon_c$ and $\varepsilon_b$ which are the relative movements of the initial midpoint of the contact line. Figure (6-11) illustrate the force-to-torque and force-to-force transmissivities (see Equations (3-18) and (3-21)) and the corresponding deviation angles. These deviation angles are measured at the midpoint of the contact line. The deviation angles measured at thetwo contact points are illustrated in Figure (6-12). $\cos\delta_{F231}$ and $\cos\delta_{F232}$ denote the deviation angles for internal force transmission. $\cos\delta_{FR1}$ and $\cos\delta_{FR2}$ denote the deviation angles for producing output rotational motion. Figure (6-13) shows the deviation angles for moment transmissions and the torque-to-torque transmissivity(see Equation (3-23)). Figures (6-14) and (6-15) show the normal forces with and without friction, respectively. The positive and negative values indicate the direction of the normal force. $F_{n1}$ and $F_{n2}$ denote the normal forces at the two contact points with friction. $F_{n1}^*$ $F_{n2}^*$ denote the normal

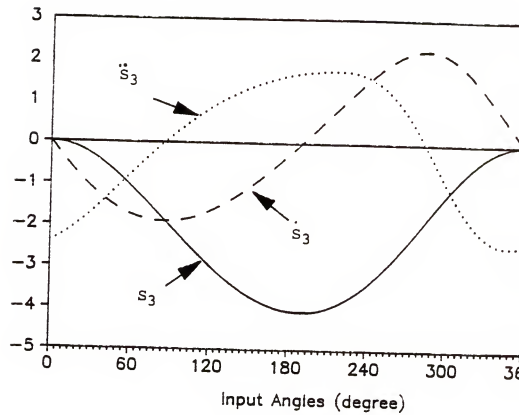


$s_3$: displacement (in)

$\dot{s}_3$: velocity (in/sec)

$\ddot{s}_3$: acceleration (in/sec$^2$)

Figure 6-8 Output translational motion of R-Cp-C mechanism.

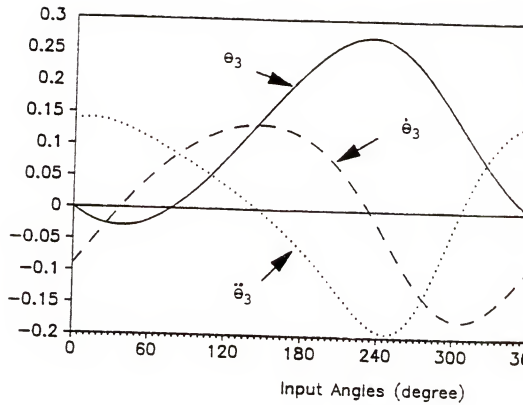


$\theta_3$: displacement (rad)

$\dot{\theta}_3$: velocity (rad/sec)

$\ddot{\theta}_3$: acceleration (rad/sec$^2$)

Figure 6-9 Output rotational motion of R-Cp-C mechanism.

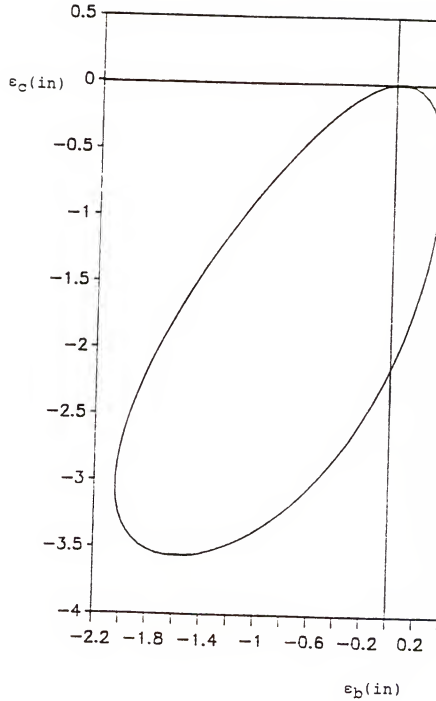


Figure 6-10 Relative displacement of the initial contact point(initially the midpoint of the contact line) at the Cp pair.

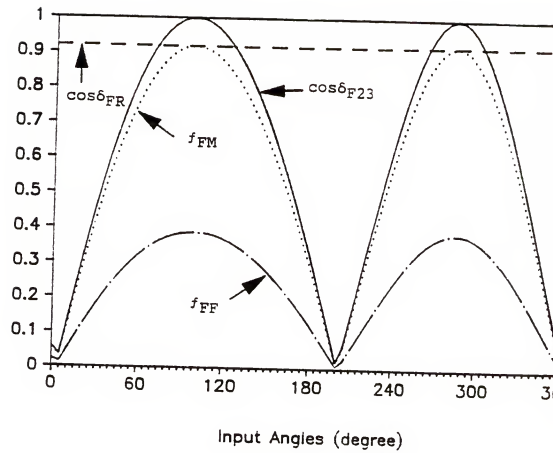


Figure 6-11 Force-to-Force and Force-to-Torque Transmissivities and the corresponding deviation angles.

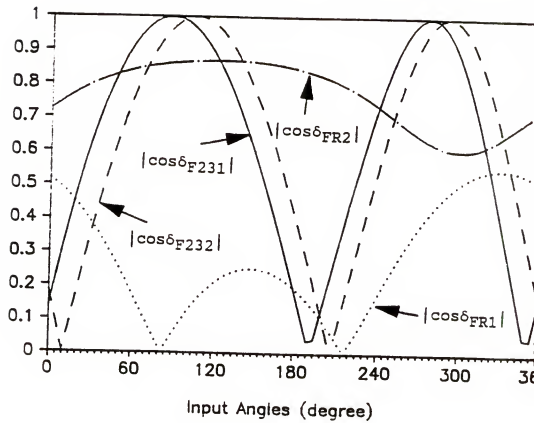


Figure 6-12 Deviation angles at the contact points.

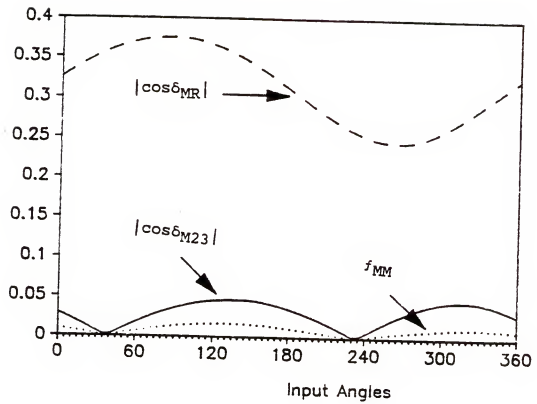


Figure 6-13 Torque-to-torque transmissivity and the corresponding deviation angles.

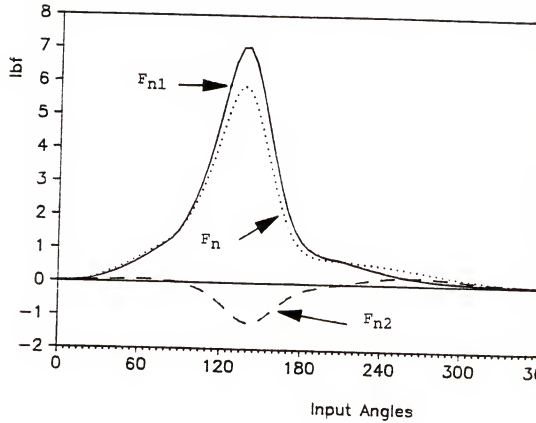


Figure 6-14 Normal forces at the Cp pair with firctional effects.

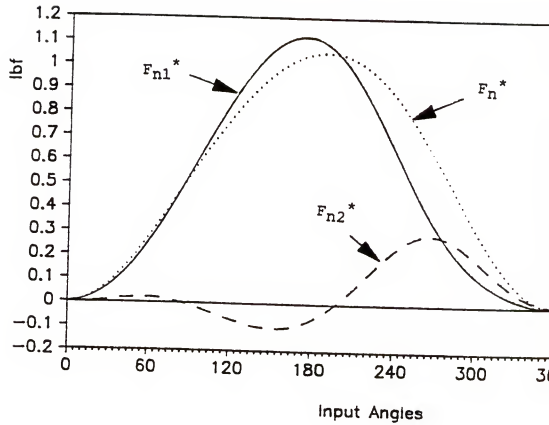


Figure 6-15 Normal forces at the Cp pair without frictional effects.

forces at the two contact points without friction. $F_n$ and $F_n^*$ denote the resultant normal forces with and without friction, respectively. In Figure (6-16), $|M_n|$ and $|M_n^*|$ are the magnitudes of the normal moments at the midpoint of the contact line of the Cp pair with and without friction, respectively. $|M_f|$ is the magnitude of the friction moment. Figure (6-17) illustrates the input power and power loss. The positive and negative values of the input and output power represent a positive and negative work contributed by the input joint or the output joint, respectively. Figure (6-18) shows the instantaneous efficiency. The first portion of the curve is the ratio of the output power at joint 3 to the input power at joint 2. The second portion of the curve is the reverse ratio since now joint 3 becomes the input and joint 2 becomes the output. The instantaneous efficiencies for output rotation and translation are not illustrated. The mechanical advantages are shown in Figure (6-19). The input force and output force are assumed applied at unity distance from joint 2 and joint 3, respectively. Then, the mechanical advantages are obtained from the ratios of output force and torque to input torque, respectively.

## 6.3 R-$P_L$-C-R Mechanisms

An R-$P_L$-C-R mechanism is shown in Figure (5-6), which is designed as a crank-crank type mechanism. The input joint is rotating with unit angular velocity ($\theta_2 = 1$

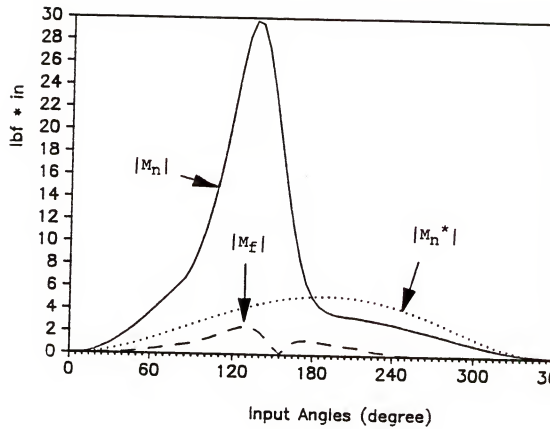


Figure 6-16 Moments at the Cp pair.

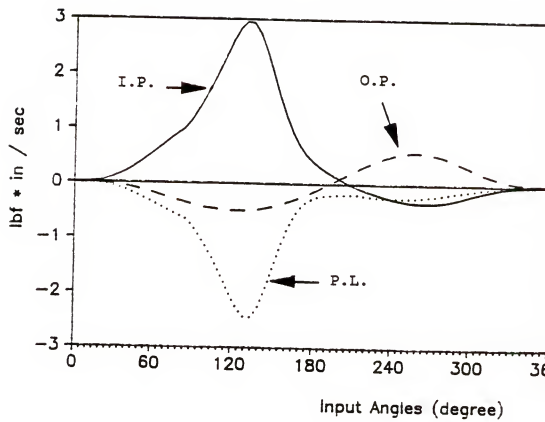


Figure 6-17 Input power(I.P.), output power(O.P.), and power loss(P.L.).

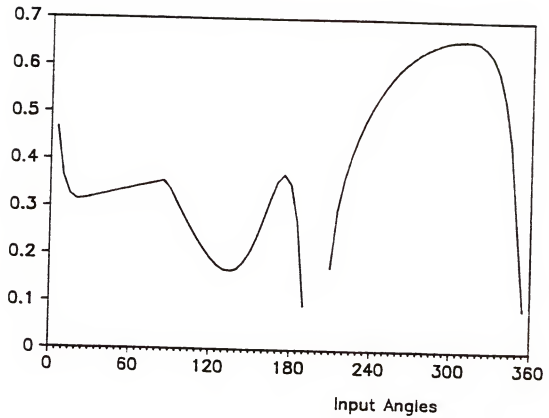


Figure 6-18 Instantaneous efficiency.

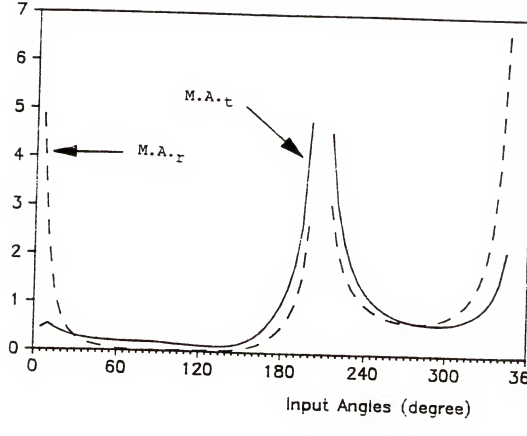


$M.A._t$: mechanical advantage for translatioal motion

$M.A._r$: mechanical advantage for rotational motion

Figure 6-19 Mechanical advantages.

rad/sec) and unit input torque ($M_d$ = 1 lbf·in). The static friction coefficient is set at $\mu$ = 0.27. The given variables are:

$$\underline{u}_2 = (1.000000,\ 0.000000,\ 0.000000)^T$$

$$\underline{D}_2 = (0.000000,\ 0.000000,\ 0.000000)^T$$

$$\underline{u}_4 = (0.866025,\ 0.000000,\ 0.500000)^T$$

$$\underline{D}_4 = (0.000000,\ 1.000000,\ 0.000000)^T$$

The input and output link lengths are set at 0.8 and 0.4, respectively. The wighting factors are chosen as

$$k_i = 1; \quad i = 1, 2, 3, 4, 5, 6, 7, 8, 9, 11, 13$$

$$k_j = 3; \quad j = 10, 12$$

The optimal design variables based on Equation (5-42) with the above weighting factors for one of the branches are found at

$$\underline{X} = [\ 0.64428810E+00,\ \ 0.22138480E+01,\ \ 0.14650180E+01$$
$$0.28783130E+01,\ \ 0.11716420E+01,\ \ 0.19570740E+01$$
$$0.16722840E+01,\ \ 0.99362500E+00,\ -0.40688370E+00$$
$$0.75471430E+00,\ -0.88621710E-02,\ -0.38934150E+00$$
$$0.88036170E+00]^T.$$

The corresponding parameters are obtained as

$$\underline{a} = (-0.082442,\ \ 0.311164,\ -0.946774)^T$$

$$\underline{b} = (\ 0.481539,\ -0.819312,\ -0.311203)^T$$

$$\underline{c} = (-0.916835,\ -0.396079,\ -0.050339)^T$$

$$\underline{P} = (\ 0.993625,\ -0.406884,\ \ 0.754714)^T$$

$$\underline{u}_3 = (\ 0.046998,\ \ 0.965289,\ -0.256921)^T$$

$$\underline{D}_3 = (-0.008862,\ -0.389342,\ \ 0.880362)^T$$

The input and output link lengths are equal to 0.799992 and

0.39995. The minimum inner plane length along the direction of the moving axis $\underline{c}^*$ is 1.4049. The minimum outer plane length along the direction of the moving axis $\underline{b}$ is 3.4710. The fixed deviation angles $\delta_{F34}$ and $\delta_{M23}$ are found at $\cos\delta_{F34} = 0.841836$ and $\cos\delta_{M23} = 0.996596$. Similar to the R-Cp-C mechanism, the widths of the plane elements affect the magnitudes of the normal forces. The sufficient widths for both plane elements are 2.4, for which Equations (4-34) to (4-36) can yield positive values for the reaction forces with proper signs of the normal force vectors.

Figure (6-20) shows the output motions. The rotational and translational motions of link 3 with respect to link 4, connected by the floating C joint are shown in Figure (6-21) and (6-22), respectively. The relative displacement of the $P_L$ pair is shown in Figure (6-23). The path is the relative movement of the initial gravity center of link 2 between the two plane elements, refered to the plane elememt of link 3. Figure (6-24) shows the deviation angles for force transmission at the three contact points on the $P_L$ pair (see Appendix C). Figure (6-25) shows the force-to-torque transmissivity (see Equation (3-26)) which is the product of $\cos\delta_{F23}$, $\cos\delta_{FR}$ and the invariant $\cos\delta_{F34}$. The curve of $\cos\delta_{F23}$ is taken from the assumption that the force is transmitted at the gravity center of the contact surface. Figure (6-26) shows the torque-to-torque transmissivity (see Equation (3-30) and the corresponding cosines of deviation angles $\delta_{M34}$ and $\delta_{MR}$.

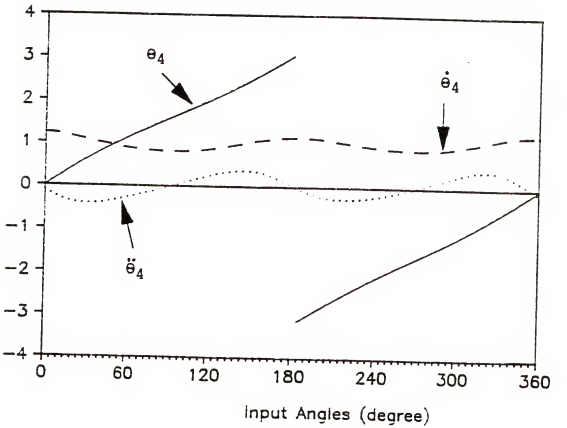


$\theta_4$: displacement (rad)

$\dot{\theta}_4$: velocity (rad/sec)

$\ddot{\theta}_4$: acceleration (rad/sec$^2$)

Figure 6-20 Output motion of R-$P_L$-C-R mechanism.

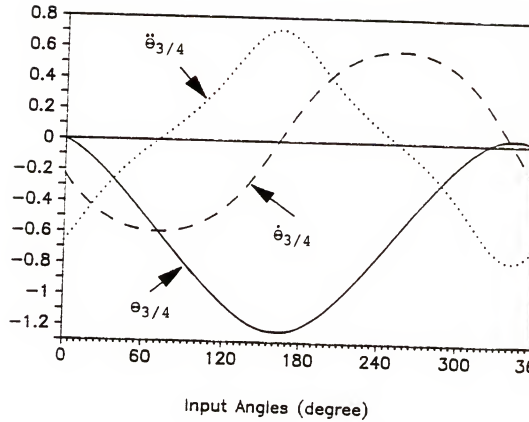


$\theta_3$: displacement (rad)

$\theta_3$: velocity (rad/sec)

$\theta_3$: acceleration (rad/sec$^2$)

Figure 6-21 Relative rotational motion of link 3 with respect to link 4 in the C joint.

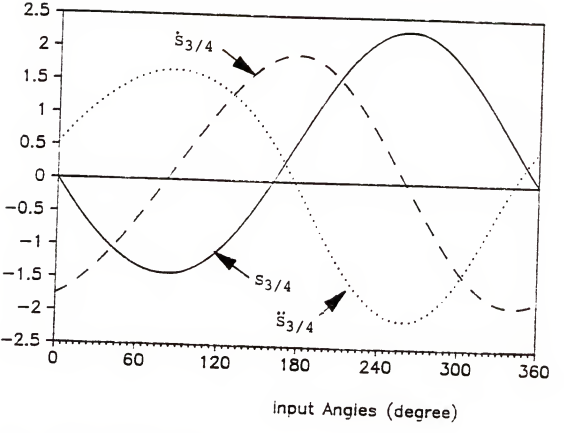


$s_3$: displacement (in)

$\dot{s}_3$: velocity (in/sec)

$\ddot{s}_3$: acceleration (in/sec$^2$)

Figure 6-22 Relative translational motion of link 3 with respect to link 4 in the C joint.

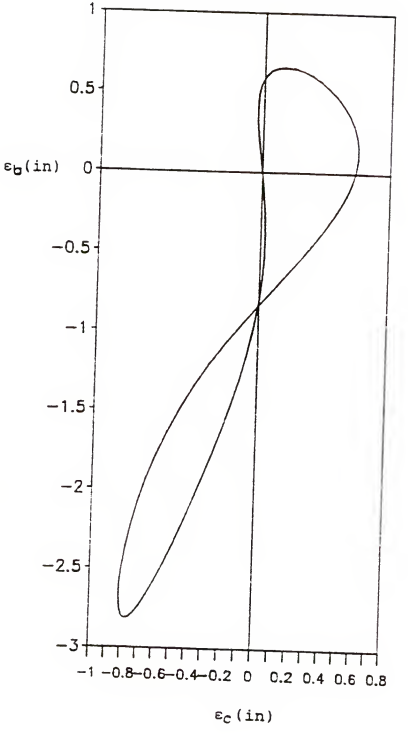


Figure 6-23 Relative displacement of elements of the $P_L$ pair: path of a point of link 2 with respect to link 3.

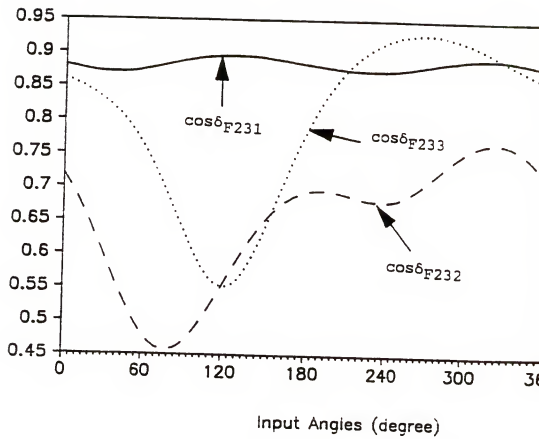


Figure 6-24 Deviation angles for internal force transmission at the three contact points.

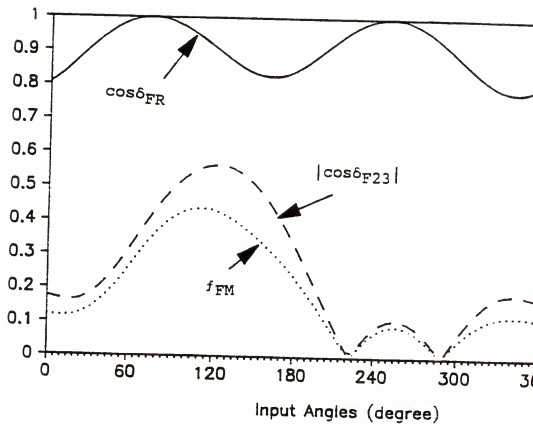


Figure 6-25 Force-to-torque transmissivity and the corresponding deviation angles ($\cos\delta_{F34}$ = 0.841836).

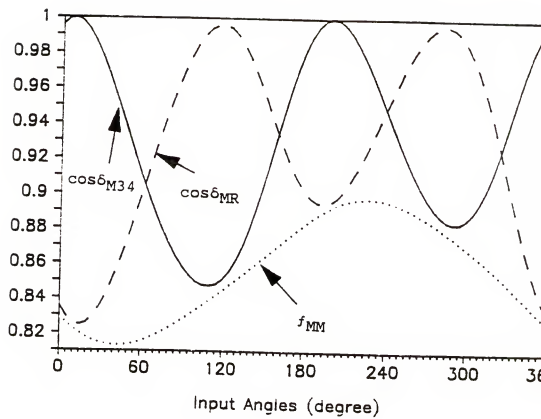


Figure 6-26 Torque-to-torque transmissivity and the corresponding deviation angles ($\cos\delta_{M23}$ = 0.996596).

Figure (6-27) shows the (force torque)[1]-to-torque transmissivity (see Equation (3-36) and the corresponding cosines of deviation angles $\delta_{FM34}$, $\delta_{FMR}$. Figure (6-28) and (6-29) show the transmitted normal forces at the three contact points and the summation of these three normal forces with and without frictional effects, respectively.

When there is no friction, the summation of the three normal forces is zero. This indicates there is no force transmitted through the $P_L$ pair. This can be explaned by the free-body diagram of the R-$P_L$-C-R mechanism (Figure 4-3) and the facts:

1. The C joint is assumed frictionless so that there is no force transmitted along the direction of the joint axis (see Equation (4-30)).
2. The normal of the plane element can not be perpendicular to the axis of the C joint to prevent the infinite sliding (see Equation (F-7)).

The moments taken at the gravity center of the $P_L$ pair are shown in Figure (6-30). $|M_n|$ and $|M_n^*|$ denote the magnitudes of the normal moments with and without friction. $|M_f|$ denotes the absolute magnitude of the friction moment. Figure (6-31) shows the magnitudes of the output torque with and without frictional effects, the output power, and the power loss. $|M_r|$ denotes the output torque with friction. $|M_r^*|$ denote the output torque without friction. Since the

---

1. The torque exerted by the transmitted force in the $P_L$ pair induced at the C joint

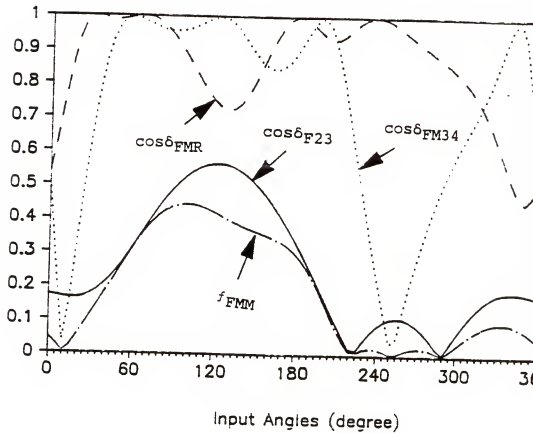


Figure 6-27 Force torque-to-torque transmissivity and the corresponding deviation angles.

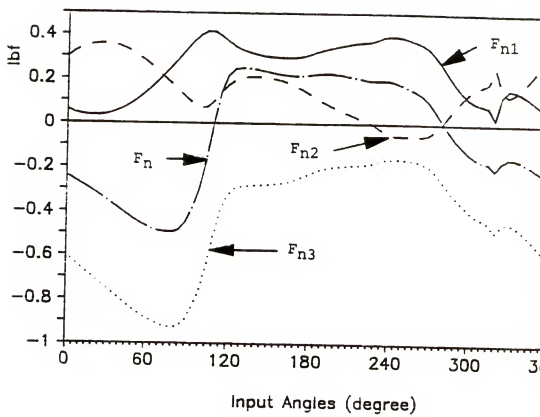


Figure 6-28 Transmitted normal forces at the $P_L$ pair with fricitonal effects.

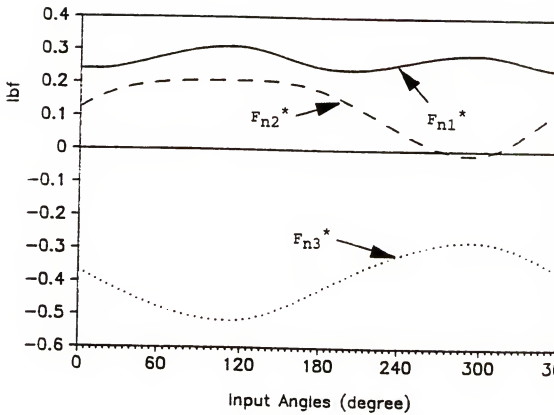


Figure 6-29 Transmitted normal forces at the $P_L$ pair without fricitonal effects.

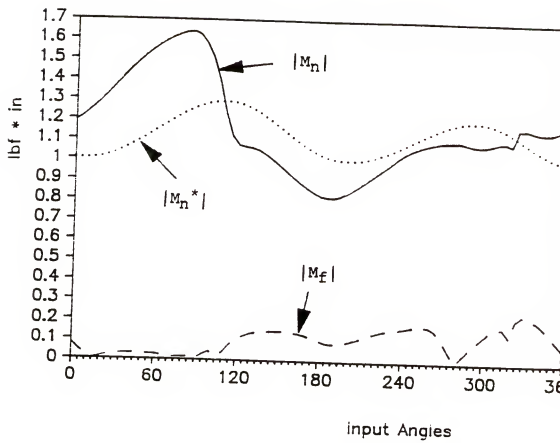


Figure 6-30 Moments at the gravity center of the $P_L$ pair.

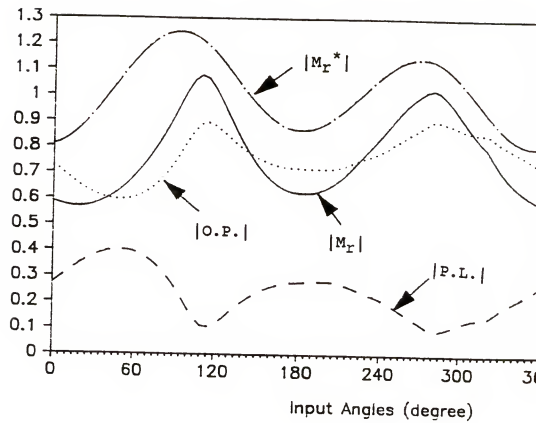


Figure 6-31 Output torque with friction ($M_r$), output torque without friction ($M_r^*$), output power(O.P.), and power loss(P.L.).

input torque is unity, the mechanical advantage is numerically equal to the output torque. Also, the input power is unity, thus, the instantaneous efficiency is numerically equal to the output power.

# CHAPTER 7
# CONCLUSIONS AND RECOMMENDATIONS FOR FUTURE RESEARCH

## 7.1 Conclusions

The transmission characteristics of spatial mechanisms containing one higher pair has been illustrated by the use of deviation angles and transmissivities. Similar definitions are applied to spatial mechanisms containing lower pairs only. This study provides a full understanding of the way to improve transmission quality. The deviation angles for internal force and moment transmissions provide a clear view of the characteristics of each specific pair. Thereafter, the transmissivities link the corresponding deviation angles to show the contributions of the input force or torque to the resistant force and/or torque. Thus, the transmission quality of mechanisms can be improved by using the criteria developed in this work in the design optimization.

The force analysis of the higher pairs and some lower pairs in Chapter 2 provides a basic understanding of these pairs. The way how the forces and torques are transmitted is related to the geometric constraints of the pairs. It has been shown that the force-closed higher pairs possess a transmission characteristic that needs to be paid more attentions to prevent separation of the pair elements. After

the transmission of force and torque at each pair are analyzed, the deviation angles and transmissivities can be defined as shown in Chapter 3. With all those criteria and the numerous design variables, the search of a mechanism with better transmission quality has not been easy. Thus, a feasible mechanism must be found before all the constraints are taken into account. Then, the mechanisms can be further optimized according to the objectives. However, the examples are quite general in their design purposes. These examples are only used to show the characteristics of these particular mechanisms. The emphasis should be on the potential usages of these design criteria. They can be included as constraints or part of the objective function for the design of other types of mechanisms.

Friction always plays a significant role in mechanism design. When friction is involved, the way of modeling the reaction forces and moments becomes important. There is more than one way to model the forces and moments acting in specific pairs for static force and torque analysis. The forces and moments in this work have been modeled in such a way that the frictional effects can be obtained directly. From the examples in Chapter 6, we observed that friction does affect the dimensions of the higher pairs. Of course, friction also affects the efficiency of the mechanisms. It can be foreseen that with the consideration of friction in each joint, friction needs much more careful attentions. If all joints are considered with friction, the force and

torques will have to be solved for iteratively. This is especially true when link masses are included. If the masses are considered, elastic analysis will be needed for those mechanisms that are statically indeterminate.

The main objective of this work is to look into the transmission characteristics and it has been done by the use of deviation angles and transmissivities. Including the static force and torque analysis exposes the significant frictional effects. It is hoped that this work fulfilled the absence of the definitions of transmission criteria in spatial mechanisms containing higher pairs. It is also hoped that this work brought more attentions to the area of frictional effects in mechanism design.

## 7.2 Recommendations

With the design criteria of transmission quality having been defined, including these criteria in the synthesis procedures becomes possible. These synthesis procedures can include motion generation or path generation.

The examples in this work are limited to mechanisms whose configuration has two branches only. Otherwise, it would be difficult to optimize the mechanisms to satisfy the constraints during the entire range of motion. For those mechanisms having more than two branches, the avoidance of branching and sequence defects becomes essential.

As mentioned in the previous section, dynamic analysis including the frictional effects is a worthwhile objective

for further research. However, it can be expected that a certain degree of difficulties will be encountered.

## APPENDIX A
## RELATIVE DISPLACEMENTS OF AN Sp PAIR

The contour of the plane in the Sp pair has been derived by Hernandez (1983), which also includes the design of the inner sphere and its' inserted rod. In this work, the detailed design of the pair elements is not considered except for the physical size of the plane element. It is necessary to limit the size of the plane element in the optimization process since the contour of the plane may be very large to satisfy some of the constraints. Therefore, a procedure similar to that illustrated by Hernandez to determine the contour of the plane element is adopted here. A coordinate system consisting of $\underline{a}$, $\underline{b}$, and $\underline{c}$ axes is attached to the plane where the origin is located at the initial contact point P, as shown in Figure (A-1). Let $\underline{a}$ be the normal of the plane element; $\underline{b}$ and $\underline{c}$ are on the contacting plane. The j-th position vectors of the initial contact point derived by starting out from the input and output joint axes are denoted as $\underline{P}_j$ and $\underline{P}_{j'}$, respectively. Then we may write the following equation

$$\underline{P}_j = \underline{P}_{j'} + \varepsilon_{bj}\underline{b}_{j'} + \varepsilon_{cj}\underline{c}_{j'} \qquad \text{(A-1)}$$

where $\varepsilon_{bj}$ and $\varepsilon_{cj}$ denote the relative displacements between the contact point along $\underline{b}_{j'}$ and $\underline{c}_{j'}$ axes, respectively; here $\underline{b}_{j'}$ and $\underline{c}_{j'}$ are obtained by starting out from the output

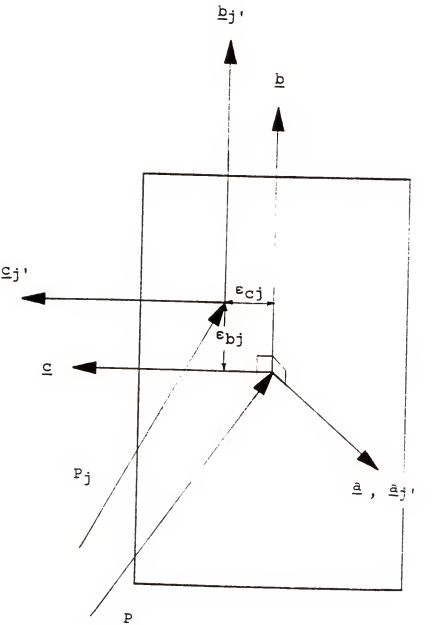


Figure A-1 Relative displacements of the Sp pair.

joint axis, since the plane is assumed to be connected to the output joint. The scalars $\varepsilon_{bj}$ and $\varepsilon_{cj}$ may be obtained by taking the dot product of Equation (A-1) with $\underline{b}_{j'}$ and $\underline{c}_{j'}$, respectively, which gives

$$\varepsilon_{bj} = (\underline{P}_j - \underline{P}_{j'}) \cdot \underline{b}_{j'} \tag{A-2}$$

and

$$\varepsilon_{cj} = (\underline{P}_j - \underline{P}_{j'}) \cdot \underline{c}_{j'} \tag{A-3}$$

The difference of the maximum positive and negative values of $\varepsilon_{bj}$ gives the extent along axis $\underline{b}$ of the plane element needed. Similarly, the extent along axis $\underline{c}$ is determined by the maximum positive and negative values of $\varepsilon_{cj}$. The plot of the two scalars $\varepsilon_{bj}$ and $\varepsilon_{cj}$ gives the contour of the plane element.

## APPENDIX B
## RELATIVE DISPLACEMENTS OF A Cp PAIR

The line of action of the force in the Cp pair can be considered to pass through the axis of the cylinder. Thus, the contact line can be assumed to be parallel to the axis of the cylinder. Figure (B-1) shows the initial and j-th position of the mid-point P of contact line $\underline{c}^*$. A mooving coordinate system consists of the normal of the plane, $\underline{a}$, and the vectors $\underline{b}$ and $\underline{c}$. The vector $\underline{c}^*$ is the axis of the cylinder element and forms an angle $\beta$ with $\underline{b}$. Thus, we may consider $\underline{c}^*$ to be rotated about $\underline{a}$ by the relative rotation angle $\beta$ formed with $\underline{b}$. Then we may write

$$\underline{c}^* = \cos\beta\underline{b} + \sin\beta(\underline{a} \times \underline{b}) \qquad \text{(B-1)}$$

The two scalars $\varepsilon_{cj}$ and $\varepsilon_{bj}$ define the required extent of the plane and length of the cylinder to prevent separation at this j-th position. Then, we may have the relationship of the position vectors of point P expressed as

$$\underline{P}_{j'} + \varepsilon_{bj}\underline{b}_{j'} = \underline{P}_j + \varepsilon^*_{cj}\underline{c}^*_j \qquad \text{(B-2)}$$

where for the case of $P_2$-Cp-$P_2$ three-link mechanism with the plane connected to the input link and the cylinder connected to the output link, and:

$$\underline{c}^*_j = \underline{c}^* + (\cos\theta_2 - 1)\underline{U}_{2c}{}^* + \sin\theta_2(\underline{u}_2 \times \underline{c}^*) \qquad \text{(B-3)}$$

$$\underline{b}_{j'} = \underline{b} + (\cos\theta_3 - 1)\underline{U}_{3b} + \sin\theta_3(\underline{u}_3 \times \underline{b}) \qquad \text{(B-4)}$$

$$\underline{P}_j = \underline{P} + (\cos\theta_2 - 1)\underline{U}_{2Q2} + \sin\theta_2(\underline{u}_2 \times \underline{Q}_2) \qquad \text{(B-5)}$$

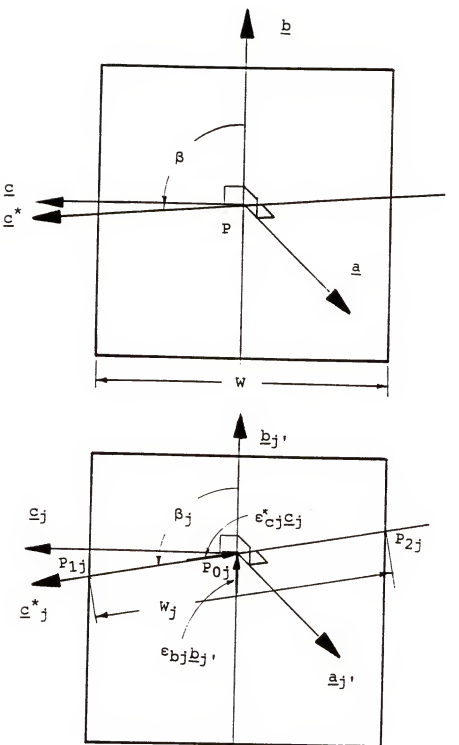


Figure B-1 Relative displacements of the Cp pair.

$$\underline{P}_{j'} = \underline{P} + (\cos\theta_3 - 1)\underline{U}_{3\underline{Q}3} + \sin\theta_3(\underline{u}_3 \times \underline{Q}_3) \qquad \text{(B-6)}$$

where

$$\underline{U}_{2\underline{c}}{}^* = (\underline{u}_2 \times \underline{c}^*) \times \underline{u}_2;$$

$$\underline{U}_{3\underline{b}} = (\underline{u}_3 \times \underline{b}) \times \underline{u}_3;$$

$$\underline{U}_{i\underline{Q}i} = (\underline{u}_i \times \underline{Q}_i) \times \underline{u}_i;$$

$$\underline{Q}_i = \underline{P}_i - \underline{D}_i; \quad i = 2, 3$$

$\underline{P}_j$ and $\underline{c}^*{}_j$ are the j-th position vector of the contact point and the unit vector of the direction of the cylinder element axis, respectively, derived by starting out from the input axis (i.e., a point fixed to the plane that is connected to the input link). $\underline{P}_{j'}$ and $\underline{b}_{j'}$ are the j-th position vectors of the same contact point and the unit vector parallel to the U-shape element, respectively, derived from the output axis (i.e., a point fixed to the inner plane which is connected to the output link). $\underline{P}$ is the initial position vector of the contact point; $\underline{D}_i$ is the vector from the origin to the axis $\underline{u}_i$; $\theta_i$ is the relative rotation of the i-th joint.

By taking the scalar product of Equation (B-2) with $(\underline{c}^*{}_j \times \underline{P}_j)$ and $(\underline{b}_{j'} \times \underline{P}_{j'})$ respectively, gives the two scalars as

$$\varepsilon_{bj} = - \frac{\underline{P}_{j'} \cdot \underline{c}^*{}_j \times \underline{P}_j}{\underline{b}_{j'} \cdot \underline{c}^*{}_j \times \underline{P}_j} \qquad \text{(B-7)}$$

and

$$\varepsilon^*{}_{cj} = - \frac{\underline{P}_j \cdot \underline{b}_{j'} \times \underline{P}_{j'}}{\underline{c}^*{}_j \cdot \underline{b}_{j'} \times \underline{P}_{j'}} \qquad \text{(B-8)}$$

The contour of the plane element can be obtained by plotting the scalar $\varepsilon_{bj}$ along the $\underline{b}$ axis and $\sin\beta_j \varepsilon^*_{cj}$ along $\underline{c}$ axis. The largest values of $\varepsilon_{bj}$ and $\varepsilon^*_{cj}$ determine the extent of the plane and the minimum length of the cylinder, respectively. If the width of the plane is denoted as W, the end points of the contact line can be expressed as

$$\underline{P}_{1j} = \underline{P}_{0j} + (W_j/2)\underline{c}^*_j \qquad \text{(B-9)}$$

$$\underline{P}_{2j} = \underline{P}_{0j} - (W_j/2)\underline{c}^*_j \qquad \text{(B-10)}$$

where

$$\underline{P}_{0j} = \underline{P}_j + \varepsilon^*_{cj}\underline{c}^*_j = \underline{P}_{j'} + \varepsilon_{bj}\underline{b}_{j'} \text{ and}$$

$$W_j = W/\sin\beta_j.$$

## APPENDIX C
## RELATIVE DISPLACEMENTS OF A $P_L$ PAIR

A procedure similar to that in Appendix B can be used to derive the position of the contact points of the $P_L$ pair (see Figure C-1). The same coordinate system is used to derive the two scalars $\varepsilon_{bj}$ and $\varepsilon^*_{cj}$ as in Equations (B-3, B-4). The lengths of the inner plane and the U-Shaped outer plane element are determined by the positive maximum values of $\varepsilon^*_{cj}$ and $\varepsilon_{bj}$, respectively. The position of the four possible contact points, i.e, the four corners of the contact surface, can be expressed as

$$\underline{P}_{1j} = \underline{P}_{0j} + (H_j/2)\underline{b}_{j'} + (W_j/2)\underline{c}^*_j \qquad \text{(C-1)}$$

$$\underline{P}_{2j} = \underline{P}_{0j} + (H_j/2)\underline{b}_{j'} - (W_j/2)\underline{c}^*_j \qquad \text{(C-2)}$$

$$\underline{P}_{3j} = \underline{P}_{0j} - (H_j/2)\underline{b}_{j'} - (W_j/2)\underline{c}^*_j \qquad \text{(C-3)}$$

$$\underline{P}_{4j} = \underline{P}_{0j} - (H_j/2)\underline{b}_{j'} + (W_j/2)\underline{c}^*_j \qquad \text{(C-4)}$$

where $\underline{P}_{0j}$, $W_j$ ,and $\underline{c}^*_j$ are defined the as in Appendix B; and

$$\underline{b}_{j'} = \underline{b}_{j3} + (\cos\theta_4 - 1)\underline{U}_4\underline{b}_{j3} + \sin\theta_4(\underline{u}_4 \times \underline{b}_{j3})$$

$$\underline{b}_{j3} = \underline{b} + (\cos\theta_3 - 1)\underline{U}_3\underline{b} + \sin\theta_3(\underline{u}_3 \times \underline{b})$$

$$H_j = H/\sin\beta_j$$

The quantity H is the width of the inner plane element, W is the width of the U-Shaped outer plane element. Then, the three contact points as used in Chapter 2 for modeling the reaction force and moment can be arbitrarily chosen from the four corner points. Similar to the Cp pair, the contour of

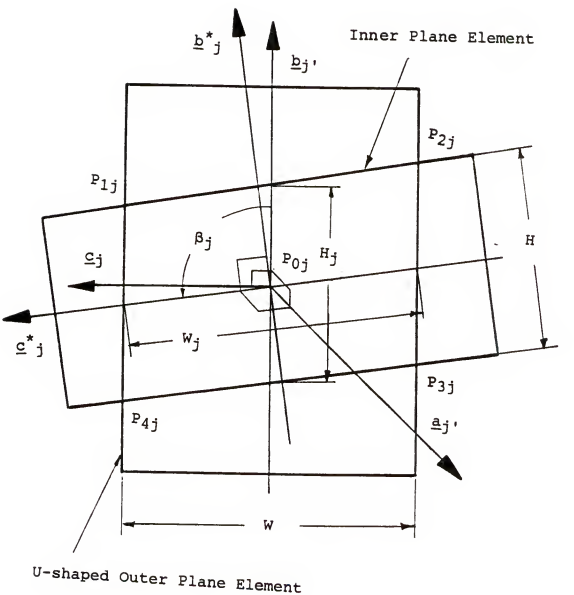


Figure C-1 Relative displacements of the $P_L$ pair.

the U-shaped outer plane element can be plotted by the two scalars $e_{bj}$ and $\sin\beta_j \varepsilon^*_{cj}$ which are the relative displacements along the in-plane coordinates $\underline{b}$ and $\underline{c}$, respectively.

## APPENDIX D
## DISPLACEMENT EQUATIONS OF R-Sp-R MECHANISM

Figure (D-1) shows the j-th position of an R-Sp-R mechanism. The constraint equation is

$$(\underline{P}_j' - \underline{P}_j) \cdot \underline{a}_j' = 0 \qquad \text{(D-1)}$$

where

$$\underline{P}_j = \underline{P} + (\cos\theta_2 - 1)\underline{U}_{2\underline{Q}2} + \sin\theta_2(\underline{u}_2 \times \underline{Q}_2)$$

$$\underline{P}_j' = \underline{P} + (\cos\theta_3 - 1)\underline{U}_{3\underline{Q}3} + \sin\theta_3(\underline{u}_3 \times \underline{Q}_3)$$

$$\underline{a}_j' = \underline{a} + (\cos\theta_3 - 1)\underline{U}_{3\underline{a}} + \sin\theta_3(\underline{u}_3 \times \underline{a})$$

and

$$\underline{U}_{i\underline{Q}3} = (\underline{u}_i \times \underline{Q}_i) \times \underline{u}_i; \qquad \underline{Q}_i = \underline{P} - \underline{D}_i \qquad i = 2, 3$$

$$\underline{U}_{3\underline{a}} = (\underline{u}_3 \times \underline{a}) \times \underline{u}_3.$$

By rewriting

$$\underline{P}_j' = \underline{Q}_3 + (\cos\theta_3 - 1)\underline{U}_{3\underline{Q}3} + \sin\theta_3(\underline{u}_3 \times \underline{Q}_3) + \underline{D}_3 \qquad \text{(D-2)}$$

which can be denoted as $\underline{Q}_{3j}'$, the constraint equation can be simplified to be

$$\underline{Q}_3 \cdot \underline{a} + (\underline{D}_3 - \underline{P}_j) \cdot \underline{a}_j' = 0 \qquad \text{(D-3)}$$

Then, the above equation can be rearranged into a quadratic equation in terms of $X_3$, where $X_3 = \tan^{-1}(\theta_3/2)$, $\cos\theta_3 = (1 - X_3^2)/(1 + X_3^2)$, and $\sin\theta_3 = 2X_3/(1 + X_3^2)$, as

$$aX_3^2 + bX_3 + c = 0 \qquad \text{(D-4)}$$

where

$$a = (\underline{P} - \underline{P}_j) \cdot \underline{a} - 2(\underline{D}_3 - \underline{P}_j) \cdot \underline{U}_{3\underline{a}}$$

$$b = 2(\underline{D}_3 - \underline{P}_j) \cdot \underline{u}_3 \times \underline{a}$$

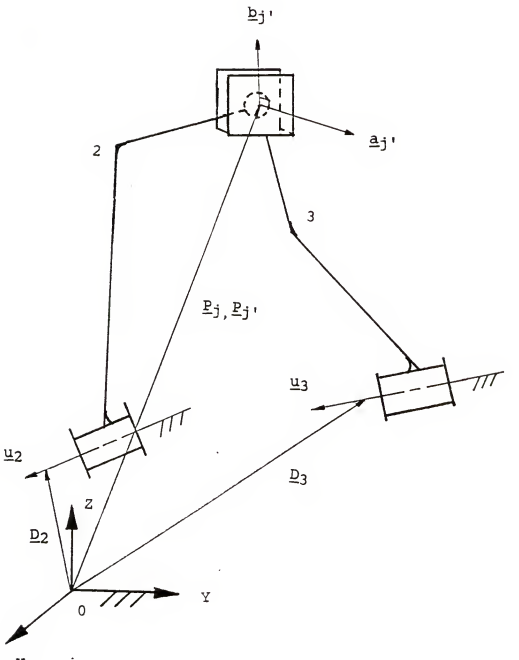


Figure D-1 The R-Sp-R mechanism in the j-th position.

$$c = (\underline{P} - \underline{P}_j) \cdot \underline{a}$$

The angular velocity $\dot{\theta}_3$ is obtained by taking time derivative of Equation (D-1) with $\dot{\theta}_2$ constant, which gives

$$\dot{\theta}_3 = \left[ \frac{\underline{P}'_j \cdot \underline{a}_{j'}}{\underline{P}'_{j'} \cdot \underline{a}_{j'} + (\underline{P}_{j'} - \underline{P}_j) \cdot \underline{a}'_{j'}} \right] \dot{\theta}_2 \qquad \text{(D-5)}$$

where

$$\underline{P}'_j = - \sin\theta_2 \underline{U}_2 \underline{Q}_2 + \cos\theta_2 (\underline{u}_2 \times \underline{Q}_2)$$

$$\underline{a}'_{j'} = - \sin\theta_3 \underline{U}_3 \underline{a} + \cos\theta_3 (\underline{u}_3 \times \underline{a})$$

$$\underline{P}'_{j'} = - \sin\theta_3 \underline{U}_3 \underline{Q}_3 + \cos\theta_3 (\underline{u}_3 \times \underline{Q}_3)$$

By taking time derivatives twice of Equation (D-2) gives the angular acceleration of the output link, as

$$\ddot{\theta}_3 = \frac{-(d\dot{\theta}_3^2 + e\dot{\theta}_2\dot{\theta}_3 + f\dot{\theta}_2^2)}{g} \qquad \text{(D-6)}$$

where

$$d = \underline{P}''_{j'} \cdot \underline{a}_{j'} + 2(\underline{P}'_{j'} \cdot \underline{a}'_{j'}) + (\underline{P}_{j'} - \underline{P}_j) \cdot \underline{a}''_{j'}$$

$$e = - 2\underline{P}'_j \cdot \underline{a}'_{j'}$$

$$f = - \underline{P}''_j \cdot \underline{a}_{j'}$$

$$g = \underline{P}'_{j'} \cdot \underline{a}_{j'} + (\underline{P}_{j'} - \underline{P}_j) \cdot \underline{a}'_{j'}$$

and

$$\underline{P}''_{j'} = - \cos\theta_3 \underline{U}_3 \underline{Q}_3 - \sin\theta_3 (\underline{u}_3 \times \underline{Q}_3)$$

$$\underline{a}''_{j'} = - \cos\theta_3 \underline{U}_3 \underline{a} - \sin\theta_3 (\underline{u}_3 \times \underline{a})$$

## APPENDIX E
## DISPLACEMENT EQUATION OF R-Cp-C MECHANISM

Figure (E-1) shows the j-th position of the R-Cp-C mechanism. The constraint equations are written

$$(\underline{P}_{j'} - \underline{P}_j) \cdot \underline{a}_{j'} = 0 \tag{E-1}$$

$$\underline{a}_{j'} \cdot \underline{c}^*_j = 0 \tag{E-2}$$

where

$$\underline{P}_{j'} = \underline{P} + (\cos\theta_3 - 1)\underline{U}_3\underline{Q}_3 + \sin\theta_3(\underline{u}_3 \times \underline{Q}_3) + S_3\underline{u}_3$$

$$\underline{P}_j = \underline{P} + (\cos\theta_2 - 1)\underline{U}_2\underline{Q}_2 + \sin\theta_2(\underline{u}_2 \times \underline{Q}_2)$$

$$\underline{a}_{j'} = \underline{a} + (\cos\theta_3 - 1)\underline{U}_3\underline{a} + \sin\theta_3(\underline{u}_3 \times \underline{a})$$

$$\underline{c}^*_j = \underline{c}^* + (\cos\theta_2 - 1)\underline{U}_2\underline{c}^* + \sin\theta_2(\underline{u}_2 \times \underline{c}^*)$$

and

$$\underline{U}_3\underline{Q}_3 = (\underline{u}_3 \times \underline{Q}_3) \times \underline{u}_3; \qquad \underline{U}_2\underline{Q}_2 = (\underline{u}_2 \times \underline{Q}_2) \times \underline{u}_2;$$

$$\underline{U}_3\underline{a} = (\underline{u}_3 \times \underline{a}) \times \underline{u}_3; \qquad \underline{U}_2\underline{c}^* = (\underline{u}_2 \times \underline{c}^*) \times \underline{u}_2;$$

$$\underline{Q}_i = \underline{P} - \underline{D}_i \qquad i = 2, 3$$

By the use of the tangent of the half angle of $\theta_3$, Equation (E-2) can be written into a quadratic equation.

$$aX_3^2 + bX_3 + c = 0 \tag{E-3}$$

where

$$a = (\underline{a} - 2\underline{U}_3\underline{a}) \cdot \underline{c}^*_j$$

$$b = 2\underline{u}_3 \times \underline{a} \cdot \underline{c}^*_j$$

$$c = \underline{a} \cdot \underline{c}^*_j$$

The coefficients a, b, and c are functions of the input angle $\theta_2$.

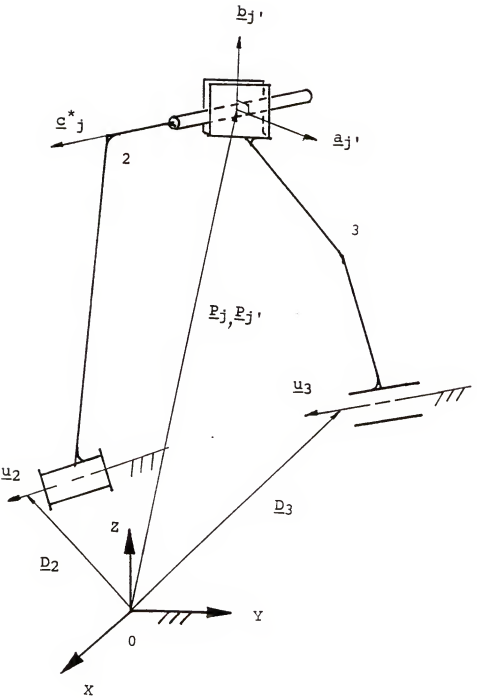


Figure E-1 The R-Cp-C mechanism in the j-th position.

The sliding displacement $S_3$ can now be found from Equation (E-1). This gives

$$S_3 = \frac{(\underline{P}_j - \underline{P}_j^*) \cdot \underline{a}_{j'}}{\underline{u}_3 \cdot \underline{a}_{j'}} \tag{E-4}$$

where

$$\underline{P}_j^* = \underline{P} + (\cos\theta_3 - 1)\underline{U}_3\underline{Q}_3 + \sin\theta_3(\underline{u}_3 \times \underline{Q}_3)$$

From the denominator of Equation (E-4), we can observe that $\underline{u}_3$ can not be perpendicular to $\underline{a}_{j'}$. Otherwise, the sliding of the $C_P$ pair may go to infinity.

The angular velocity $\dot{\theta}_3$ is obtained by taking time derivative of Equation (E-2) with $\dot{\theta}_2$ constant, which gives

$$\dot{\theta}_3 = - \frac{\underline{c}^{*\prime}_j \cdot \underline{a}_{j'}}{\underline{c}^*_j \cdot \underline{a}'_{j'}} \dot{\theta}_2 \tag{E-5}$$

where

$$\underline{c}^{*\prime}_j = - \sin\theta_2\underline{U}_2\underline{c}^* + \cos\theta_2(\underline{u}_2 \times \underline{c}^*)$$

$$\underline{a}'_{j'} = - \sin\theta_3\underline{U}_3\underline{a} + \cos\theta_3(\underline{u}_3 \times \underline{a})$$

The translational velocity $\dot{S}_3$ is then solved by taking time derivative of Equation (E-4) with $\dot{\theta}_2$ constant. This leads to

$$\dot{S}_3 = \frac{\dot{\theta}_2(\underline{P}'_j \cdot \underline{a}_{j'}) + \dot{\theta}_3[(\underline{P}_j - \underline{P}_{j'}) \cdot \underline{a}'_{j'} - \underline{P}'_{j'}^* \cdot \underline{a}_{j'}]}{\underline{u}_3 \cdot \underline{a}_{j'}} \tag{E-6}$$

where

$$\underline{P}'_j = - \sin\theta_2\underline{U}_2\underline{Q}_2 + \cos\theta_2(\underline{u}_2 \times \underline{Q}_2)$$

$$\underline{P}'_{j'}^* = - \sin\theta_3\underline{U}_3\underline{Q}_3 + \cos\theta_3(\underline{u}_3 \times \underline{Q}_3)$$

The angular acceleration is given as

$$\ddot{\theta}_3 = \frac{-[\dot{\theta}_3{}^2(\underline{a}''_{j'} \cdot \underline{c}^*_j) + 2\dot{\theta}_2\dot{\theta}_3(\underline{a}'_{j'} \cdot \underline{c}^{*\prime}_j) + \dot{\theta}_2{}^2(\underline{a}_{j'} \cdot \underline{c}^{*\prime\prime}_j)}{\underline{a}'_{j'} \cdot \underline{c}^*_j} \tag{E-7}$$

where

$$\underline{a}''_{j'} = -\cos\theta_3\underline{U}_3\underline{a} - \sin\theta_3(\underline{u}_3 \times \underline{a})$$

$$\underline{c}^{*\prime\prime}_j = -\cos\theta_2\underline{U}_2\underline{c}^* - \sin\theta_2(\underline{u}_2 \times \underline{c}^*)$$

The linear acceleration of the output link is

$$\ddot{s}_3 = \frac{-[d\ddot{\theta}_3 + e\dot{\theta}_3{}^2 + \dot{\theta}_3(f\dot{\theta}_2 + g\dot{s}_3) + g\dot{\theta}_2{}^2]}{\underline{u}_3 \cdot \underline{a}_{j'}} \tag{E-8}$$

where

$$d = \underline{P}'_{j'}{}^* \cdot \underline{a}_{j'} + (\underline{P}_{j'} - \underline{P}_j) \cdot \underline{a}'_{j'}$$

$$e = \underline{P}''_{j'}{}^* \cdot \underline{a}_{j'} + 2(\underline{P}'_{j'}{}^* \cdot \underline{a}'_{j'}) + (\underline{P}_{j'} - \underline{P}_j) \cdot \underline{a}''_{j'}$$

$$f = -2\underline{P}'_j \cdot \underline{a}'_{j'}$$

$$g = \underline{u}_3 \cdot \underline{a}'_{j'}$$

$$h = -\underline{P}''_j \cdot \underline{a}_{j'}$$

and

$$\underline{P}''_{j'}{}^* = -\cos\theta_3\underline{U}_3\underline{Q}_3 - \sin\theta_3(\underline{u}_3 \times \underline{Q}_3)$$

$$\underline{P}''_j = -\cos\theta_1\underline{U}_1\underline{Q}_1 - \sin\theta_1(\underline{u}_1 \times \underline{Q}_1)$$

$$\underline{P}'_{j'}{}^* = -\sin\theta_3\underline{U}_3\underline{Q}_3 + \cos\theta_3(\underline{u}_3 \times \underline{Q}_3)$$

$$\underline{P}'_j = -\sin\theta_2\underline{U}_2\underline{Q}_2 + \cos\theta_2(\underline{u}_2 \times \underline{Q}_2)$$

## APPENDIX F
## DISPLACEMENT EQUATIONS OF R-$P_L$-C-R MECHANISM

The finite screw displacements for the three, four, and five-link mechanisms containing Sp, Sg, Sc, and Cp pairs have been derived by Ghosal (1982), which does not include the $P_L$ pair. However, the displacement equations for the mechanisms containing a $P_L$ pair can be derived in a similar manner as in Ghosal's work. Figure (F-1) shows an R-$P_L$-C-R mechanism in the j-th position.

The $P_L$ pair has one rotation about the normal sectors $\underline{a}_j$ and $\underline{a}_j'$ between the two plane elements where the two normal sectors must be the same. The other relative motion between the pair elements of the $P_L$ pair is the translation on the contact plane, which indicates that the direction sector of the relative motion must be perpendicular to the normal of the plane. Thus, the constraint equations for the planar pair are expressed as follows:

$$\underline{a}_j = \underline{a}_j' \tag{F-1}$$

$$(\underline{P}_j' - \underline{P}_j) \cdot \underline{a}_j = 0 \tag{F-2}$$

where

$$\underline{a}_j = \underline{a} + (\cos\theta_2 - 1)\underline{U}_{2\underline{a}} + \sin\theta_2(\underline{u}_2 \times \underline{a})$$

$$\underline{a}_j' = \underline{a}_{j3} + (\cos\theta_4 - 1)\underline{U}_{4\underline{a}_{j3}} + \sin\theta_4(\underline{u}_4 \times \underline{a}_{j3})$$

$$\underline{a}_{j3} = \underline{a} + (\cos\theta_3 - 1)\underline{U}_{3\underline{a}} + \sin\theta_3(\underline{u}_3 \times \underline{a})$$

$$\underline{P}_j = \underline{P} + (\cos\theta_2 - 1)\underline{U}_{2\underline{Q}_2} + \sin\theta_2(\underline{u}_2 \times \underline{Q}_2)$$

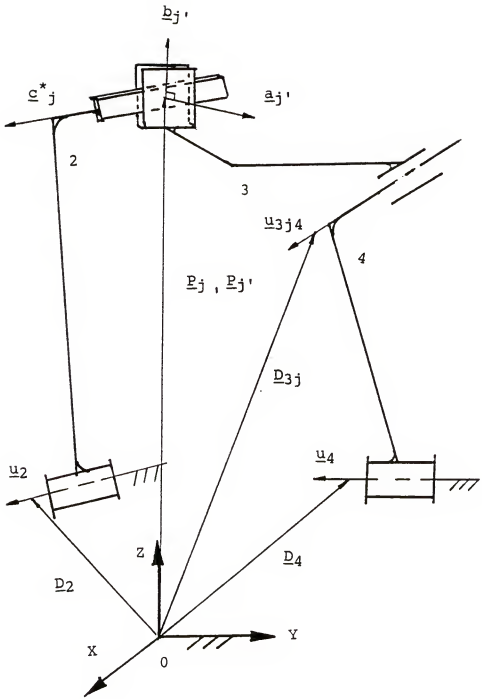


Figure F-1 The R-$P_L$-C-R mechanism in the j-th position.

$$\underline{P}_{j'} = \underline{P}_{j3} + (\cos\Theta_4 - 1)\underline{U}_4\underline{Q}_{j4} + \sin\Theta_4(\underline{u}_4 \times \underline{Q}_{j4}) + S_3\underline{u}_{3j4}$$

$$\underline{P}_{j3} = \underline{P} + (\cos\Theta_3 - 1)\underline{U}_3\underline{Q}_3 + \sin\Theta_3(\underline{u}_3 \times \underline{Q}_3)$$

$$\underline{Q}_{j4} = \underline{P}_{j3} - \underline{D}_4$$

By taking scalar product with $\underline{u}_4$ of Equation (F-1), gives one equation correlating $\Theta_2$ and $\Theta_3$ as

$$[\underline{a} + (\cos\Theta_3 - 1)\underline{U}_3\underline{a} + \sin\Theta_3(\underline{u}_3 \times \underline{a}) - \underline{a}_j] \cdot \underline{u}_4 = 0 \qquad \text{(F-3)}$$

With the use of tangent of the half angle formulations using $\tan(\Theta_3/2)$ Equation (F-3) can be rearranged into a quadratic form as

$$aX_3^2 + bX_3 + c = 0 \qquad \text{(F-4)}$$

where

$$a = (\underline{a} - \underline{a}_j - 2\underline{U}_3\underline{a}) \cdot \underline{u}_4$$

$$b = 2(\underline{u}_3 \times \underline{a}) \cdot \underline{u}_4$$

$$c = (\underline{a} - \underline{a}_j) \cdot \underline{u}_4$$

Then, the output angular displacement $\Theta_4$ can be obtained by taking the scalar product of Equation (F-1) with $\underline{U}_4\underline{a}_{j3}$ and $\underline{u}_4 \times \underline{a}_{j3}$ to eliminate $\sin\Theta_3$ and $(\cos\Theta_4 - 1)$, respectively, as

$$\cos\Theta_4 = d/e \qquad \text{(F-5)}$$

$$\sin\Theta_4 = f/e \qquad \text{(F-6)}$$

where

$$d = \underline{a}_j \cdot \underline{U}_4\underline{a}_{j3}$$

$$e = 1 - (\underline{a}_{j3} \cdot \underline{u}_4)^2$$

$$f = \underline{a}_j \cdot \underline{u}_4 \times \underline{a}_{j3}$$

Then, $\Theta_4 = \tan^{-1}(\sin\Theta_4/\cos\Theta_4)$. Note that in programming,

the function ATAN2 should be used in stead of ATAN to avoid getting an improper sign of $\theta_4$.

The linear displacement of joint 3, $S_3$, now can be obtained directly from the other constraint-equation (F-2), as

$$S_3 = \frac{(\underline{P}_j - \underline{P}_{j'}^*) \cdot \underline{a}_j}{\underline{u}_{3j4} \cdot \underline{a}_j} \qquad \text{(F-7)}$$

where

$$\underline{P}_{j'}^* = \underline{P}_{j3} + (\cos\theta_4 - 1)\underline{U}_4\underline{Q}_{j4} + \sin\theta_4(\underline{u}_4 \times \underline{Q}_{j4})$$

$$\underline{u}_{3j4} = \underline{u}_3 + (\cos\theta_4 - 1)\underline{U}_4\underline{u}_3 + \sin\theta_4(\underline{u}_4 \times \underline{u}_3)$$

Similar to the R-Cp-C mechanism, the denominator of the above equation tells that $\underline{u}_{3j4}$ can not be perpendicular to $\underline{a}_{j'}$. Otherwise, an infinite sliding will occur.

To derive the angular velocities, we can take the time derivative of Equation (F-1) with $\dot{\theta}_2$ constant, which gives the following equation

$$\dot{\theta}_3\underline{a}^3{}_{j'} + \dot{\theta}_4\underline{a}^4{}_{j'} = \dot{\theta}_2\underline{a}'_j \qquad \text{(F-8)}$$

where

$$\underline{a}^3{}_{j'} = \underline{a}'_{j3} + (\cos\theta_4 - 1)\underline{U}_4\underline{a}'_{j3} + \sin\theta_4(\underline{u}_4 \times \underline{a}'_{j3})$$

$$\underline{a}^4{}_{j'} = -\sin\theta_4\underline{U}_4\underline{a}_{j3} + \cos\theta_4(\underline{u}_4 \times \underline{a}_{j3})$$

$$\underline{a}'_{j3} = -\sin\theta_3\underline{U}_3\underline{a} + \cos\theta_3(\underline{u}_3 \times \underline{a})$$

Then, $\dot{\theta}_3$ and $\dot{\theta}_4$ are given by taking dot products of Equation (F-8) with $\underline{u}_3 \times \underline{a}^4{}_{j'}$ and $\underline{u}_3 \times \underline{a}^3{}_{j'}$, respectively, as

$$\dot{\theta}_3 = \frac{(\underline{a}'_j \cdot \underline{u}_3 \times \underline{a}^4{}_{j'})\dot{\theta}_2}{\underline{a}^3{}_{j'} \cdot \underline{u}_3 \times \underline{a}^4{}_{j'}} \qquad \text{(F-9)}$$

and

$$\dot{\theta}_4 = \frac{(\underline{a}'_j \cdot \underline{u}_3 \times \underline{a}^3{}_{j'})\dot{\theta}_2}{\underline{a}^4{}_{j'} \cdot \underline{u}_3 \times \underline{a}^3{}_{j'}} \qquad \text{(F-10)}$$

where

$$\underline{a}'_j = -\sin\theta_2 \underline{U}_{2\underline{a}} + \cos\theta_2(\underline{u}_2 \times \underline{a})$$

The sliding velocity of joint 3, $\dot{S}_3$, can be obtained by taking time derivatives of Equation (F-2), which gives

$$\dot{S}_3 = \frac{\dot{\theta}_2 g - [\dot{\theta}_3 \underline{P}^3{}_{j'} + \dot{\theta}_4(\underline{P}^4{}_{j'} + S_3 \underline{u}'_{3j4})] \cdot \underline{a}_j}{\underline{u}_{3j4} \cdot \underline{a}_j} \qquad \text{(F-11)}$$

where

$$g = \underline{P}'_j \cdot \underline{a}_j + (\underline{P}_j - \underline{P}_{j'}) \cdot \underline{a}'_j$$

$$\underline{P}'_j = -\sin\theta_2 \underline{U}_{2\underline{Q}2} + \cos\theta_2(\underline{u}_2 \times \underline{Q}_2)$$

$$\underline{P}^4{}_{j'} = -\sin\theta_4 \underline{U}_{4\underline{Q}j4} + \cos\theta_4(\underline{u}_4 \times \underline{Q}_{j4})$$

$$\underline{P}^3{}_{j'} = \underline{P}'_{j3} + (\cos\theta_4 - 1)\underline{U}_4 \underline{P}'_{j3} + \sin\theta_4(\underline{u}_4 \times \underline{P}'_{j3})$$

$$\underline{P}'_{j3} = -\sin\theta_3 \underline{U}_{3\underline{Q}3} + \cos\theta_3(\underline{u}_3 \times \underline{Q}_3)$$

$$\underline{u}'_{3j4} = -\sin\theta_4 \underline{U}_4 \underline{u}_3 + \cos\theta(\underline{u}_4 \times \underline{u}_3)$$

The angular accelerations $\ddot{\theta}_3$ and $\ddot{\theta}_4$ can be obtained by first taking the time derivative again of Equation (F-8), which gives

$$\ddot{\theta}_3 \underline{a}^3{}_{j'} + \dot{\theta}_3{}^2 \underline{a}^{33}{}_{j'} + 2\dot{\theta}_3 \dot{\theta}_4 \underline{a}^{34}{}_{j'} + \ddot{\theta}_4 \underline{a}^4{}_{j'} + \dot{\theta}_4{}^2 \underline{a}^{44}{}_{j'} = \dot{\theta}_2{}^2 \underline{a}''_j \qquad \text{(F-12)}$$

where

$$\underline{a}''_j = -\cos\theta_2 \underline{U}_{2\underline{a}} - \sin\theta_2(\underline{u}_2 \times \underline{a})$$

$$\underline{a}''_{j3} = -\cos\theta_3 \underline{U}_{3\underline{a}} - \sin\theta_3(\underline{u}_3 \times \underline{a})$$

$$\underline{a}^{33}{}_{j'} = \underline{a}''_{j3} + (\cos\theta_4 - 1)\underline{U}_4 \underline{a}''_{j3} + \sin\theta_4(\underline{u}_4 \times \underline{a}''_{j3})$$

$$\underline{a}^{34}{}_{j'} = -\sin\theta_4 \underline{U}_4 \underline{a}'_{j3} + \cos\theta_4(\underline{u}_4 \times \underline{a}'_{j3})$$

$$\underline{a}^{44}{}_{j'} = -\cos\theta_4 \underline{U}_4 \underline{a}_{j3} - \sin\theta_4(\underline{u}_4 \times \underline{a}_{j3})$$

Then, by taking dot products with $\underline{u}_3 \times \underline{a}^3{}_{j'}$ and $\underline{u}_3 \times \underline{a}^4{}_{j'}$, respectively, gives

$$\ddot{\theta}_3 = \frac{\underline{h} \cdot \underline{u}_3 \times \underline{a}^4{}_{j'}}{\underline{a}^3{}_{j'} \cdot \underline{u}_3 \times \underline{a}^4{}_{j'}} \qquad \text{(F-13)}$$

and

$$\ddot{\theta}_4 = \frac{\underline{h} \cdot \underline{u}_3 \times \underline{a}^3{}_{j'}}{\underline{a}^4{}_{j'} \cdot \underline{u}_3 \times \underline{a}^3{}_{j'}} \qquad \text{(F-14)}$$

where

$$\underline{h} = \dot{\theta}_2{}^2\underline{a}"_j - \dot{\theta}_3{}^2\underline{a}^{33}{}_{j'} - 2\dot{\theta}_3\dot{\theta}_4\underline{a}^{34}{}_{j'} - \dot{\theta}_4{}^2\underline{a}^{44}{}_{j'}$$

The relative linear acceleration in joint 3 is obtained by taking the time derivative again of Equation (F-11), which gives

$$\begin{aligned}\ddot{\underline{s}}_3 = \{&[\dot{\theta}_2{}^2\underline{P}"_j - \dot{\theta}_3{}^2\underline{P}^{33}{}_{j'} - \dot{\theta}_4{}^2(\underline{P}^{44}{}_{j'} + S_3\underline{u}"_{3j4}) - \\ &\ddot{\theta}_3\underline{P}^3{}_{j'} - \ddot{\theta}_4(\underline{P}^4{}_{j'} + S_3\underline{u}'_{3j4}) - 2\dot{\theta}_3\dot{\theta}_4\underline{P}^{34}{}_{j'} - \\ &2\dot{\theta}_4\dot{S}_3\underline{u}'_{3j4}] \cdot \underline{a}_j + [2\dot{\theta}_2(\dot{\theta}_2\underline{P}'_j - \dot{\theta}_3\underline{P}^3{}_{j'} - \dot{\theta}_4(\underline{P}^4{}_{j'} + \\ &S_3\underline{u}'_{3j4}) - \dot{S}_3\underline{u}_{3j4}] \cdot \underline{a}'_j + \dot{\theta}_2(\underline{P}_j - \underline{P}_{j'}{}^* - \\ &S_3\underline{u}_{3j4}) \cdot \underline{a}"_j\} / (\underline{u}_{3j4} \cdot \underline{a}_j)\end{aligned}$$

where

$$\underline{P}"_j = -\cos\theta_2\underline{U}_2\underline{Q}_2 + \sin\theta_2(\underline{u}_2 \times \underline{Q}_2)$$

$$\underline{P}^{33}{}_{j'} = \underline{P}"_{j3} + (\cos\theta_4 - 1)\underline{U}_4\underline{P}"_{j3} + \sin\theta_4(\underline{u}_4 \times \underline{P}"_{j3})$$

$$\underline{P}^{34}{}_{j'} = -\sin\theta_4\underline{U}_4\underline{P}'_{j3} + \cos\theta_4(\underline{u}_4 \times \underline{P}'_{j3})$$

$$\underline{P}^{44}{}_{j'} = -\cos\theta_4\underline{U}_4\underline{Q}_{j4} - \sin\theta_4(\underline{u}_4 \times \underline{Q}_{j4})$$

$$\underline{u}"_{3j4} = -\cos\theta_4\underline{U}_4\underline{u}_3 - \sin\theta_4(\underline{u}_4 \times \underline{u}_3)$$

$$\underline{P}"_{j3} = -\cos\theta_3\underline{U}_3\underline{Q}_3 - \sin\theta_3(\underline{u}_3 \times \underline{Q}_3)$$

## APPENDIX G
## ROTATABILITY OF R-Sp-R MECHANISM

The constraint equation for the R-Sp-R mechanism can be written, as

$$(\underline{P}_{j'} - \underline{P}_j) \cdot \underline{a}_{j'} = 0 \qquad \text{(G-1)}$$

where $\underline{P}_j$, $\underline{P}_{j'}$, and $\underline{a}_{j'}$ are denoted in Appendix D. By the use of tangent of the half angle of the output joint rotation angle, $\theta_3$, the above equation can be rearranged into a quadratic equation of $X_3$, where $X_3 = \tan(\theta_3/2)$:

$$aX_3^2 + bX_3 + c = 0 \qquad \text{(G-2)}$$

The coefficients of Equation (G-2) are listed in Appendix D. The two roots of Equation (G-2) correspond to the two possible values of the output angle $\theta_3$. When the input link reaches a limit position, the two output angles become the same, i.e., the determinant of Equation (G-2) must be equal to zero. The discriminant

$$D = b^2 - 4ac \qquad \text{(G-3)}$$

can be rearranged into a quartic equation in terms of the output angle by the use of tangent of the half angle formulations for the input rotation angle, which gives

$$d_4X_2^4 + d_3X_2^3 + d_2X_2^2 + d_1X_2 + d_0 = 0 \qquad \text{(G-4)}$$

where

$$d_4 = e_0 - 2e_1 + 4e_4$$

$$d_3 = 2e_2 - 4e_3$$

$$d_2 = 2e_0 - 2e_1 + 4e_5$$

$$d_1 = 2e_2$$

$$d_0 = e_0$$

and

$$e_0 = (\underline{Q}_3 \cdot \underline{u}_3 \times \underline{a})^2$$

$$e_1 = 2(\underline{Q}_3 \cdot \underline{u}_3 \times \underline{a})(\underline{U}_{2\underline{Q}2} \cdot \underline{u}_3 \times \underline{a}) + 2(\underline{Q}_3 \cdot \underline{U}_{3\underline{a}})(\underline{U}_{2\underline{Q}2} \cdot \underline{a})$$

$$e_2 = 2(\underline{Q}_3 \cdot \underline{u}_3 \times \underline{a})(\underline{u}_2 \times \underline{Q}_2 \cdot \underline{u}_3 \times \underline{a}) + 2(\underline{Q}_3 \cdot \underline{U}_{3\underline{a}})(\underline{u}_2 \times \underline{Q}_2 \cdot \underline{a})$$

$$e_3 = 2(\underline{U}_{2\underline{Q}2} \cdot \underline{u}_3 \times \underline{a})(\underline{u}_2 \times \underline{Q}_2 \cdot \underline{u}_3 \times \underline{a}) - 2(\underline{U}_{2\underline{Q}2} \cdot \underline{a})(\underline{u}_2 \times \underline{Q}_2 \cdot \underline{a}) + 2(\underline{U}_{2\underline{Q}2} \cdot \underline{a})(\underline{u}_2 \times \underline{Q}_2 \cdot \underline{U}_{3\underline{a}}) + (\underline{u}_2 \times \underline{Q}_2 \cdot \underline{a})(\underline{U}_{2\underline{Q}2} \cdot \underline{U}_{3\underline{a}})$$

$$e_4 = (\underline{U}_{2\underline{Q}2} \cdot \underline{u}_3 \times \underline{a})^2 - (\underline{U}_{2\underline{Q}2} \cdot \underline{a})^2 + 2(\underline{U}_{2\underline{Q}2} \cdot \underline{a})(\underline{U}_{2\underline{Q}2} \cdot \underline{U}_{3\underline{a}})$$

$$e_5 = (\underline{u}_2 \times \underline{Q}_2 \cdot \underline{u}_3 \times \underline{a})^2 - (\underline{u}_2 \times \underline{Q}_2 \cdot \underline{a})^2 + 2(\underline{u}_2 \times \underline{Q}_2 \cdot \underline{a})(\underline{u}_2 \times \underline{Q}_2 \cdot \underline{U}_{3\underline{a}})$$

Solving Equation (G-4) will yield four values of the input angle corresponding to the four possible limit positions. However, if an input crank link is desired, no limit positions should exist, therefore, Equation (G-4) should have no real roots.

Similarly, to ensure a fully rotatable output link, we may write the out-input equation by reversing the roles of the input and output rotation angles in Equation (G-2), which gives

$$fX_2^2 + gX_2 + h = 0 \qquad \text{(G-5)}$$

where

$$f = \underline{Q}_3 \cdot (\underline{a}_{j'} - \underline{a}) - 2\underline{U}_{2\underline{Q}2} \cdot \underline{a}_{j'}$$

$$g = \underline{u}_2 \times \underline{Q}_2 \cdot \underline{a}_{j'}$$

$$h = \underline{Q}_3 \cdot (\underline{a}_{j'} - \underline{a})$$

The discriminant of Equation (G-5) can be rearranged into a quartic equation in terms of $X_3$, as

$$i_4 X_3^4 + i_3 X_3^3 + i_2 X_3^2 + i_1 X_3 + i_0 = 0 \qquad \text{(G-6)}$$

where

$$i_4 = j_0 - 2j_1 + 4j_4$$

$$i_3 = 2j_2 - 4j_3$$

$$i_2 = 2j_0 - 2j_1 + 4j_5$$

$$i_1 = 2j_2; \qquad i_0 = j_0$$

and

$$j_0 = (\underline{u}_2 \times \underline{Q}_2 \cdot \underline{a})^2$$

$$j_1 = 2[(\underline{u}_2 \times \underline{Q}_2 \cdot \underline{a})(\underline{u}_2 \times \underline{Q}_2 \cdot \underline{U}_{3\underline{a}}) + (\underline{U}_{2\underline{Q}2} \cdot \underline{a})(\underline{Q}_3 \cdot \underline{U}_{3\underline{a}})]$$

$$j_2 = 2[(\underline{u}_2 \times \underline{Q}_2 \cdot \underline{a})(\underline{u}_2 \times \underline{Q}_2 \cdot \underline{u}_3 \times \underline{a}) + (\underline{U}_{2\underline{Q}2} \cdot \underline{a})(\underline{Q}_3 \cdot \underline{u}_3 \times \underline{a})]$$

$$j_3 = 2[(\underline{u}_2 \times \underline{Q}_2 \cdot \underline{U}_{3\underline{a}})(\underline{u}_2 \times \underline{Q}_2 \cdot \underline{u}_3 \times \underline{a}) - (\underline{Q}_3 \cdot \underline{U}_{3\underline{a}})(\underline{Q}_3 \cdot \underline{u}_3 \times \underline{a}) + (\underline{Q}_3 \cdot \underline{U}_{3\underline{a}})(\underline{U}_{2\underline{Q}2} \cdot \underline{u}_3 \times \underline{a}) + (\underline{Q}_3 \cdot \underline{u}_3 \times \underline{a})(\underline{U}_{2\underline{Q}2} \cdot \underline{U}_{3\underline{a}})$$

$$j_4 = (\underline{u}_2 \times \underline{Q}_2 \cdot \underline{U}_{3\underline{a}})^2 - (\underline{Q}_3 \cdot \underline{U}_{3\underline{a}})^2 + 2(\underline{Q}_3 \cdot \underline{U}_{3\underline{a}})(\underline{U}_{2\underline{Q}2} \cdot \underline{U}_{3\underline{a}})$$

$$j_5 = (\underline{u}_2 \times \underline{Q}_2 \cdot \underline{u}_3 \times \underline{a})^2 - (\underline{Q}_3 \cdot \underline{u}_3 \times \underline{a})^2 + 2(\underline{Q}_3 \cdot \underline{u}_3 \times \underline{a})(\underline{U}_{2\underline{Q}2} \cdot \underline{u}_3 \times \underline{a})$$

If a fully rotatable output link is desired, Equation (G-6) must have no real roots so that there are no limit positions of the output rotation angle.

## REFERENCE


Alizade, R. I. & Sandor G. N., "Determination of the Condition of Existence of Complete Crank Rotation and of the Instantaneous Efficiency of Spatial Four-Bar Mechanisms," Mechanism and Machine Theory, Vol. 20, No. 3., 1975, pp. 155-163.

Angeles, J. & Bernier, A., "A General Method of Four-Bar Linkage Mobility Analysis," ASME paper 86-DET-65, 1986.

Bagci, C., "Static Force and Torque Analysis Using 3x3 Screw Matrix, and Transmission Criteria for Space Mechanisms," ASME Journal of Engineering for Industry, Vol. 90, Feb. 1971, pp. 90-101.

Bagci, C. "Design of Spherical Crank-Rocker Mechanism with Optimal Transmission," ASME Journal of Engineering for Industry, Vol. 95, B, No. 2, May 1973, pp. 577-583.

Bagci, C., "Dynamic Motion Analysis of Plane Mechanisms with Coulomb and Viscous Damping via the Joint Force Analysis," ASME Journal of Engineering for Industry, Vol. 97, May 1975a, pp. 551-560.

Bagci, C., "Simplified Synthesis of the Double-Crank (Drag-Link) Four-Bar Plane Mechanism with Most Favorable Transmission via the Pole Technique," Proceedings of the 4th OSU Applied Mechanisms Conference, Nov. 2-5, 1975b, Chicago, Ill, pp. 26-1 to 26-13.

Bagci, C. & Khosravi, F., "Dynamics of Spatial Mechanisms with Coulomb and Viscous Friction Forces in Bearings with Surface Contacts," ASME paper 86-DET-192.

Balaji Rao, L. V. & Lakshminarayana, K., "Optimal Designs of the RSSR Crank-Rocker Mechanism-I. General Time Ratio," Mechanism and Machine Theory, Vol. 19, No. 4/5, 1984, pp. 431-441.

Balaji Rao, L. V. & Lakshminarayana, K., "Optimal Designs of the RSSR Crank-Rocker Mechanism-II. Unit Time Ratio and Limits of Capability," Mechanism and Machine Theory, Vol. 19, No. 4/5, 1984, pp. 443-448.

Bell, R. & Burdekin, M., "Dynamic Behavior of Plain Slideways," Proceeding for Institution of Mechanical Engineers, Vol. 181,, 1966, Pt. 1, No. 8.

Brasfield, R. L. & Bagci, C., "Matrix-Displacement-Direct-Element Method for Force and Torque Analysis of Determinate and Indeterminate Space Mechanisms With Arbitrary Skew Angles," ASME Journal of Engineering for Industry, May 1975, pp. 671-681.

Cajori, F., An Introduction to Theory of Equations, Macmillan, New York, 1943.

Chen, F. Y., Mechanics and Design of Cam Mechanims, Pergamon Press, 1982, New York.

Chen, P. & Roth, B., "Design Equations for the Finite and Infinitesimally Separated Position Synthesis of Binary Links and Combined Link Chains," ASME Journal of Engineering for Industry, Series B, No. 1, Vol. 91, Feb. 1969, pp. 208-218.

Chew, M., "Application of Kinematically Compatible Rolling-Contact Pairs to the Design of Low-Friction Rocker-Pivots," ASME Journal of Mechanisms, Transmission, and Automation in Design, Vol. 107, Sep. 1985, pp. 388-393.

Chiang, C. H., "Design of Spherical and Planar Crank-Rockers and Double-Rockers as Function Generators-I: Crank-Rockers," Mechanism and Machine Theory, Vol. 21, No. 4, 1986, pp. 287-296.

Chiang, C. H., "Design of Spherical and Planar Crank-Rockers and Double-Rockers as Function Generators-II: Double-Rockers," Mechanism and Machine Theory, Vol. 21, No. 4, 1986, pp. 297-305.

Duffy, J., Analysis of Mechanisms and Robot Manipulators, John Wiley & Sons, New York, 1980.

Dukkipati, R. V. & Soni, A. H., "How to Design Spherical Four-Bar with Optimum Transmission Angle and Optimum Structural Error," Proceedings of the 4th OSU Applied Mechanisms Conference, Nov. 2-5, 1975, Chicago, Ill, pp. 17-1 to 17-8.

Eason, E. D. & Fenton, R. G., "A Comparison of Numerical Optimization Methods for Engineering Design," ASME Journal of Engineering for Industry, Feb. 1974, pp. 196-200.

Erdman, A. G. & Sandor G. N., Mechanism Design: Analysis and Synthesis, Vol. 1, Prentice-Hall, New Jersey, 1984.

Fiacco V. & G. P. McCormick, Nonlinear Programming: Sequentially Unconstrained Minimization Techniques, John Wiley & Sons, Inc., New York, 1968.

Fox, R. L. & Gupta, K. C., "Optimization Technology as Applied to Mechanism Design," ASME Journal of Engineering for Industry, May 1973, pp. 657-663.

Freudenstein, F. & Chew, M. S., "Optimization of Crank-and-Rocker Linkages with Size and Transmission Constraints," ASME Journal of Mechanical Design, Vol. 191, 1979, pp. 51-57.

Freudenstein, F. & Primrose, E. J. F., "The Classical Transmission Angle Problem," Proc. Conference on Mechanisms, Institute of Mechanical Engineers, London, 1972, pp. 105-110.

Funabashi, H. & Freudenstein, F., "Performance Criteria for High-Speed Crank-and-Rocker Linkages Part I: Plane Crank-and-Rocker Linkages," ASME Journal of Mechanical Design, Jan. 1979, Vol. 101, pp. 20-25.

Funabashi, H. & Freudenstein, F., "Performance Criteria for High-Speed Crank-and-Rocker Linkages Part II: Spherical Crank-and-Rocker Linkages," ASME Journal of Mechanical Design, Jan. 1979, Vol. 101, pp. 26-31.

Ghosal, A., "Analysis of Spatial Mechanisms Containing Higher Pairs, " M.S. Thesis, University of Florida, 1982.

Ghosal, A., Kohli, D., & Sandor, G. N., "Kinematic Analysis of Four-Link Space Mechanisms Containing Sphere-Groove and Sphere-Slotted-Cylinder Higher Pairs," ASME paper 82-DET-123, 1982

Gilmartin M. J., and Duffy J., "Type and Mobility Analysis of the Spherical Four-Link Mechanism,", Proc. Conference on Mechanisms, Institute of Mechanical Engineers, London, 1972, pp. 90-97.

Gupta, K. C., "Design of Four-Bar Function Generators with Mini-Max Transmission Angle," ASME Journal of Engineering for Industry, Vol 99, No. 2, May 1977, pp. 360-366.

Gupta, K. C., "A General Theory for Synthesizing Crank-Type Four-Bar Function Generators with Transmission Angle Control," ASME Journal of Applied Mechanics, June 1978, Vol. 45, pp. 415-421.

Gupta, K. C. & Kazerounian, S. M. K., "Synthesis of Fully Rotatable R-S-S-R Linkages," Mechanism and Machine Theory, Vol. 18, No. 3, pp. 199-205, 1983.

Hain, Kurt, "Optimization of a Cam Mechanism-to give good transmissivility, maximal output angle of swing and minimal acceleration," Journal of Mechanism, Vol. 6, 1971, pp. 419-434.

Hall, A. S., Kinematics and Linkage Design, Balt, West Lafayette, Indiana, 1966.

Hamid, S. & Soni, A. H., "Design of an RSSR Crank-Rocker Mechanism for Optimum Force Transmission," Proceedings of the 2nd OSU Applied Mechanisms Conference, Oct. 7-8, 1971, Stillwater, Oklahoma, Paper No. 17.

Hamid, S. & Soni, A. H., "Design of s Space Slider-Crank RSSP Mechanism with Optimum Force Transmission," ASME paper 72-Mech-82, 1972.

Hernandez Jr., M. V., "Kinematic Synthesis and Analysis of Three-Link Spatial Function Generators with Higher Pairs," Ph.D. Dissertation, University of Florida, 1983.

Hock, W. & Schittkowske, K., "A Comparative Performance Evaluation of 27 Nonlinear Programming Codes," Computing, Vol. 30, 1983, pp. 335-358.

Hossne G., A. J., "Design of Spherical Double-Rocker Linkages," Proceedings of the 6th OSU Applied Mechanisms Conference, Oct. 1-3, 1979, Denever, Colorado, pp. XX 1-7.

Huang, M. & Soni, A. H., "Design of Spherical and Spatial Four-Link Crank-Rocker Mechanisms With or Without Passive Constraints," Proceedings of the 1st OSU Applied Mechanisms Conference, Stillwater, Oklahoma, 1969, pp. 22.1-22.5.

Huang, M., Pamidi, P. R., & Soni, A. H., "Design of a Spherical Four-Link Crank-Rocker Mechanism," ASME Journal of Mechanisms, Vol. 5, 1970, pp. 5-10.

Hunt, K. H., Kinematic Geometry of Mechanisms, Clarendon Press, Oxford, 1978.

Imam, I., Skreiner, M., & Sadler, J. P., "A New Solution to Columb Friction in Mechanism Bearing: Theory and Application," ASME Journal of Mechanical Design, Vol. 103, Oct. 1981, pp. 764-775.

Keler, M. L., "Kinematics and Statics Including Friction in Single-Loop Mechanisms by Screw Calculus and Dual Vectors," ASME Journal of Engineering for Industry, May 1973, pp. 471-480.

Kohli, D. & Soni, A. H., "Displacement Analysis of Single-Loop Spatial Mechanisms," Proceedings of IFToMM, International Symposium on Linkages, Bucharest, Romania, June 6-13, 1973.

Kohli, D. & Soni, A. H., "Displacement Analysis of Spatial Two-Loop Mechanisms," Proceedings of IFToMM, International Symposium on Linkages, Bucharest, Romania, June 6-13, 1973.

Kohli, D. & Soni, A. H., "Kinematic Analysis of Spatial Mechanism Via Successive Screw Displacements," ASME Journal of Engineering for Industry, Series B, No. 2, Vol. 97, May, 1975, pp. 739-747.

Lakshminarayana, K. & Balaji Rao, L. V., "Graphical Synthesis of the RSSR Crank-Rocker Mechanism," Mechanism and Machine Theory, Vol. 19, No. 3, 1984, pp. 331-336.

Lee, I.-P. J. & Bagci, C., "The RCRRC Five-Link Space Mechanism-Displacement Analysis, Force and Torque Analysis and Its Transmission Criteria," ASME Journal of Engineering for Industry, May 1975, pp. 581-594.

Litvin, F. L., "Criteria of Force Transmission for Linkages and Their Application for Synthesis," ASME Journal of Mechanisms, Transmission, and Automation in Design, Vol. 102, Jan. 1980, pp. 38-44.

Litvin, F. L. & Coy, J. J., "Special Cases of Friction and Applications," ASME Journal of Mechanisms, Transmission, and Automation in Design, Vol. 106, June 1984, pp. 256-260.

Litvin, F. L. & Gutman, Y. I., "Analysis and Synthesis of a Three-Link Linkage with an Intermediate Higher Kinematic Pair," Paper Presented to the ASME Design Engineering Conference, Beverly Hills, California, Sep. 28-Oct. 1, 1980.

Midha A., Hall, A. S., Jr., Her I., & Bubel G. M., "Mechanical Advantage of Single-Input and Multiple-Output Ports Mechanical Device," ASME Journal of Mechanisms, Transmissions, and Automation in Desing, Vol. 106, Dec. 1984, pp. 462-469.

Miesch, T. C., "Optimization of a Three-Link Spatial Mechanism with a Higher Pair," M.S. Thesis, University of Florida, 1984.

Pisano, A. P., "Coulomb Friction in Hig-Speed Cam Systems," ASME Journal of Mechanisms, Transmission, and Automation in Design, Vol. 106, Dec. 1984, pp. 470-474.

Rao, S. S., Optimization, Theory and Applications, John Wiley & Sons, New York, 1979.

Reiinholtz, C. F., "Optimization of Spatial Mechanisms,", Ph.D. Dissertation, University of Florida, 1983.

Reklaitis G. V., Ravindran A. R., & Ragsdell K. M., Engineering Optimizaiton, John Wiley and Sons, New York, 1983.

Rooney, G. T., & Deravi, P. "Coulomb Friction in Mechanism Sliding Joints," Journal of Mechanism and Machine Theory, Vol. 17, No. 3, 1982, pp. 207-211.

Roth, B., Freudenstein, F., & Sandor, G. N., "Synthesis of Four-link Path-Generating Mechanisms with Optimum Transmission Characteristics," Proceedings of the 7th conference on Mechanisms, Purdue University, West Lafayette, Ind., Oct. 8-10, 1962, pp. 44-48.

Sadler, J. P., "Dynamic Analysis of Mechanisms Including Coulomb Friction Via Equilibrium Equations," Proceedings of the 3rd OSU Applied Mechanisms Conference, Stillwater, Oklahoma, 1973, pp. 13-1 to 13-11.

Sandgren, E. & Ragsdell, K. M., "The Utility of Nonlinear Programming Algorithms: A Comparative Study - Part I & II", ASME Journal of Mechanical Design, Vol. 102, July 1980, pp. 540-551.

Sandor, G. N., Kohli, D., Hernandez, M. V., & Ghosal, A., "Kinematic Analysis of Three-Link Spatial Mechanisms Containing Sphere-Plane and Sphere-Groove Pair," Proceedings of the 7th OSU Applied Mechanism Conference, Dec. 7-9, 1981, pp. XXXII-1 to XXXII-11.

Shoup, T. E. & Pelan, B. J., "Design of Four-Bar Mechanisms for Optimum Transmission Angle and Optimum Structural Error," Proceedings of the 2nd OSU Applied Mechanism Conference, Oct. 7-8, 1971, Stillwater, Oklahoma, pp. 4-1 to 4-9.

Shoup, T. E., Steffen, J. R., & Weatherford, R. E., "Design of Spatial Mechanisms for Optimum Load Transmission," ASME paper, 72-Mech-88, 1972.

Singh, Y. P. & Kohli, D., "Kinematic Analysis of Spatial Mechanisms Containing Lower and Higher Pairs," Proceedings of the 6th OSU Conference of Applied Mechanisms, Oct. 1-3, 1979, pp. 35-1 to 35-13.

Soni, A. H. & Harrisberger, L., "The Design of the Spherical Drag-Link Mechanism," ASME Journal of Engineering for Industry, Vol. 89, B, No. 1, Feb. 1967, pp. 177-186.

Soni, A. H. & Harrisberger, L., "Design of a Spatial Four-Link Mechanism With or Without Passive Constraint," Journal of Mechanisms, Vol. 4, No. 4, 1969, pp. 337-348.

Soni, A. H. & Harrisberger, L., "Design of Spatial Four-Link Crank-Rocker Mechanism With or Without Passive COnstraint," ASME Journal of Engineering Industry, Vol. 93, No. 1, Feb. 1971, pp. 34-38.

Soylemez E. & Freudenstein, F., "Transmission Optimization of Spatial 4-Link Mechanisms," Mechanism and Machine Theory, Vol. 17, No. 4, 1982, pp. 263-283.

Sun, J. W. H. & Waldron, K. J., "Graphical Transmission Angle control in Planar," Mechanism and Machine Theory, Vol. 16, No. 4, 1981, pp. 385-397.

Sutherland, G. & Roth, B., "A Transmission Index for Spatial Mechanisms," ASME Journal of Engineering for Industry, May 1973, pp. 589-597.

Sutherland, G. H., "Quality of Motion and Force Transmission," Mechanism and Machine Theory, Vol. 16, 1981, pp. 221-225.

Tsai, L.-W., "Design of Drag-Link Mechanisms with Optimum Transmission Angle," ASME Journal of Mechanisms, Transmissions, and Automation in Design, June 1983, Vol. 105, pp. 254-258.

Vanderplatts G. N., Numerical Optimization Techniques for Engineering Design With Application, McGraw-Hill, New York, 1984.

## BIOGRAPHICAL SKETCH

Chin-Hung Jwo was born 1956 in Chun-Li, Taiwan. He received a Bachelor of Engineering degree from Feng Chia University at Taichung in 1979. After two years military service as an Administration Officer in the Army, he worked as a sales engineer in a machinary and auto parts exporting company and as a claim specialist in an auto dealer.

On August 7, 1982, he arrived at Gainesville, Florida, starting his graduate studies in the Department of Mechanical Engineering at the University of Florida. In December 1985, he received a Master of Engineering degree. He is currently continuing his graduate studies for the doctoral degree at the University of Florida.

Chin-Hung is married to the former Ms. Mei-Jung Chang on the Christmas of 1985 in Taipei, Taiwan. In September of 1986, Kai-Wei(Kevin) was born in Alachua General Hospital, Gainesville, Florida.

I certify that I have read this study and that in my opinion it conforms to acceptable standards of scholarly presentation and is fully adequate, in scope and quality, as a dissertation for the degree of Doctor of Philosophy.

George N. Sandor, Chair
Professor of Mechanical Engineering

I certify that I have read this study and that in my opinion it conforms to acceptable standards of scholarly presentation and is fully adequate, in scope and quality, as a dissertation for the degree of Doctor of Philosophy.

Joseph Duffy
Professor of Mechanical Engineering

I certify that I have read this study and that in my opinion it conforms to acceptable standards of scholarly presentation and is fully adequate, in scope and quality, as a dissertation for the degree of Doctor of Philosophy.

Don W. Dareing
Professor of Mechanical Engineering

I certify that I have read this study and that in my opinion it conforms to acceptable standards of scholarly presentation and is fully adequate, in scope and quality, as a dissertation for the degree of Doctor of Philosophy.

Carl D. Crane
Assistant Professor of Mechanical Engineering

I certify that I have read this study and that in my opinion it conforms to acceptable standards of scholarly presentation and is fully adequate, in scope and quality, as a dissertation for the degree of Doctor of Philosophy.

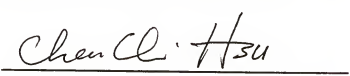

Chen-Chi Hsu
Professor of Aerospace Engineering, Mechanics, and Engineering Sciences

This dissertation was submitted to the Graduate Faculty of the College of Engineering and to the Graduate School and was accepted as partial fulfillment of the requirements for the degree of Doctor of Philosophy.

May 1989

Dean, College of Engineering

Dean, Graduate School